NATIONAL AERONAUTICS AND SPACE ADMINISTRATION

Technical Report No. 32-970

Fission-Electric Cell Irradiation

Walter F. Krieve

JET PROPULSION LABORATORY
CALIFORNIA INSTITUTE OF TECHNOLOGY
PASADENA, CALIFORNIA

March 1, 1967

NATIONAL AERONAUTICS AND SPACE ADMINISTRATION

Technical Report No. 32-970

Fission-Electric Cell Irradiation

Walter F. Krieve

Approved by:

Robert J. Mackin, Jr.

Robert J. Mackin, Jr., *Manager*
Physics Section

JET PROPULSION LABORATORY
CALIFORNIA INSTITUTE OF TECHNOLOGY
PASADENA, CALIFORNIA

March 1, 1967

Prepared Under Contract No. NAS 7-100
National Aeronautics & Space Administration

CONTENTS

TABLES

FIGURES

FIGURES (Cont'd)

FIGURES (Cont'd)

ABSTRACT

A series of capsule reactor irradiation experiments was performed to study the component behavior of fission-electric cell devices under relatively high-radiation intensity and with sufficient fuel burnup to establish operational trends. This Technical Report gives a detailed account of these experiments. It includes complete descriptions of the designs of the various fission-electric cell capsules, discussions of some of the specialized fabrication techniques, and a description of the experiments themselves. The experiments were concerned with electrical characteristics of the cells and with the materials problems associated with extended irradiation periods. In addition to the in-pile measurements of cell performance (as well as calibration runs in intense gamma fluxes), the experiments included extensive post-irradiation, microscopic, and radiochemical analyses. The rationale for the fission-electric cell program and the general conclusions of these experiments are reported elsewhere.

I. INTRODUCTION

A series of capsule reactor irradiation experiments was performed to study the component behavior of fission-electric cell devices under relatively high-radiation intensity and with sufficient fuel burnup to establish operational trends. A fission-electric cell (Refs. 1 through 5)[1] is a device for converting the kinetic energy of charged fission fragments into electrical energy. Because of the short range and the large kinetic energy-to-charge ratio of the fragments, a full-scale fission-electric cell is necessarily a high-voltage, low-current device. Several studies (Ref. 5) have shown the potential advantages to a space power system using a fission-cell reactor if certain operating parameters can be achieved.

The basic components of a fission-electric cell are the cathode, which is covered with a thin layer of fissionable material and serves as the source of the fission fragments; an anode, which serves as the collector of the fragments; and a charge separator, which may be either a magnetic field or an electrostatic grid or both. Fragments originating from the fissioning of fissile atoms are charged. A portion of the fragments produced by neutron bombardment of the fissionable material on the cathode will

[1] See also "Weight of Cavity-Type Fission Cell Reactor," by C. J. Heindl, Section Report No. 363-3, Jet Propulsion Laboratory, Pasadena, April 28, 1966.

emerge from the surface. Of these fragments emerging from the cathode surface, a fraction can be collected on a suitably placed anode. Because of the short range of the fragments in matter, the space between the cathode and anode must be evacuated. The fragments that penetrate the surface of the cathode material are accompanied by a large number of electrons. A net fragment current can be realized by suppressing these electrons with either a magnetic field or an electrostatic grid.

These basic components were encapsulated in an evacuated housing to form miniature fission-electric cells. During irradiation, the output current and voltage were monitored to follow component behavior. Following the irradiation period, the capsules were disassembled and the components were inspected visually and via gamma scanning. Fragment and uranium distributions within the capsules were determined by radiochemical analysis.

Seven cells were irradiated in the General Electric Test Reactor (GETR) in 1961–1963 and three in the General Electric Nuclear Test Reactor (NTR) in 1961 and 1963–1964. Both reactors are at the General Electric Vallecitos site.

II. EXPERIMENT

A. Capsule Design

The capsule (Fig. 1) is formed by a pair of concentric cylinders with the inner space hermetically sealed and evacuated. Suspended within the inner space via either quartz or alumina standoffs is the cylindrical anode. A portion of the inner cylinder supports the fissionable material and serves as the cathode.

A solenoid surrounds the capsule and is the source of magnetic field for suppression of the δ- or follow-out electrons that accompany the fission fragments. An ion pump is attached to the capsule to maintain vacuum and also to monitor the inner space pressure. The pump and electrical terminals are sealed in a container attached to the capsule and coil housing. Electrical leads are strung through a tube that extends from the pump housing to a convenient terminal location. An assembled aluminum capsule is shown in Fig. 2.

Capsule envelopes were fabricated of either aluminum or stainless steel. For the aluminum capsules, the interior of the vacuum chamber was either a polished surface or one that was platinum plated and then plated with platinum black.

The outer shell of the aluminum capsules was 2.00 in. in diameter; the inner cylinder was 0.50 in. in diameter (except in regions expanded for fragment interception). Total capsule length was 9.0 in. The fuel was deposited on the central 3-in. section of the inner cylinder. Fuel element area was 30.4 cm^2 for the non-gridded capsules and 18.3 cm^2 for the gridded. Nominal wall thickness was 0.025 in. and the material, 6061-T6 aluminum. The anode was 1.50 in. in diameter except in contracted regions and was 6.10 in. long. The field coil container had an ID of 2.16 in., an OD of 2.68 in., and a length of 9.5 in. The diameters for the stainless steel capsules were essentially the same as for the aluminum; however, the stainless capsule and field coil containers had a basic length of 12.25 in. The anode was 9.25 in. in length. Fuel was deposited on the central 5-in. section of the inner cylinder and the fuel element area was 36.0 cm^2. Nominal wall thickness was 0.016 in. and the material, type 347 SS.

The fissionable material used in all of the capsules was fully enriched U-235 (93.15%) in the form of UO_2. The UO_2 was electro-deposited on the cathode. Plating techniques and solutions are described in Appendix A. Prior to the plating of the UO_2 on the aluminum cathodes, the aluminum was first zincated and then covered with a thin layer of either (1) copper and then zinc, (2) electrolysis nickel, or (3) platinum. UO_2 layer thickness was determined by uranium added to the plating solution and by weight difference of the cathode structure. Uniformity of the plating was determined by α-scanning of the uranium layer. Layer thickness of the UO_2 was in the range of 1.0 to 10.0 mg/cm^2. The cathodes were terminated on the ends via expanded sections or were sectioned with concentric ribs (Fig. 3) that acted as mechanical collimators for the fragments. These collimators were used to ensure that only those fragments intercepted by the anode would leave the cathode.

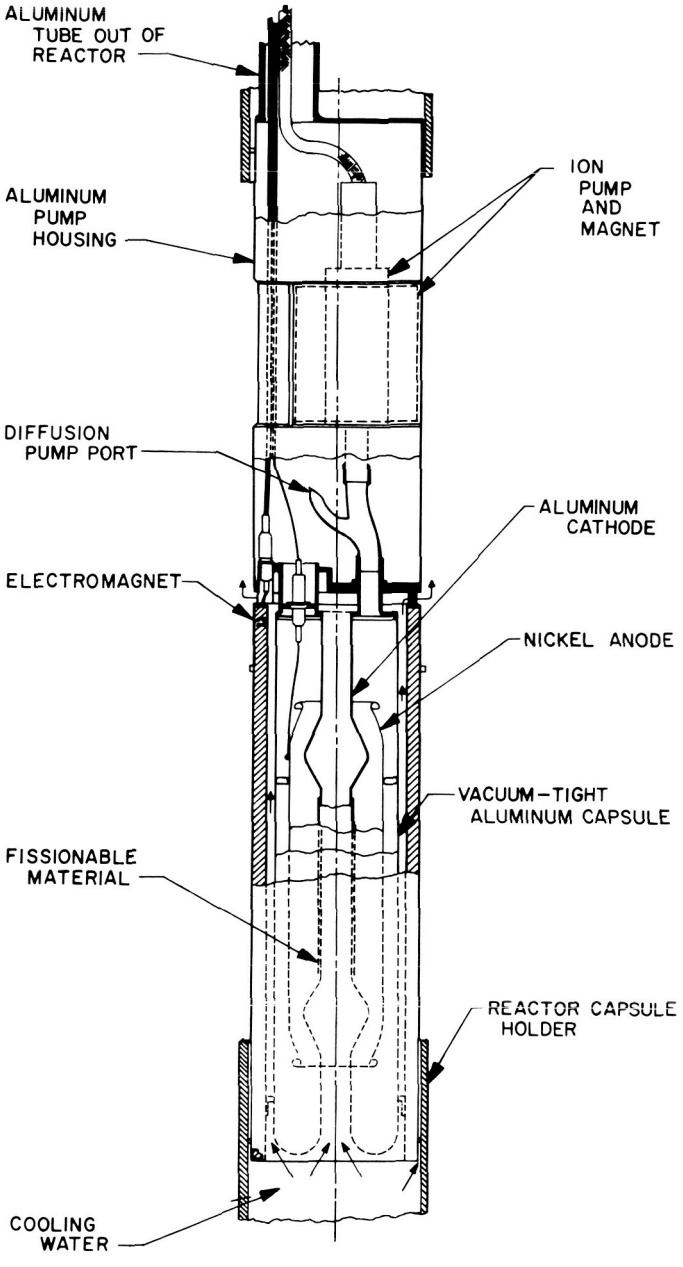

Fig. 1. Fission-electric cell capsule

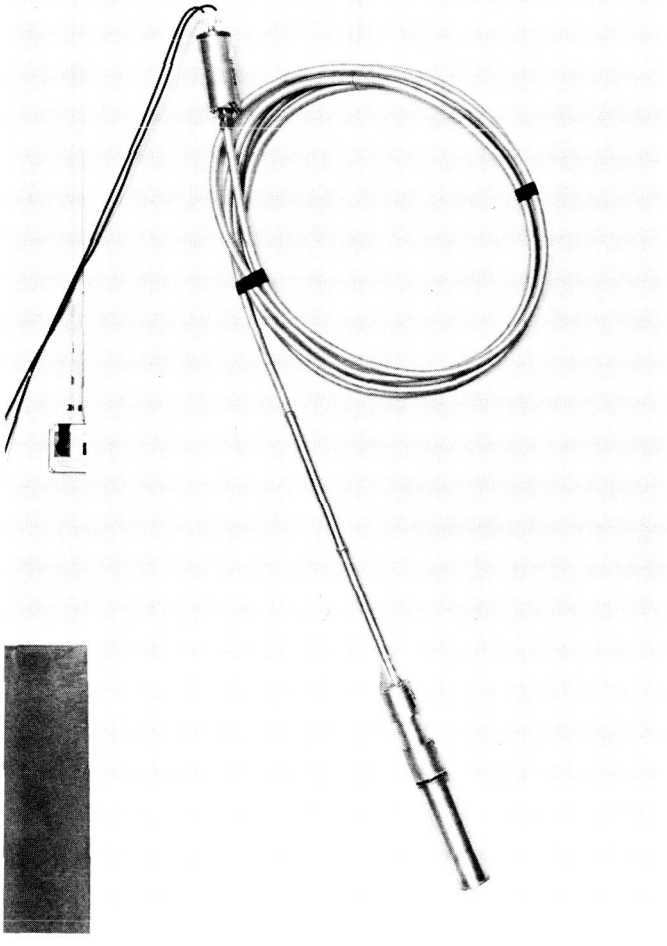

Fig. 2. Assembled aluminum capsule

The anodes for all of the capsules were electroformed from nickel. A typical example is shown in Fig. 4. Anodes for the later capsules in the series had a 50- to 100-μin. layer of platinum over the nickel base. Several of the platinum plated anodes were covered with platinum black. The anodes were between 0.0012 and 0.0015 in. thick; this thickness was chosen to minimize the capsule background current. This background current is produced from non-fission events such as electrons emitted because of gamma interactions (Compton scattering) and beta decay because of neutron activation of the structural material. The anodes were of sufficient thickness to stop all of the fission fragments, but thin enough to be essentially transparent to the high-energy electrons. Because of the thinness of the anodes, they would also represent a small source of electrons. It is theoretically possible to select an anode of mass density and material such that the rate at which the electrons are produced and escape the anode is exactly equal to the rate at which electrons produced outside of the anode are intercepted and stopped by it. For this case, the background current, as measured in the anode circuit, would be zero. In order to monitor the fragment current and to discern any operational trends associated with the fragment current, it is necessary to restrict the background current to a small fraction of the fragment current. However, another requirement imposed on the anode by the experiment was that it have sufficient thickness to have a reasonable life expectancy.

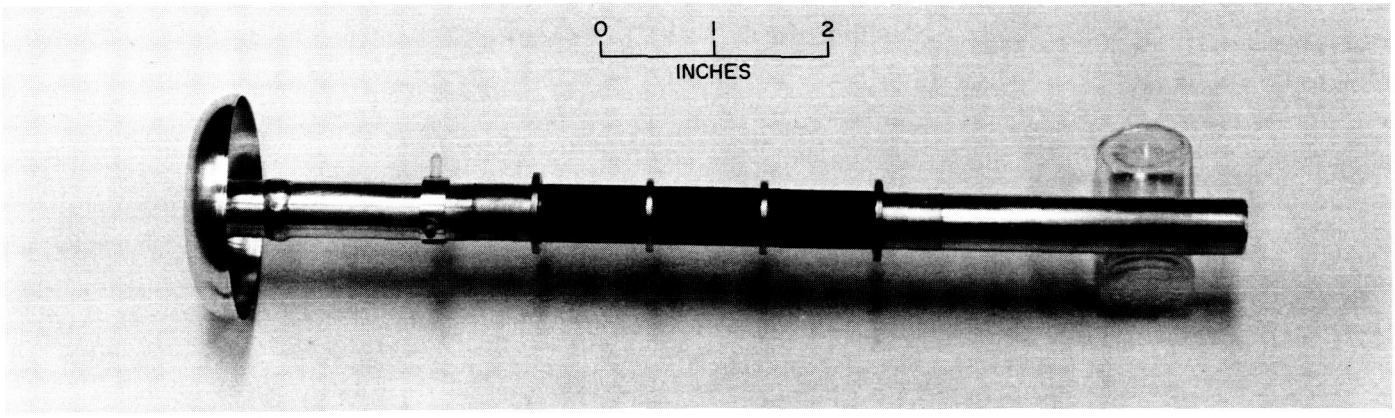

Fig. 3. Cathode sectioned with concentric ribs

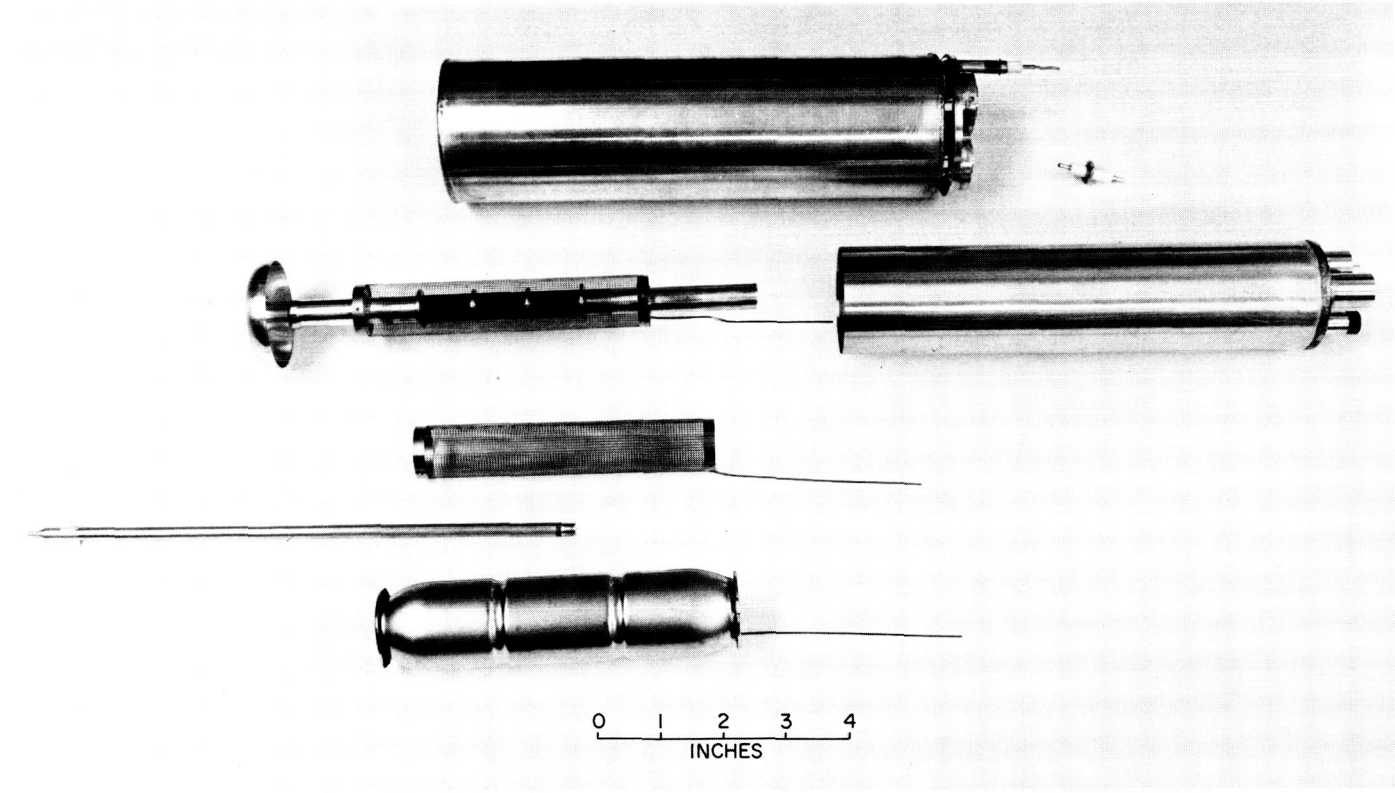

Fig. 4. Capsule components

The magnetic field was produced by a solenoid that surrounded the cell envelope. Aluminum wire was used for the windings of the first group of capsules and copper wire for the later ones. The coils were wound so that there was, effectively, a magnetic bottle within the capsules. The maximum magnetic field was at the ends of the anode and the minimum at the centerline of the anode and cathode. Ratio between the maximum and minimum magnetic flux was approximately 1.5 for all of the capsules. Maximum magnetron limitation for the capsules was between 2800 and 6400 v. Typical axial magnetic field profiles for the aluminum and stainless steel capsules are shown in Figs. 5 and 6.

Three different types of grids were used in the gridded capsules. The first was fabricated via chemical milling of a molybdenum cylinder (Fig. 4). These grids had square openings and a transparency of 75%. The second was

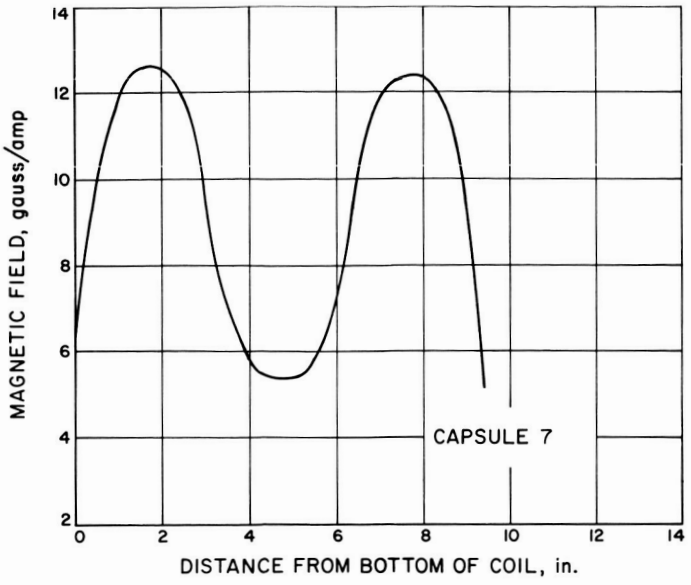

Fig. 5. Axial magnetic field profile (Capsule 7)

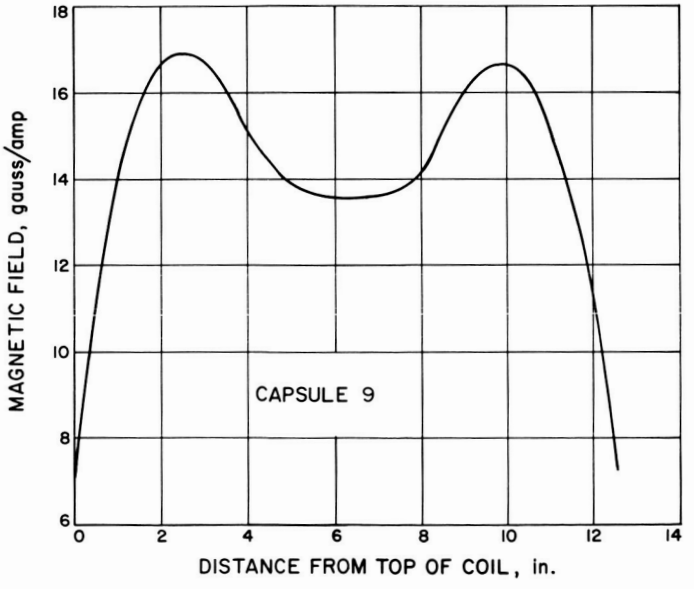

Fig. 6. Axial magnetic field profile (Capsule 9)

formed by axial nickel wires. The third type was fabricated of platinum wire (Fig. 7). Transparency of this last series varied from 91 to 97%. The grids were supported from the cathode via either quartz or aluminum oxide standoff insulators. Amplification factors for the grids were between 7 and 20.

Potential capability of the various capsules was determined by applying the appropriate form of the magnetron equation and/or grid amplification equation.

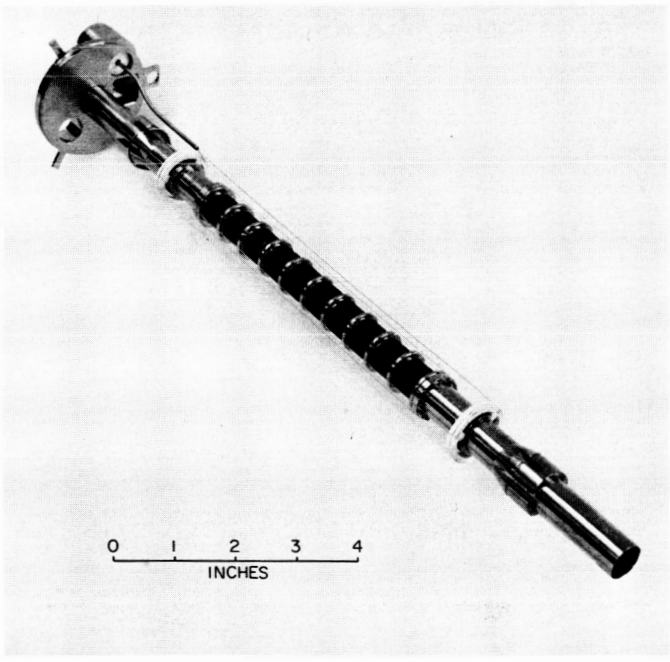

Fig. 7. Grid assembly (Capsule 9)

The magnetron equation used for determining the magnetron limitation for the capsules was (Ref. 6):

$$N = 2\pi r_a \left[\frac{(V+V_e)}{c}\right]\left[\frac{2m_oc^2}{e(V+V_e)} + 1\right]^{1/2} - 2\pi r_c \frac{(V_e)}{c}\left[\frac{2m_oc^2}{V_e e} + 1\right]^{1/2}$$

where

V = potential between cathode and anode

V_e = potential corresponding to initial electron kinetic energy

m_oc^2 = rest mass energy of an electron

c = velocity of light

r_a = radius of the anode

r_c = radius of the cathode

N = total number of Maxwells in the area between the cathode and anode (for uniform radical field, $N = B\pi\,(r_a^2 - r_c^2)$ where B = field in gauss in the centimeter-gram-second system)

Results of the various capsule experiments indicated that at complete turn-around $V_e e$ corresponded to 2300 ev.

Amplification factors for the various grids were determined from (Ref. 7):

$$\mu = \frac{2\pi n r_g \ln \frac{r_a}{r_g}}{\ln \coth 2\pi nR}$$

where

μ = amplification factors = $-E_a/E_g$

E_a = anode potential and E_g = grid potential at limiting turn-around conditions

r_g = radius of the grid

$1/n$ = grid wire spacing

r_a = radius of the anode

R = radius of the grid wires

Although the grids used in most of the gridded capsules were spiral, the equation for the amplification factor applies even though it was derived for a grid composed of wires parallel to anode and cathode. Because of the dimensions of the anode, cathode, and grid combination, the planar form of the amplification factor also gives a good approximation:

$$\mu = \frac{2\pi n(r_a - r_g)}{\ln \coth 2\pi nR}$$

The E_g used to determine the possible anode potential capability was the grid voltage minus the voltage required for complete electron turn-around under short-circuit conditions.

The ion pumps used on the capsules were Ultek Model 110, with a l-liter/sec pumping speed. Each aluminum capsule contained one pump, and the stainless steel capsules had three.

A burnup sample, located within a tube in the cooling passage of the cathode of each capsule, was a thin layer of UO_2 plated on a nickel foil. The length of the burnup sample corresponded to that of the plated region of the cathode. Capsule design characteristics are listed in Table 1.

Table 1. Capsule design characteristics

Capsule	Capsule assembly	Cathode	Anode	Grid	Field coil	Irradiated
1	Capsule of type shown in Fig. 1. Assembly of parts by soft soldering. Aluminum parts zincated, covered with copper strike, and tin plated in region of solder seal. Basic structural material (not cathode) was 0.025-in.-thick aluminum. Leads from capsule were RG 58/U coaxial cable. Field coil lead was plastic covered copper wire. Ion pump and terminals not sealed in terminal housing.	Fabricated of nickel by electroforming. Section was between 0.010 and 0.015 in. thick. Normal diameter was 0.50 in.; distance between starting points was 3.0 in. Expanded regions were 1.03-in. diameter. Attached to end caps of cell can by soft soldering. Uranium dioxide plated directly to nickel in region between expanded sections to serve as fragment collimators; 0.172 g of depleted (0.22% U-235) uranium dioxide plated on 30.4-cm^2 fueled area. 0.030 to 0.035-mg/cm^{-2} copper overlay plated on fueled region.	Fabricated of nickel by electroforming. Section between 0.0012 and 0.0015 in. thick. Nominal diameter of 1.50 in.; minimum diameter at ends was 1.1 in. Overall length was 6.10 in. Shape and positioning as shown in Fig. 1. Supported from outer cell envelope by quartz standoffs.	No grid.	Anodized aluminum wire windings with mixture of powdered alumina and sodium silicate for insulation. Magnetic flux at axial centerline of fuel element was 4.0 gauss/amp. Maximum magnetic flux near ends of anode was 8.8 gauss/amp. Maximum available field coil current was 30 amp. (Typical magnetic field profiles are shown in Figs. 5 and 6.)	NTR

Table 1. Capsule design characteristics (Continued)

Capsule	Capsule assembly	Cathode	Anode	Grid	Field coil	Irradiated
2	Capsule of type shown in Fig. 1. All aluminum seals by argon-arc welding. Feedthrough insulator and electroformed copper "Y" section attached by soft soldering. Tin plated in region of solder seal. Leads for first 2-ft section from capsule terminals of quartz-insulated platinum wire RG 58/U coaxial cable used from quartz-platinum leads to end terminal box. Leads between capsule and terminal box were inside flexible aluminum tubing which could be pressurized. (Assembled capsule is shown in Fig. 2.)	Fabricated of aluminum by hydroforming. Section between 0.020 and 0.025 in. thick. Nominal diameter was 0.50 in. Attached to end caps of cell can by argon-arc welding. Aluminum was zincated, copper plated, then zinc plated in fueled region before uranium plating. 0.109 g fully enriched (93.15% U-235) uranium dioxide plated on 30.4-cm^2 filled area. Copper overlay comparable to Capsule 1 used.	Fabricated of nickel by electroforming. Section between 0.0012 and 0.0015 in. thick. Nominal diameter of 1.50 in.; minimum diameter at ends, 1.10 in. Overall length of 6.10 in. Shape and positioning as shown in Fig. 1. Supported from outer cell envelope by quartz standoffs.	No grid.	Anodized aluminum wire windings with mixture of powdered alumina and sodium silicate for insulation. Magnetic flux at axial centerline of fuel element was 4.0 gauss/amp. Maximum magnetic flux near ends was 8.8 gauss/amp. Maximum available field coil current of 30 amp. (Typical magnetic field profiles are shown in Figs. 5 and 6.)	NTR
3	Capsule of type shown in Fig. 1. All aluminum seals by argon-arc welding. Feedthrough insulator and electroformed copper "Y" section attached by soft soldering. Tin plated in region of solder seal. Leads for first 2-ft section from capsule terminals of quartz-insulated platinum wire RG 58/U coaxial cable used from quartz-platinum leads to end terminal box. Field coil lead was quartz-insulated copper for first 2-ft section from coil and plastic-insulated copper to terminal box. Leads between capsule and terminal box were inside flexible aluminum tubing which could be pressurized.	Fabricated of aluminum by hydroforming. Nominal diameter of 0.50 in. Attached to end caps of cell can by argon-arc welding. Aluminum was zincated, copper plated, then zinc plated in fueled region prior to uranium plating. Total of 0.155 g fully enriched uranium dioxide plated on 30.4-cm^2 fueled area. Copper overlay comparable to Capsule 1 used.	Fabricated of nickel by electroforming. Section between 0.0012 and 0.0015 in. thick. Nominal diameter of 1.50 in.; minimum diameter at ends, 1.10 in. Overall length of 6.10 in. Shape and positioning as shown in Fig. 1. Supported from outer cell envelope by quartz standoffs.	No grid.	Anodized aluminum wire windings with mixture of powdered alumina and sodium silicate for insulation. Magnetic flux at axial centerline of fuel element was 4.0 gauss/amp. Maximum magnetic flux near ends of anode was 8.8 gauss/amp. Maximum available field current was 30 amp. (Typical magnetic field profiles are shown in Figs. 5 and 6.)	GETR

Table 1. Capsule design characteristics (Continued)

Capsule	Capsule assembly	Cathode	Anode	Grid	Field coil	Irradiated
4	Capsule of type shown in Fig. 1. All aluminum seals by argon-arc welding. Feedthrough insulator and electroformed copper "Y" section attached by soft soldering. Tin plated in region of solder seal. Leads for first 2-ft section from capsule terminals of quartz-insulated platinum wire. RG 58/U coaxial cable used from quartz-platinum leads to end terminal box. Field coil lead of quartz-insulated copper for first 2-ft section from coil, and plastic-insulated copper to terminal box. Leads between capsule and terminal box were inside flexible aluminum tubing which could be pressurized. (See Fig. 2.)	Fabricated of aluminum by hydroforming. Section between 0.020 and 0.025 in. thick. Nominal diameter of 0.50 in. Attached to end caps of cell can by argon-arc welding. Aluminum was zincated, copper plated, then zinc plated in fuel region prior to uranium plating. Total of 0.305 g of fully enriched uranium dioxide plated on 30.4-cm^2 fueled area. Copper overlay comparable to that of Capsule 1 used.	Fabricated of nickel by electroforming. Section between 0.0012 and 0.0015 in. thick. Nominal diameter of 1.50 in.; minimum diameter at ends, 1.10 in. Overall length of 6.10 in. Shape and positioning as shown in Fig. 1. Supported from outer cell envelope by quartz standoffs.	No grid.	Anodized aluminum wire windings with mixture of powdered alumina and sodium silicate for insulation. Magnetic flux at axial centerline of fuel element was 4.0 gauss/amp. Maximum magnetic flux near anode ends was 8.8 gauss/amp. Maximum available field coil current was 30 amp. (Typical magnetic field profiles are shown in Figs. 5 and 6.)	GETR
5	Same as Capsule 2 except for electrostatic grid, which necessitated additional feedthrough insulator. Aluminum in soft solder seal regions was zincated, then coated with electroless nickel (successful in obtaining vacuum-tight seals). Welding in vicinity of nickel plate did not destroy its adhesion. Solder seals could be reworked without losing plating.	Cathode type shown in Fig. 3. Fabricated of aluminum. Nominal diameter of 0.50 in.; wall thickness of 0.025 in. Two inner collimating ribs had diameter of 0.71 in.; rib width was 0.062 in. Distance of 1.00 in. between their centerlines. Fuel region was between rib sections. Aluminum was zincated, then plated with electrolysis nickel prior to uranium plating. Total of 0.071 g of fully enriched uranium dioxide plated on 18.6-cm^2 fueled area.	Same as Capsule 1 except that inner surface (facing cathode) was plated with 50- to 100-μin. layer of platinum.	Molybdenum grid formed by chemically milling square openings in 0.007-in.-thick sheet. Sheet was rolled into a cylinder 0.890 in. in diameter and spot-welded at seam as shown in Fig. 4. Optical transparency of 75%. Insulated from cathode with quartz standoffs.	Same as Capsule 1 except that magnetic flux at axial centerline of fuel element was 5.4 gauss/amp; maximum flux near anode ends was 12.5 gauss/amp. Maximum available field coil current was 35 amp.	Spent Fuel Element Facility and GETR

Table 1. Capsule design characteristics (Continued)

Capsule	Capsule assembly	Cathode	Anode	Grid	Field coil	Irradiated
6	Same as Capsule 2 except for electrostatic grid which necessitated additional feedthrough insulator. Aluminum in soft solder seal regions was zincated, then coated with electroless nickel (successful in obtaining vacuum-tight seals). Welding vicinity of nickel plate did not destroy its adhesion. Solder seals could be reworked without losing plating.	Cathode type shown in Fig. 3. Fabricated of aluminum. Nominal diameter of 0.50 in. wall thickness of 0.025 in.; two inner colliminating ribs had diameter of 0.70 in.; rib width was 0.062 in. Distance of 1.00 in. between their centerlines. Fuel region between rib sections. Aluminum was zincated, then plated with electrolysis prior to uranium plating. Total of 0.107 g of fully enriched uranium dioxide plated on 18.6-cm^2 fueled area.	Same as Capsule 1 except that all surfaces were plated with 50- to 100-μin. layer of platinum.	Molybdenum grid formed by chemically milling square openings in 0.007-in.-thick sheet. Sheet was rolled into a cylinder 0.890 in. in diameter and spot-welded at seam as shown in Fig. 4. Optical transparency of 70%. Insulated from cathode with quartz standoffs.	Same as Capsule 1 except that magnetic flux at axial centerline of fuel element was 5.4 gauss/amp; maximum flux near anode ends was 12.5 gauss/amp. Maximum available field coil current was 35 amp.	GETR
7	Same as Capsule 5 except that interior surface of capsule cell portion was platinum, then plated with platinum black. Quartz-insulated leads extended 5-ft from capsule.	Same as Capsule 5 except that 0.03 g of fully enriched uranium dioxide was used. Aluminum was zincated, then platinum plated prior to uranium plating.	Same as Capsule 5 except that layer of platinum was plated over platinum surfaces.	Fabricated by suspending 0.010-in.-diameter axial nickel wires between two end rings. Diameter was 0.890 in. Optical transparency of 89%. Insulated from cathode with quartz standoffs.	Copper wire windings used. Insulation same as in Capsule 1. Magnetic flux profile same as for Capsule 5. Maximum available field coil current was 50 amp.	Spent Fuel Element Facility and GETR
8	Same as Capsule 5. Capsule encased in aluminum jacket through which cooling water was passed. Cooling was required for sustained field coil operation in NTR. Provisions made on external terminal box for purging anode lead tube with various gases.	Same as Capsule 5 except that 0.195 g of fully enriched uranium dioxide was used. Aluminum was zincated, then platinum plated prior to uranium plating.	Same as Capsule 6 except that layer of platinum was plated over platinum surfaces.	Fabricated from 0.010-in.-diameter platinum wire. Grid assembly was spiral wire suspended by three axial wires (Fig. 8). Grid supported from cathode with alumina standoffs. Optical transparency of 91%.	Copper wire windings used. Insulation same as in Capsule 1. Magnetic flux profile same as Capsule 5. Maximum available field coil current was 50 amp.	NTR

Table 1. Capsule design characteristics (Continued)

Capsule	Capsule assembly	Cathode	Anode	Grid	Field coil	Irradiated
9	Capsule of basic type shown in Fig. 9. Fabricated of stainless steel (347). Basic thickness of structural material was 0.016 in. All seals made by argon-arc welding. Anode and grid leads vacuum insulated for 3-ft above cell. Each lead, as well as cell, had ion pump connected to it; by means of interconnecting passages, all volumes were pumped by three ion pumps. Interior surfaces of cell plated with platinum black.	Type shown in Fig. 10. Machined from stainless steel (347). Nominal diameter of 0.50 in.; wall thickness of 0.016 in. Collimating ribs were 0.062 in. wide and varied in OD from 0.59 in. for center one to 0.68 in. for outer ones. Distance between rib centerlines was 0.5 in. Total of 0.183 g of fully enriched uranium was plated directly to stainless steel in region between ribs. Total fueled area was 36 cm^2.	Same as Capsule 7 except that nominal diameter was 1.40 in.; length was 9.25 in. Supported from cathode with aluminum standoffs (Fig. 11).	Same as Capsule 8 except that platinum wire was 0.005 in. in diameter (Fig. 10). Optical transparency was 97%.	Copper wire windings and mixture of powdered alumina and sodium silicate used for insulation. Magnetic flux at axial centerline of fuel element was 13.5 gauss/amp; maximum flux near anode ends was 16.8 gauss/amp. Maximum available field coil current was 50 amp.	Spent Fuel Element Facility and GETR
10	Capsule of basic type shown in Fig. 9. Fabricated of stainless steel (347). Basic thickness of structural material was 0.016 in. All seals made by argon-arc welding. Anode and grid leads were vacuum-insulated for 3 ft above cell. Each lead, as well as cell proper, had ion pump connected to it; by means of interconnecting passages, all volumes were pumped by three ion pumps. Interior surfaces of cell plated with platinum black.	Type shown in Fig. 10. Machined from stainless steel (347). Nominal diameter was 0.50 in.; wall thickness was 0.016 in. Collimating ribs were 0.062 in. wide and varied in OD from 0.59 in. for center one to 0.68 for outer ones. Distance between rib centerlines was 0.5 in. Total of 0.370 g of fully enriched uranium dioxide was plated directly to stainless steel in region between ribs. Total fueled area was 36 cm^2. Spiral grid of 0.005-in.-diameter platinum wire at pitch of eight turns/in. was suspended over collimating ribs to produce zero potential region near cathode surface.	Same as Capsule 7 except that nominal diameter was 1.40 in.; length was 9.25 in. Supported from cathode with alumina standoffs (Fig. 11).	Same as Capsule 8 except that spiral platinum wire was 0.005 in. in diameter (Fig. 7). Optical transparency was 97%.	Copper wire windings and mixture of powdered alumina and sodium silicate used for insulation. Magnetic flux at axial centerline of fuel element was 13.5 gauss/amp; maximum flux near anode ends was 16.8 gauss/amp. Maximum available field coil current was 50 amp.	GETR

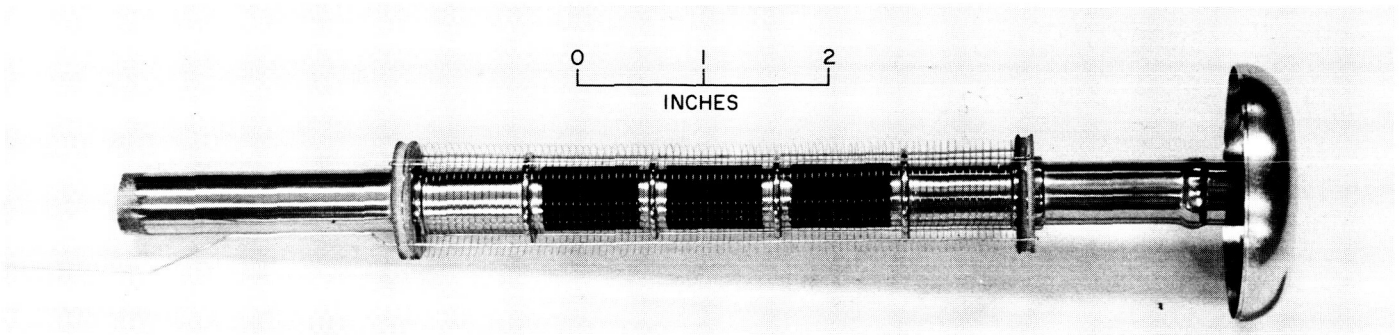

Fig. 8. Grid assembly (Capsule 8)

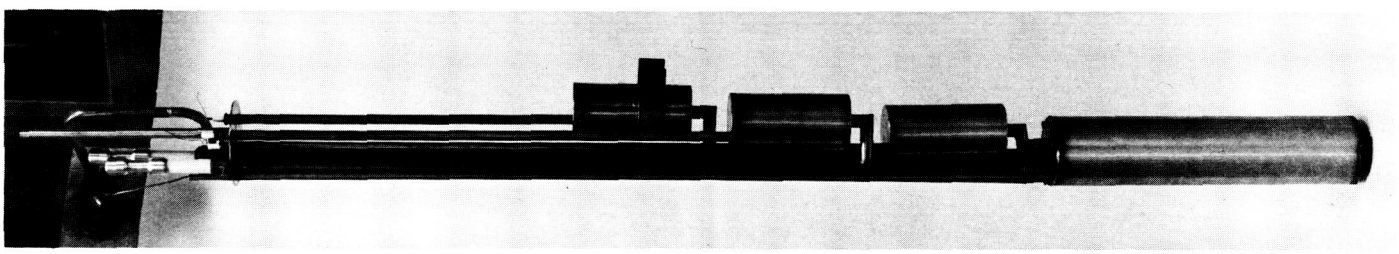

Fig. 9. Capsule (assembled)

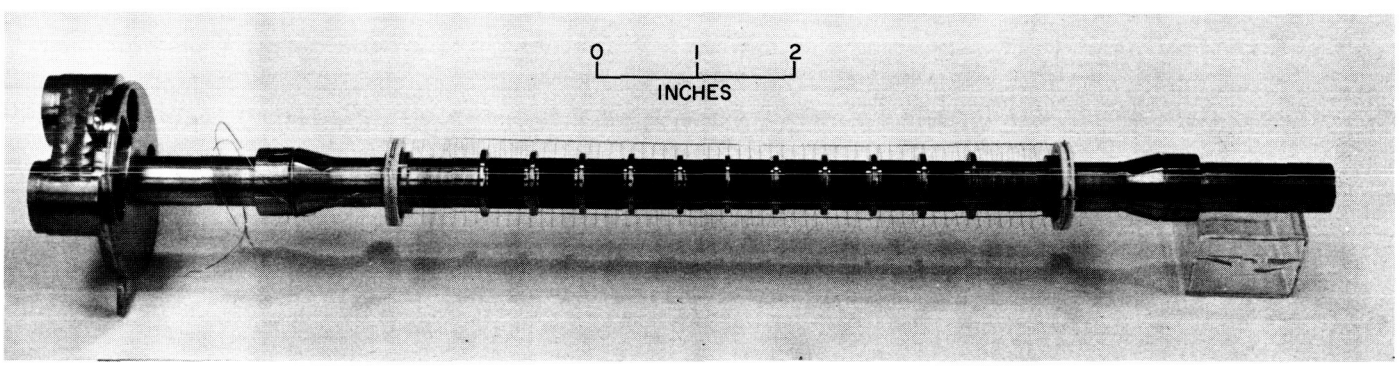

Fig. 10. Cathode and grid assembly (Capsule 9)

B. Test Facilities

The capsules were irradiated in the GETR and also in the General Electric NTR and the Spent Fuel Element Facility of the GETR for calibration purposes. In the GETR,capsules were mounted in the pool approximately 25 ft below the surface. Cycle-average unperturbed thermal neutron flux in the region occupied by the series of aluminum capsules was 3.4×10^{13} and approximately 60% of this value for the stainless steel capsules. The accompanying gamma dose rate was between 7×10^{7} and 9×10^{7} roentgens/hr.

The facility tube used at the NTR extended through the axis of the core and was open to the atmosphere. Operating power levels for the reactor were from 0.02 w to 30 kw. Unperturbed thermal neutron flux in the position used was 2.7×10^{11} at a power level of 10 kw.

The Spent Fuel Element Facility uses the irradiated elements of the GETR as a gamma source. Each fuel element used and each capsule irradiated was surrounded with cadmium to minimize the effects of photo-neutrons. Gamma dose rates of between 10^{6} and 10^{7} roentgens/hr

Fig. 11. Capsule 9 with anode in place

were available depending on the fuel element condition and the facility geometry. The capsule positions were approximately 15 ft under water.

C. *Capsule Data*

1. Irradiation Data

The basic data taken for all of the capsules on a continuous basis was the short-circuit output current from the anode. This included measurements with and without electron suppression via the magnetic field. Ion pump current was also taken at the same time to determine the operating pressure within the capsule. At periodic intervals (the beginning of the irradiation cycle, near the end of the cycle, and once or twice in between), test measurements were made on the capsule. These included:

(1) Short-circuit anode current with various magnetic field strengths.

(2) Anode current with various resistances in series with the anode and with various magnetic field strengths.

(3) Leakage current in the anode circuit with various applied potentials and magnetic fields.

In addition, with capsules that contained electrostatic grids, the following were included:

(1) Short-circuit anode current and grid leakage current with varying grid potential.

(2) Anode current with various resistances in series with the anode and with varying grid potential.

(3) Anode current with various resistances in series and with a combination of grid potential and magnetic field.

The amount of data taken depended on the condition of the capsule.

Neutron flux level varied during the irradiation cycle in the GETR. This variation was essentially proportional to the control rod position at the position occupied by the capsule.

The neutron flux level for the capsules irradiated in the NTR could be varied over six orders of magnitude. The data taken during irradiation in the NTR was the same as that taken during irradiation in the GETR with the added variations of flux level. Primary emphasis during the NTR experiments, however, was on short-circuit anode current and leakage currents with applied potential, and with varied magnetic field strength and grid potential, if a grid were present.

Calibration experiments in the Spent Fuel Element Facility consisted of measuring short-circuit anode currents and leakage currents with applied anode potentials with various magnetic field strengths and grid potentials. These data were taken at a single position in the facility which corresponded to one particular gamma dose level. Checks made at different gamma dose rates indicated that all data were proportional to the dose rate. All capsules irradiated in the Spent Fuel Element Facility contained an electrostatic grid.

2. Disassembly Procedure

Only those capsules irradiated in the GETR were subjected to a post-irradiation analysis. Because of the activity level of the capsules, their disassembly was accomplished in a hot cell facility. Gross gamma scans were made of the capsule assembly and of the various cell components. This was done to determine the location of the fragment activity within the capsules. Any gross migration of uranium could be detected by the profile of the fragment activity within the capsule. An attempt was made on the first two capsules to scan the components at discrete energy levels; however, fragment identification

by this method was not possible because of the small amount of uranium present in the capsules and the inherent background activity in a hot cell.

Photographs of the capsule assembly, subassemblies, and components were taken as well as photographs of any irregularities that appeared on the components. Observations made during the disassembly helped to explain some of the capsule behavior during the irradiation period.

3. Radiochemical Analysis

Following disassembly, the various components were dissolved and the solutions prepared for chemical analysis. The chemical analysis consisted of analyzing for the four fragments Y-91, Zr-95, Ba-140, and Ce-144, two typifying the light group and two the heavy group, and for total uranium. Both Z-95 and Ce-144 are the result of short-lived precursors, and Y-91 and Ba-140 result from long-lived precursors. Since these fragments are born as noble gases with precursors of different half-lives, any diffusion out of the component in which they are deposited would result in difference in the ratios of fragments between the various components. Differences in the ratios between the light and heavy fragments in the various components should exist because of range difference.

The uranium analysis should give the quantity of fuel material removed from the cathode during the irradiation period. Because UO_2 was the only chemical form of the fuel used, no comparison on the relative merits of various forms of fuel could be made; however, the capsules were subjected to different amounts of burnup by virtue of different irradiation cycle time and reactor fuel loading.

III. DATA

A. Calibration Data

In order to determine the background current from the various capsules, calibration tests were performed in either the NTR facility or the Spent Fuel Element Facility of the GETR. Tests run in the NTR were controlled tests in which the output current of the capsules could be determined with various neutron fluxes and ratios of gamma to neutron flux. The results were compared with those of a capsule fueled with depleted uranium. Capsules irradiated in the Spent Fuel Element Facility were exposed to a gamma flux only. The background current was composed primarily of electrons originating from Compton scattering of gamma rays; thus, the current readings of capsules exposed to gamma rays only would give a measure of the background current expected in the GETR irradiations.

For all of the capsules, background current was in the same direction as the fragment current. This meant that the anode was a source of electrons rather than a sink. The magnitude of the background current for all capsules was between 6 and 30% of the calculated fragment current. Actual value of the background current at GETR operating conditions was between 0.6 and 1.0 μamp for the various capsules. The reason for the variation among different capsules was the variation in total uranium content, material of construction and, if present, the transparency of the grid of individual capsules.

Background current was smaller for those capsules that had higher-mass anodes. The higher-mass anodes were those whose surfaces were platinum plated. This indicated that, for the range of anode mass densities used, the anode increased more rapidly as a sink than a source of electrons as the mass was increased.

The results of the calibration tests are in Figs. 12 through 19; a discussion of the tests is in Appendix B.

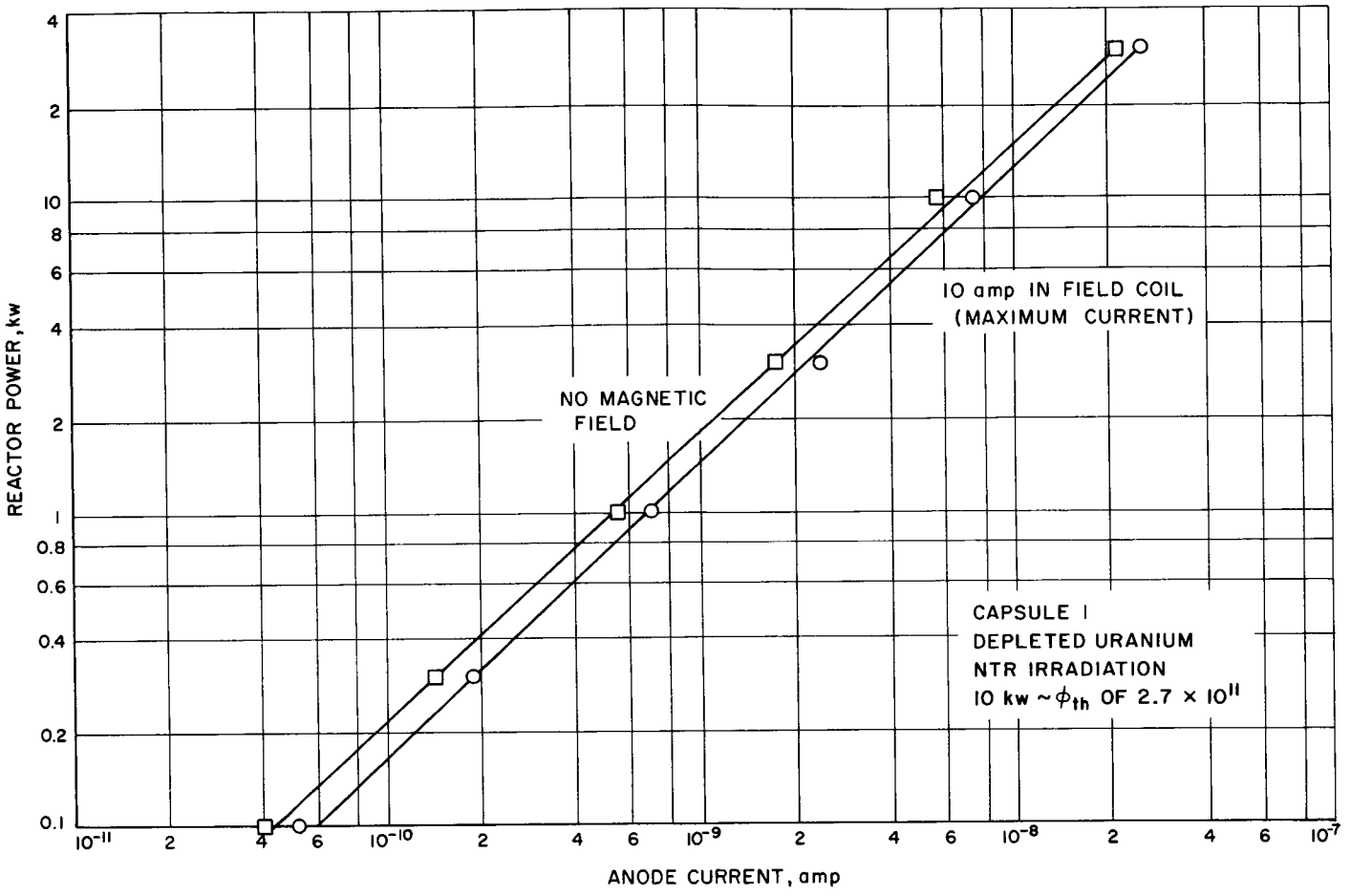

Fig. 12. Calibration data: background current

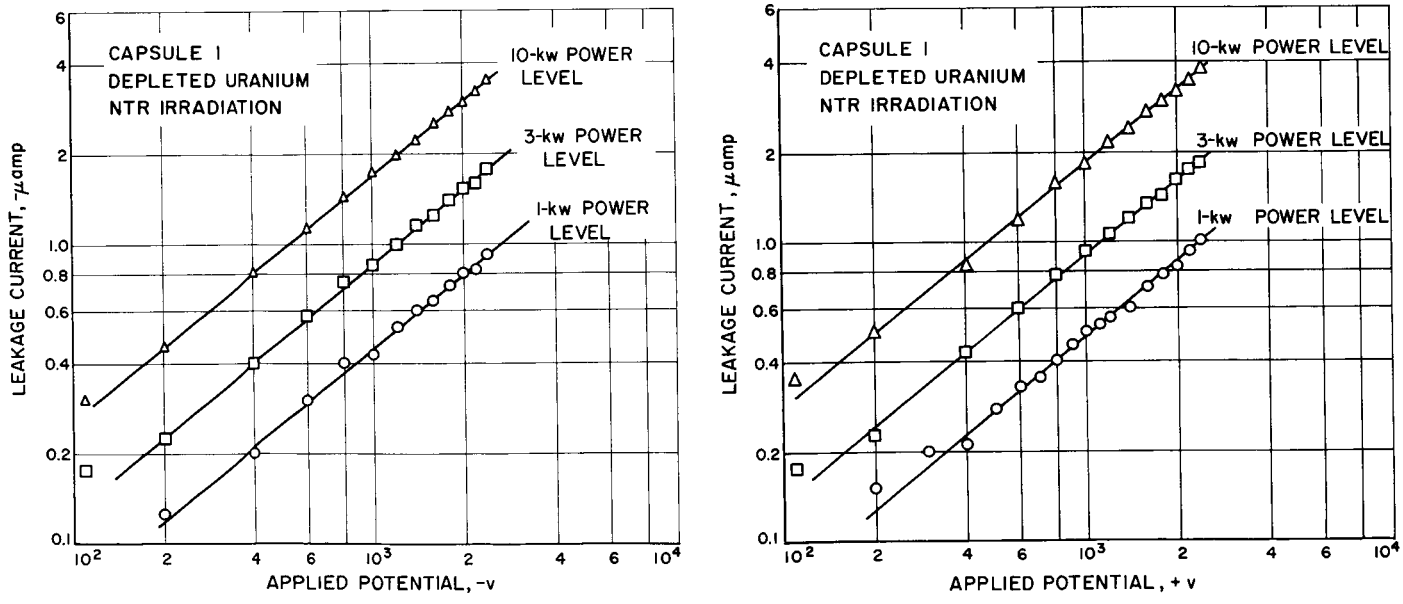

Fig. 13. Calibration leakage current: (a) negative potential and (b) positive potential

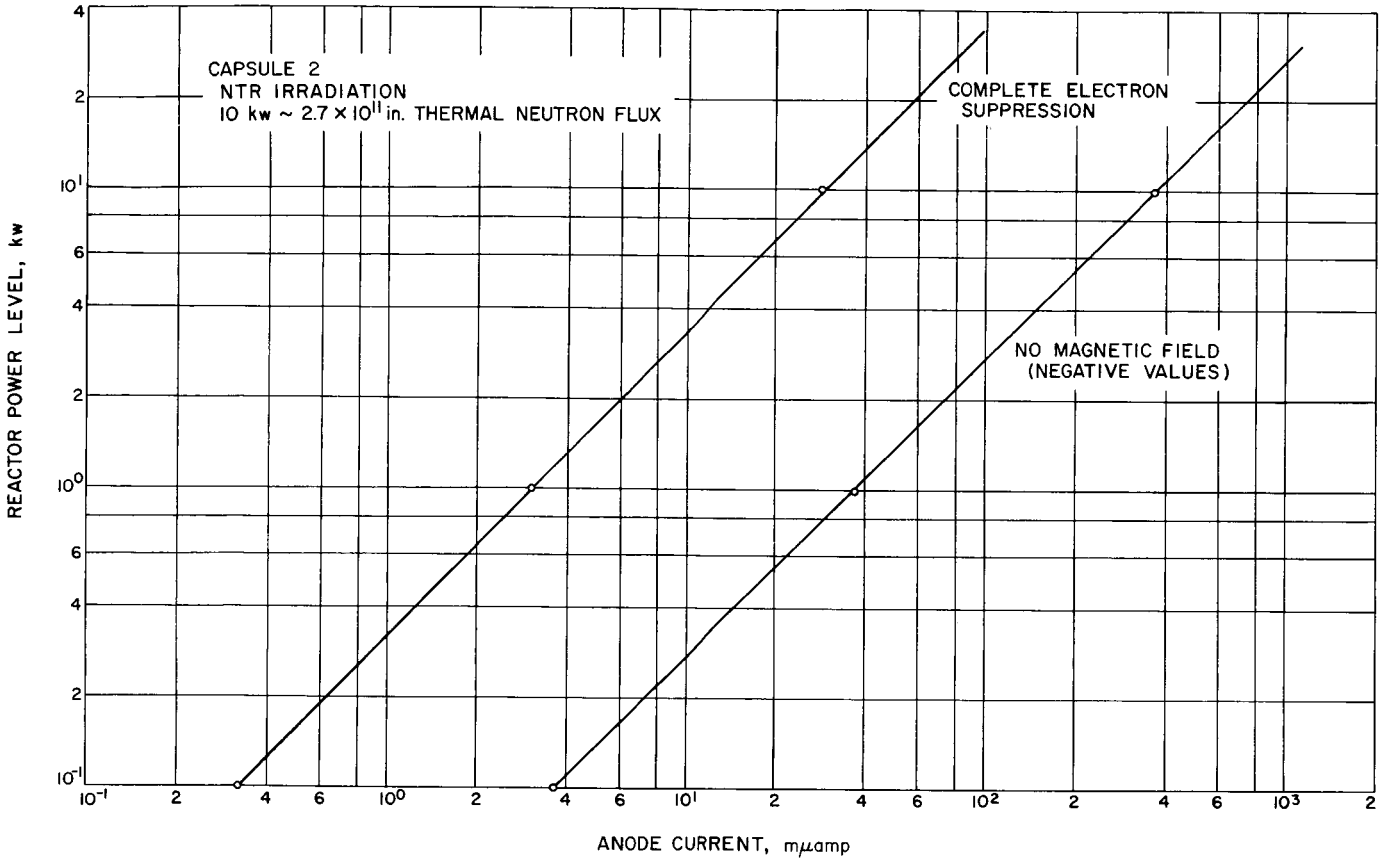

Fig. 14. Calibration data: anode current

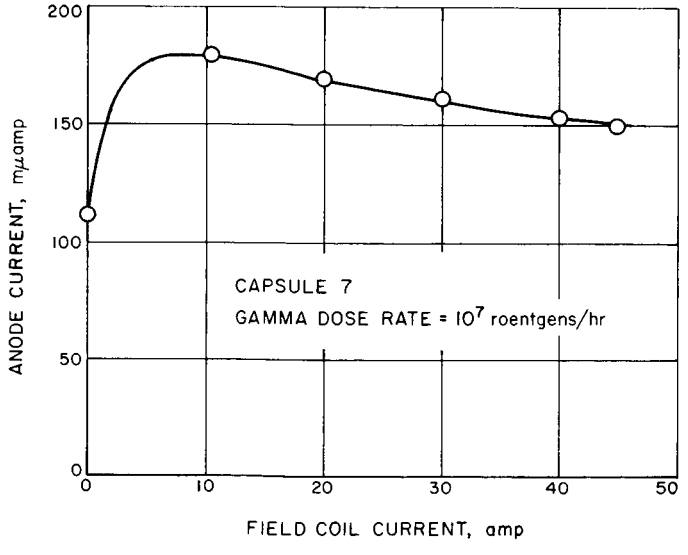

Fig. 15. Calibration data: magnetron effect

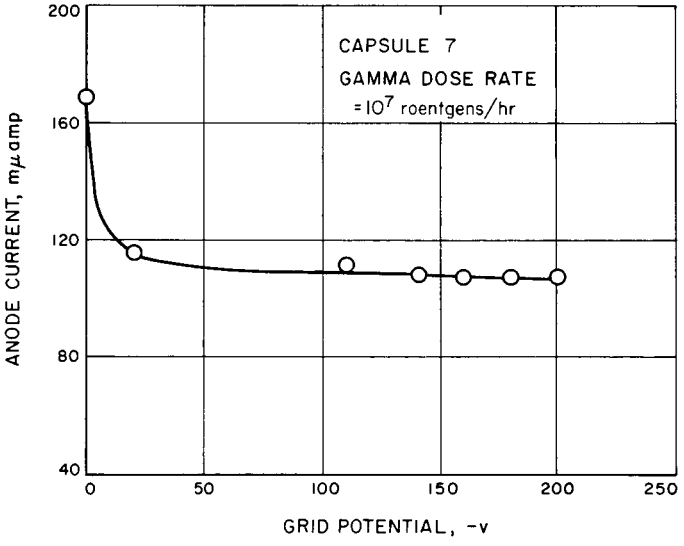

Fig. 16. Calibration data: electrostatic charge separation (aluminum capsule)

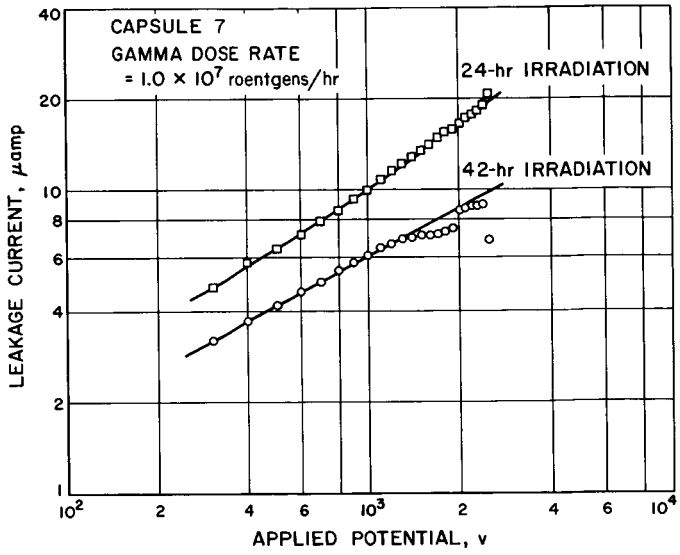

Fig. 17. Calibration data: leakage current after irradiation

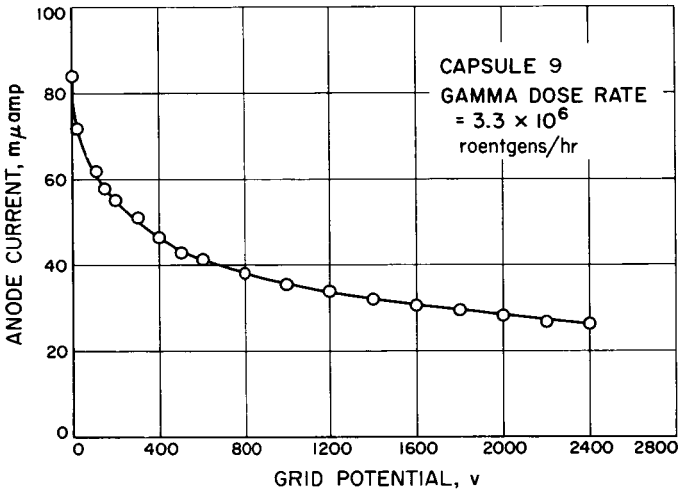

Fig. 18. Calibration data: electrostatic charge separation (stainless steel capsule)

B. Capsule Irradiation Data

The output currents from the capsules, monitored at approximately 8-hr intervals during the irradiation cycle, are presented in Figs. 20 through 28. Reactor power schedule, control rod positions, ion pump current, and other explanatory notes are also presented. Ion pump current versus pressure is shown in Fig. 29 and control rod position versus relative thermal neutron flux is shown in Fig. 30.

Malfunction of the ion pump was one of the major factors contributing to erratic currents from the capsules.

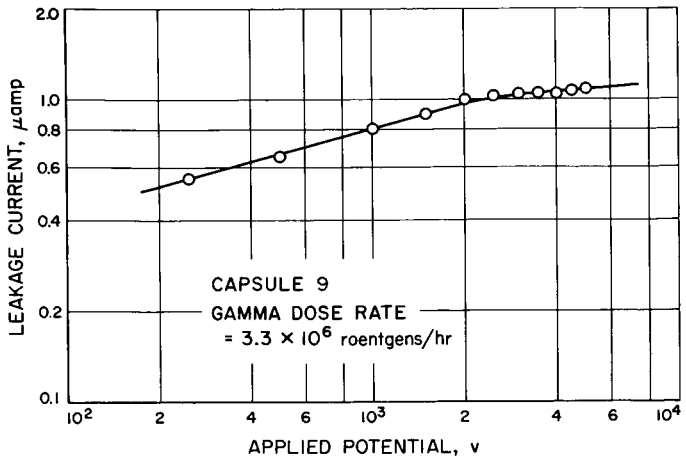

Fig. 19. Calibration data: leakage current (stainless steel capsule)

This malfunction consisted of either shorting of the pump lead or feedthrough insulators, or the failure of the pump to maintain its discharge. In either case, the pressure within the capsules rose to a level at which the fragments would make a significant number of ionizing collisions in going from the cathode to the anode. The necessity for continuous pumping was noted for Capsule 3 when the ion pump lead was severed during the irradiation cycle. During the period in which the ion pump was not operating, the output current from the capsule, with electron suppression, increased by a factor of 10 to 12. Current without suppression had the same polarity as that with suppression and approximately one-half the value. After the lead was repaired and the pump refired, the capsule recovered and output currents returned to normal.

The ion pump of Capsule 4 stopped pumping after approximately one-third of the irradiation cycle. The output currents from the capsule were very erratic and behaved similarly to those of Capsule 3. Post-irradiation examination indicated that considerable anode material had sublimed [Fig. 31(a) and (b)]. This would result in the reemission of noble gas fragments from the anode, which may have interfered with the pumping action of the ion pump.

After failure of the ion pump, the potential buildup capability of the capsule was reduced to the millivolt range. This caused the output current readings to be a function of the circuit impedance. Sublimation of the anode was also noted in both these capsules; thus, it is not known whether the voltage limitation was due to the increased gas pressure or to the coating of the insulators with anode material.

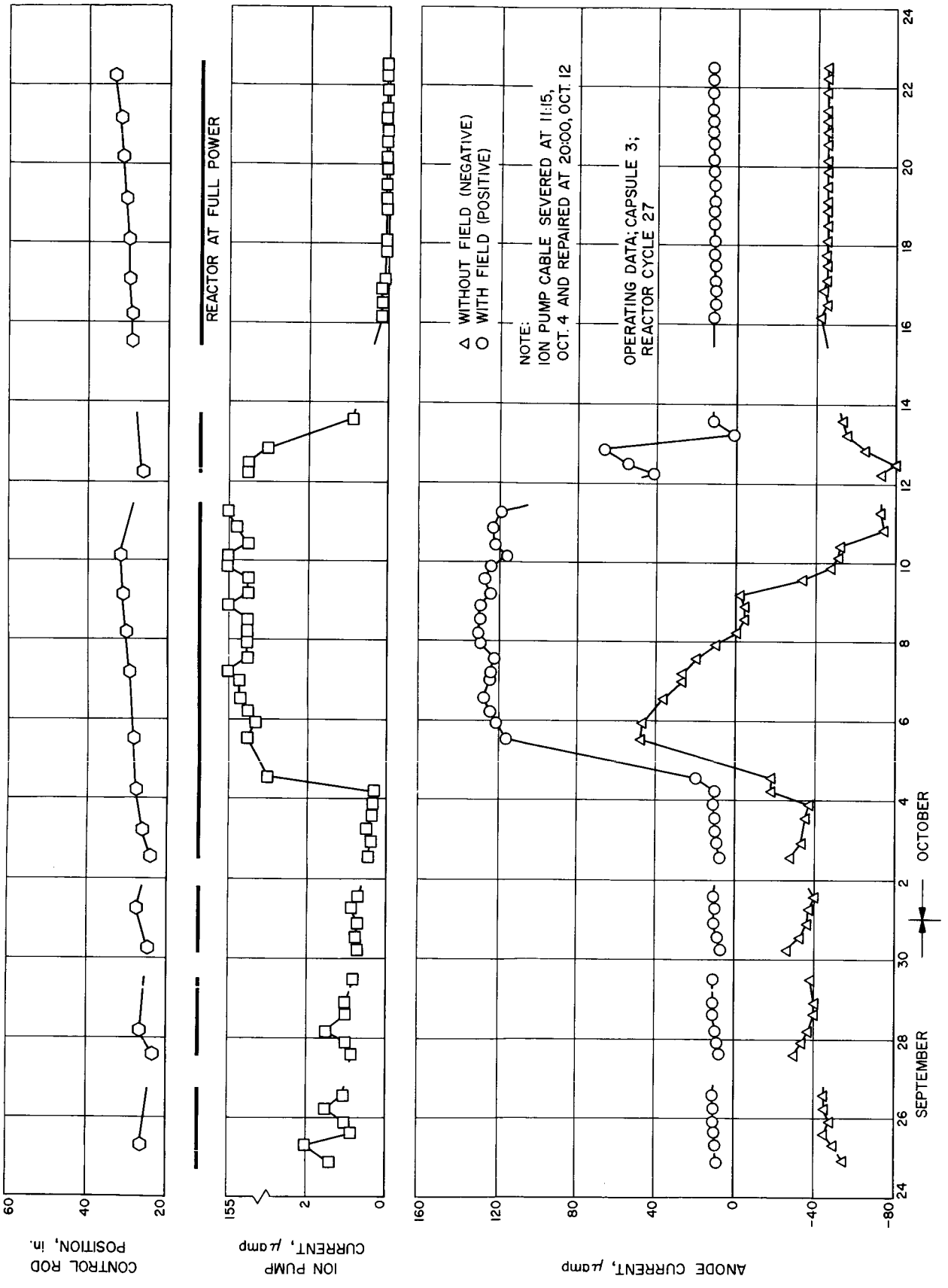

Fig. 20. Operating data (Capsule 3): Reactor Cycle 27

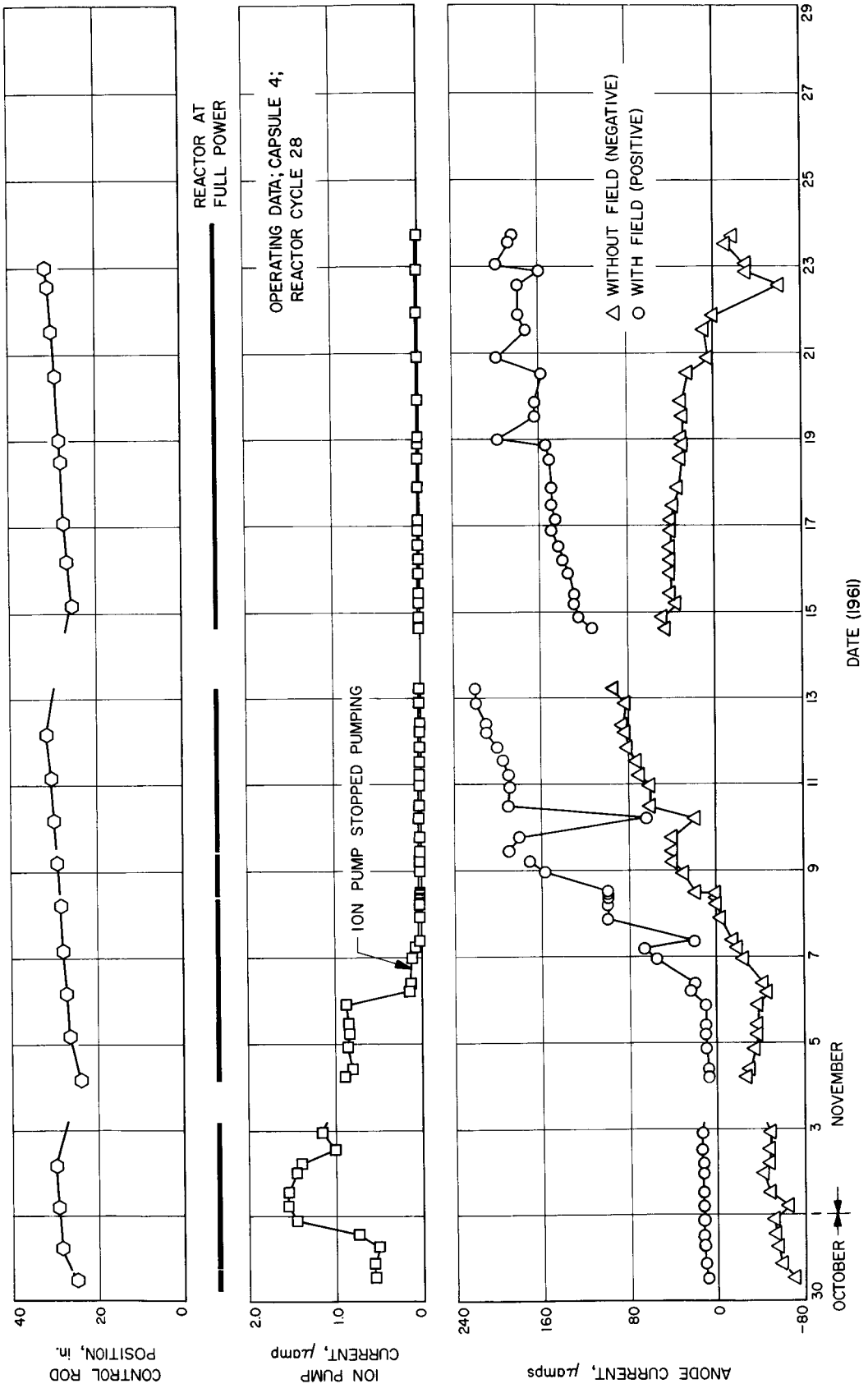

Fig. 21. Operating data (Capsule 4): Reactor Cycle 28

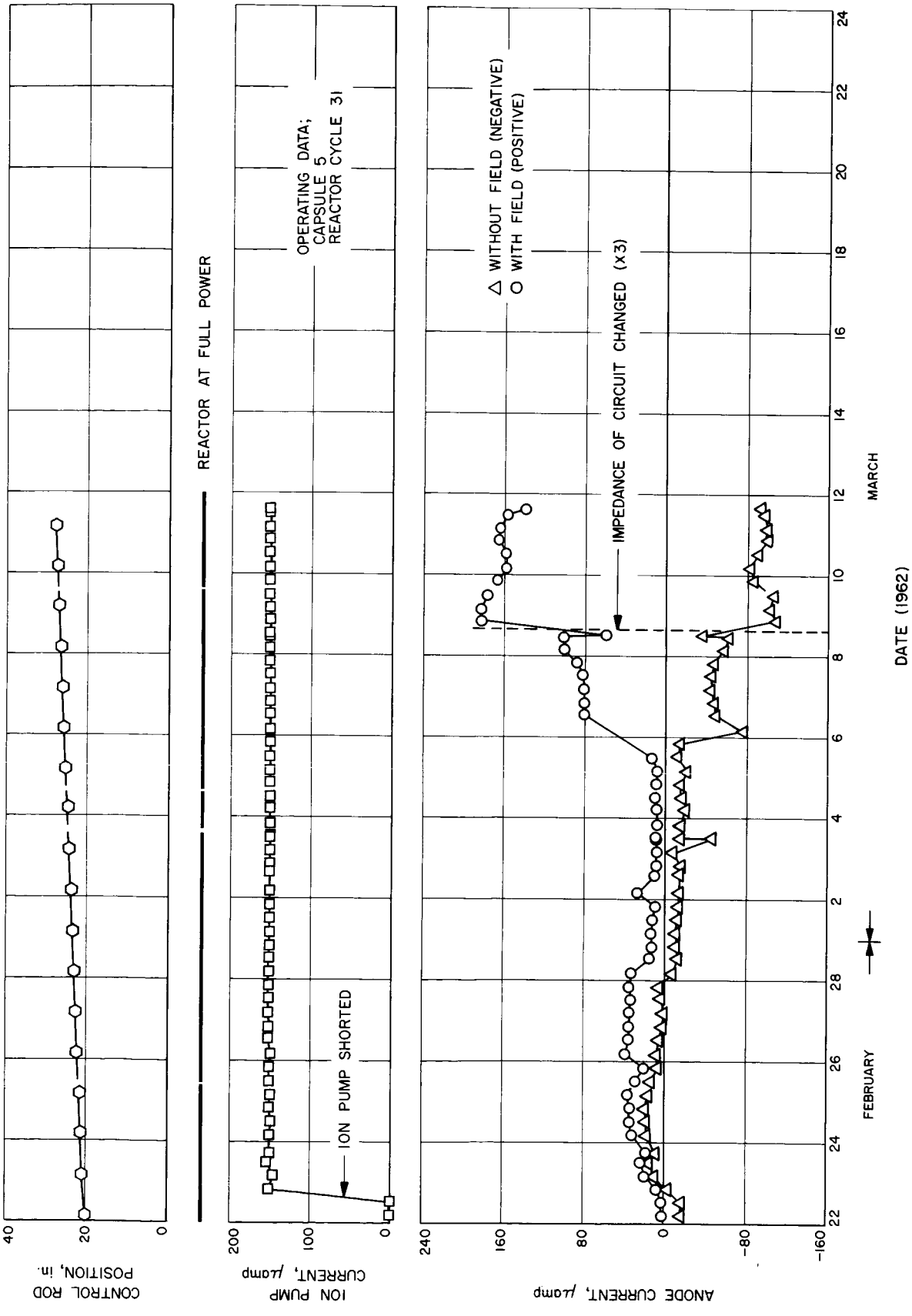

Fig. 22. Operating data (Capsule 5): Reactor Cycle 31

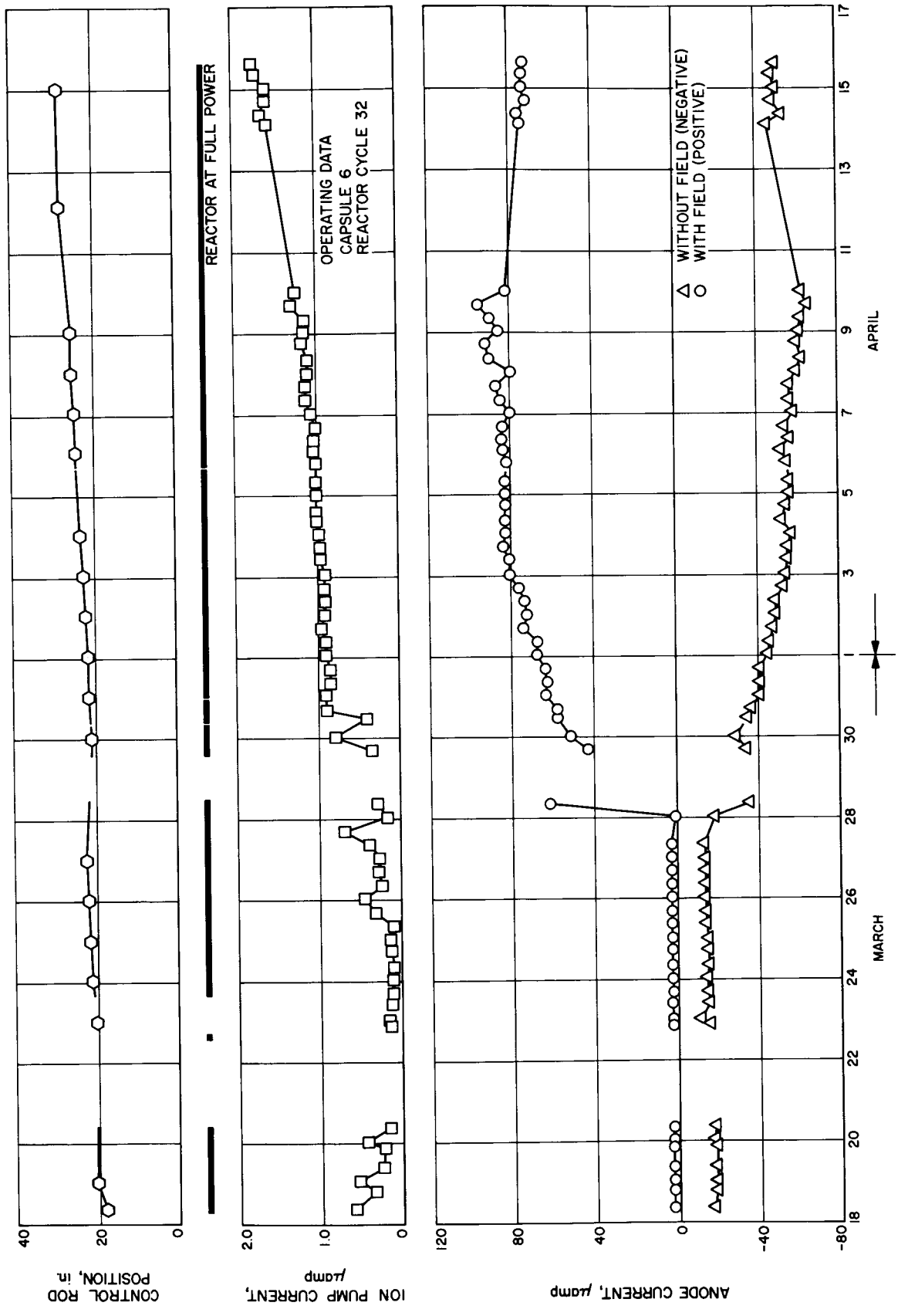

Fig. 23. Operating data (Capsule 6): Reactor Cycle 32

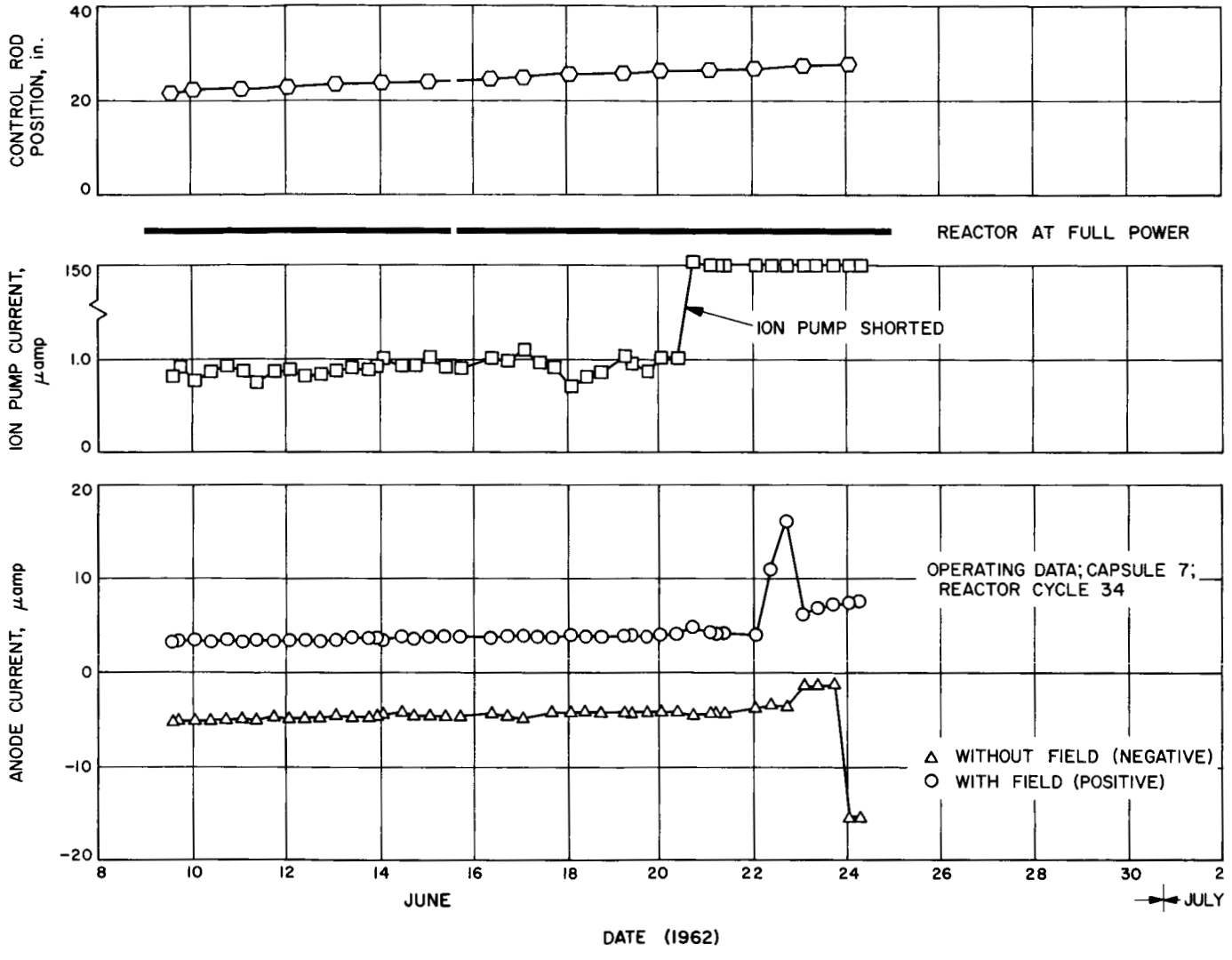

Fig. 24. Operating data (Capsule 7): Reactor Cycle 34

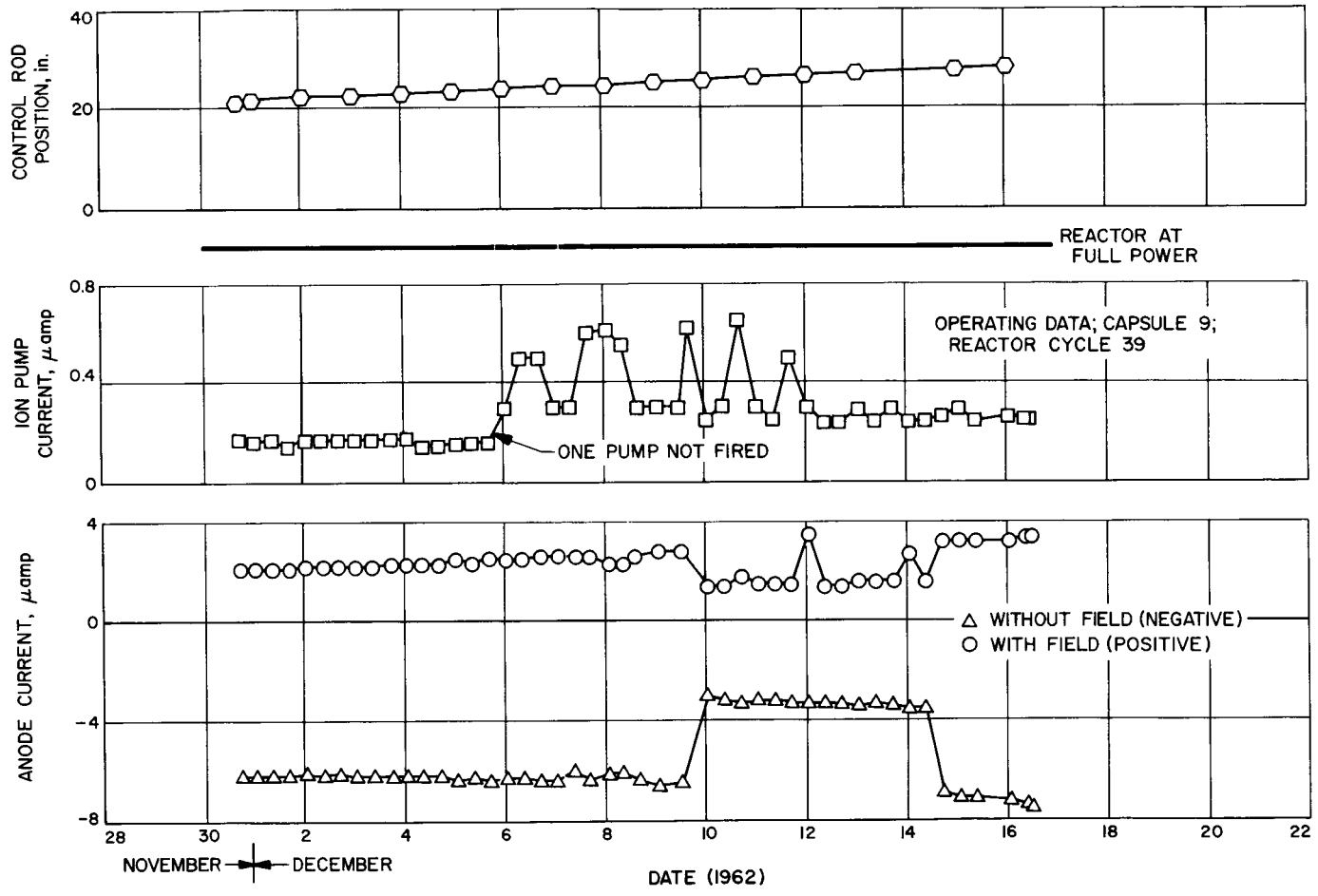

Fig. 25. Operating data (Capsule 9): Reactor Cycle 39

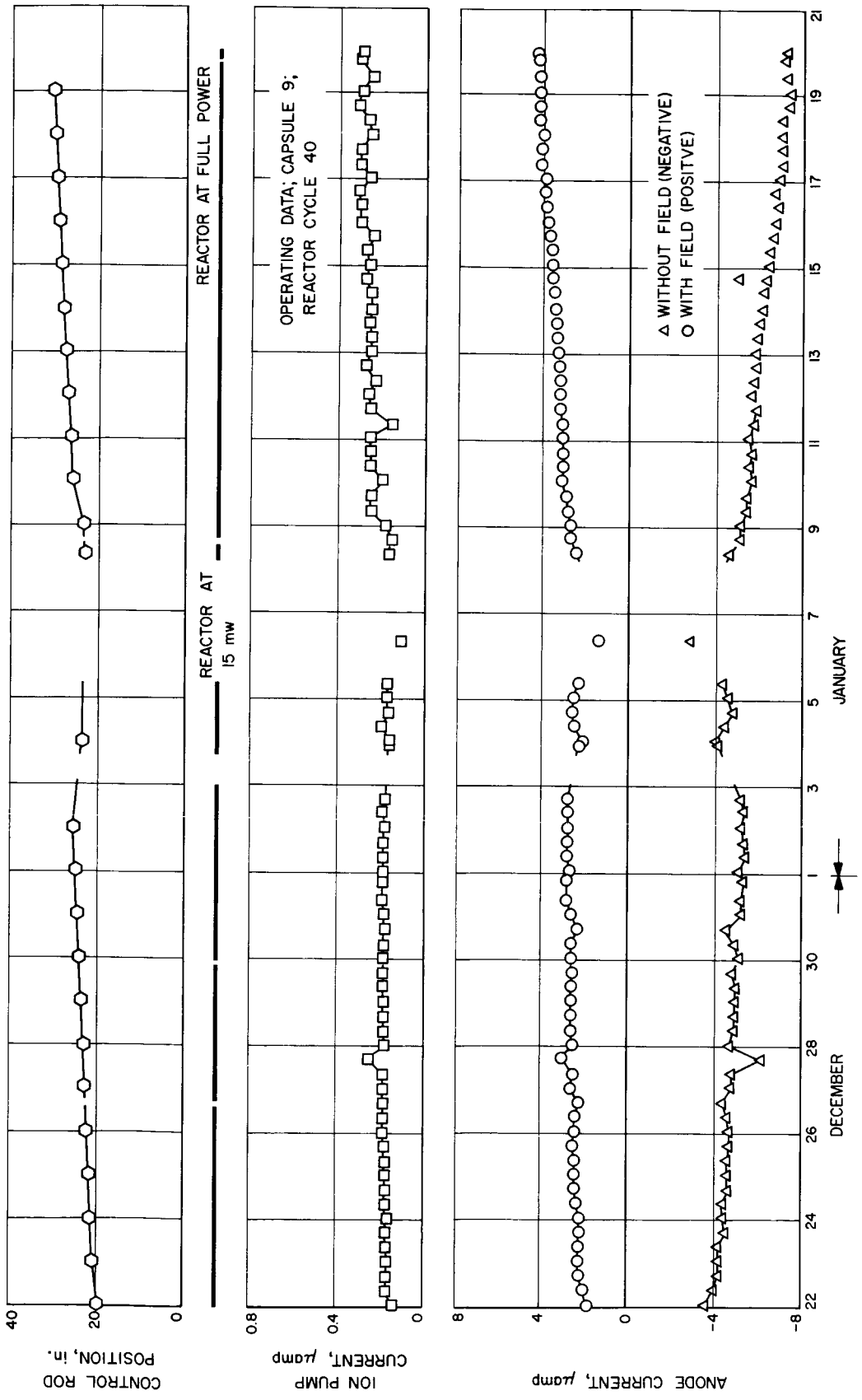

Fig. 26. Operating data (Capsule 9): Reactor Cycle 40

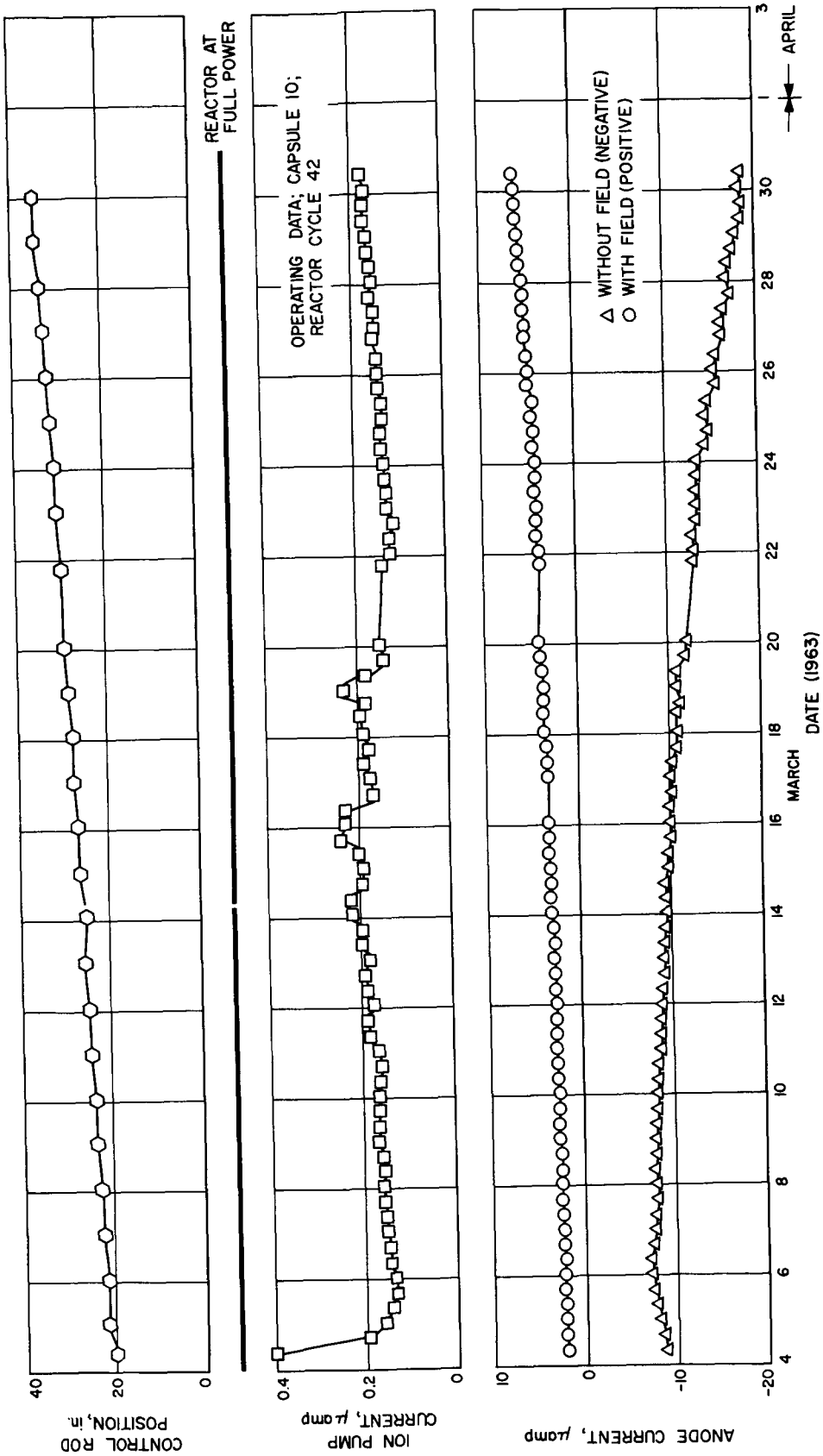

Fig. 27. Operating data (Capsule 10): Reactor Cycle 42

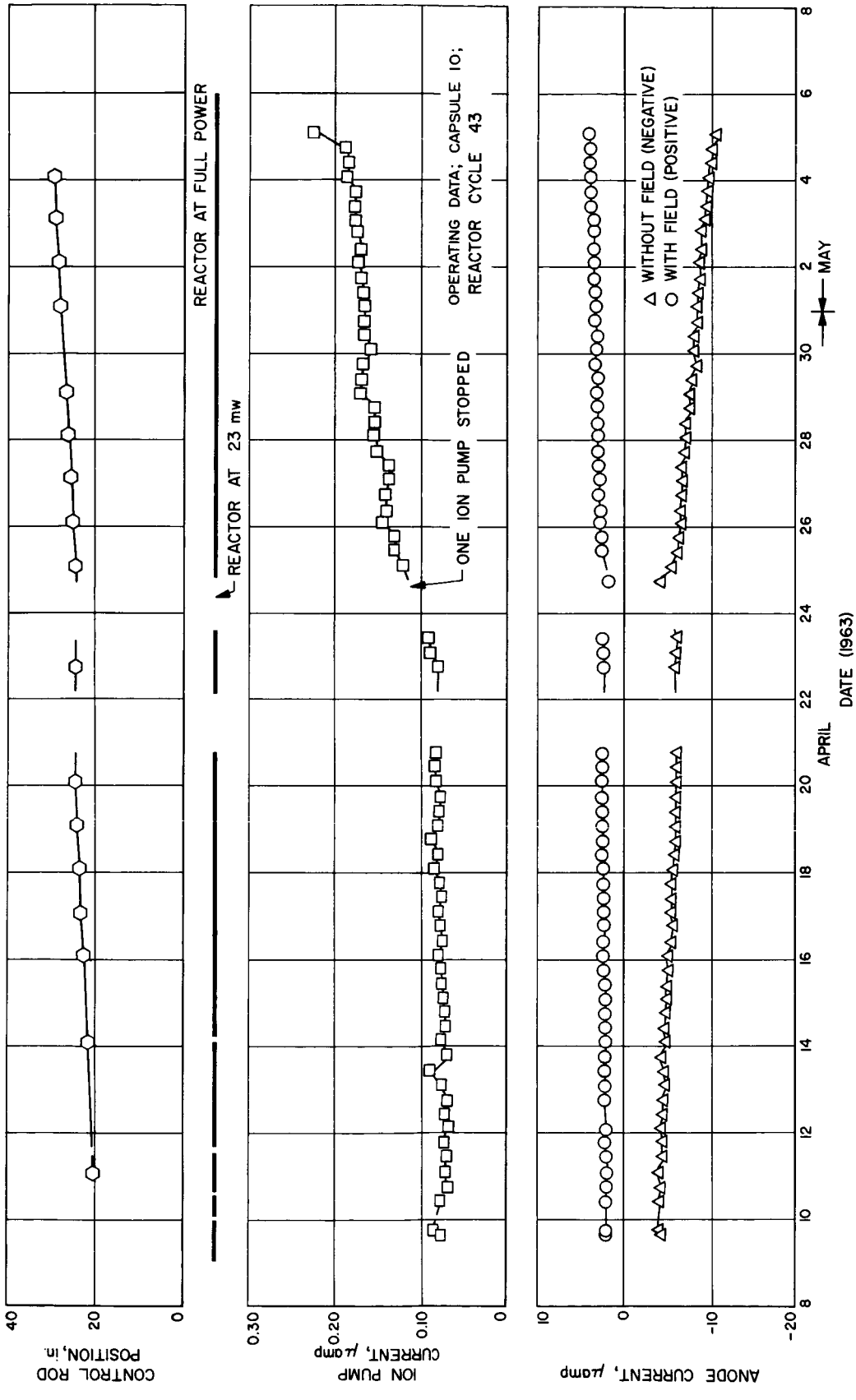

Fig. 28. Operating data (Capsule 10): Reactor Cycle 43

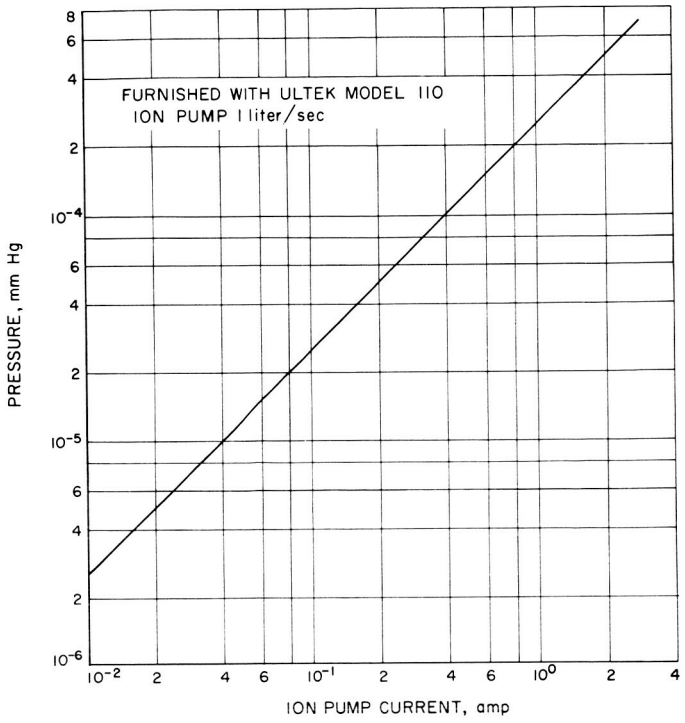

Fig. 29. Ion pump current versus pressure

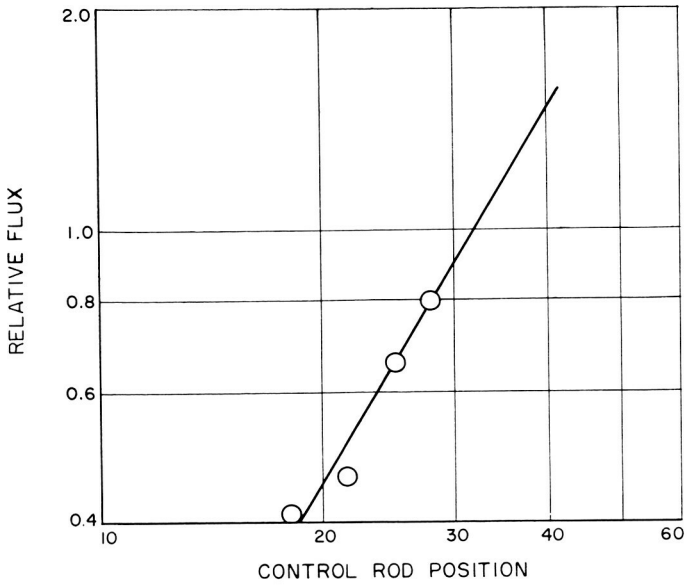

Fig. 30. Relative thermal neutron flux versus control rod position

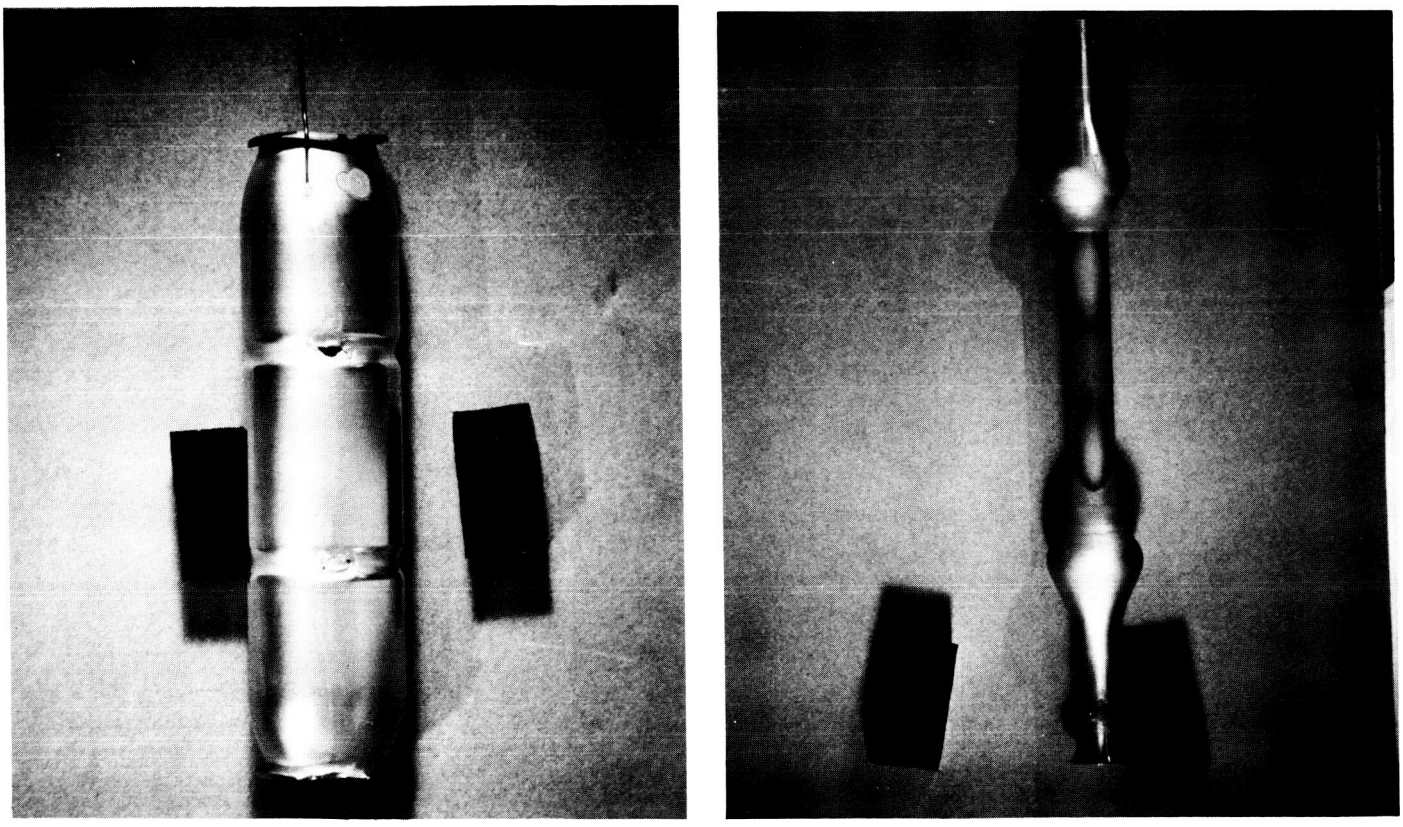

Fig. 31. After irradiation: (a) anode and (b) cathode

The buildup of noble gas fission fragments was probably the largest contributor to residual gas in the capsules and to the pumping problems. All adsorbed reactive gases would have been picked up by the pump during the early portion of the irradiation cycle. Approximately 26% of all fragments produced from fission are either Krypton or Xenon, with sufficient half-life to contribute to the residual gas in the capsules. A major portion of all of the fragments is buried in the various components to a depth from which reemission is unlikely; however, because of the overheating of components and grazing collisions, some of the long-lived noble gas fragments will accumulate in the capsule void. If all the long-lived fragments accumulated, 1% burnup of a 100-mg sample of U-235 would produce a residual pressure of 20 mm Hg in the capsules. Assuming an extrapolated average pumping speed of 0.0035 liter/sec for the Kr and Xe, the equilibrium capsule pressure would be 2×10^{-4} mm Hg for a 100-mg sample of U-235 if all noble gas atoms were reemitted. Indicated capsule pressures were lower than this for those in which the pumps functioned normally. In those cases where full power supply current was drawn by the pump, it is assumed that a short developed in the pump electrical circuit. Accumulation of noble gas in the system would cause the pump to cease firing. In these cases, the pump drew only a leakage current because of the ionizing radiation on the lead and insulator. Ion pump currents for the capsules are shown in Figs. 20 through 28.

During normal capsule operation, the ratio of current without suppression to that with suppression decreased with accumulated irradiation time. The ratio increased immediately after a mid-cycle start-up over the value just prior to the shutdown. Accumulation of uranium on the anode would give a source of δ-electrons on the anode, which cancels a portion of the δ-electrons from the cathode. Results of the radiochemical analysis, however, indicated that this effect should reach an equilibrium value and would not cause the fluctuation from the trend during mid-cycle interruptions in irradiation. Accumulation of beta decaying fission fragments and neutron activation of the anode structural material would cause a decrease in the current ratio and would be a function of the irradiation and mid-cycle cooling periods. This electron current would enhance the apparent fragment current, just as observed.

The capsule output data presented below, taken with various applied conditions, are those obtained only when capsule operation was considered normal. This data for the various capsules, with accompanying definition of conditions, is shown in Figs. 32 through 47. The key measurement made on all capsules was the output current with various magnetic field strengths. The shape of these curves varied with the total accumulated irradiation of the capsule. This was expected from the variation in the currents with and without full suppression. For those capsules with high magnetic-field capability, the current with suppression reached a maximum value and then decreased with increasing field. This is the expected effect of the magnetic field on the background current.

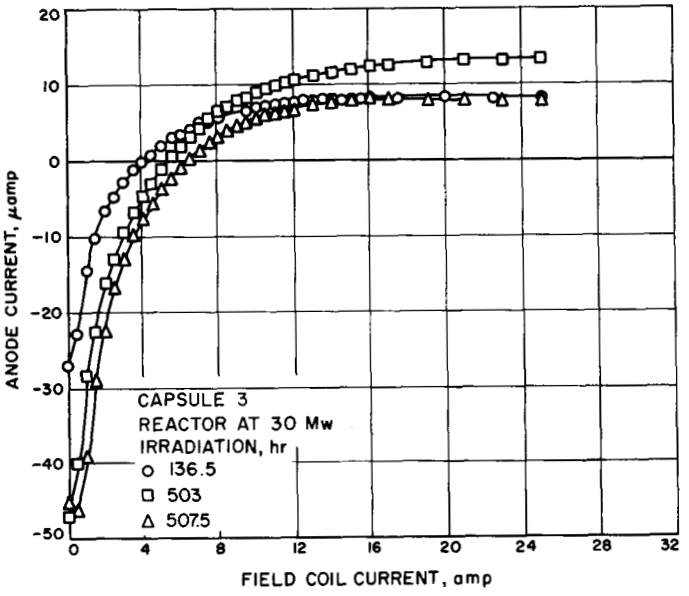

Fig. 32. Magnetron effect: anode current (Capsule 3)

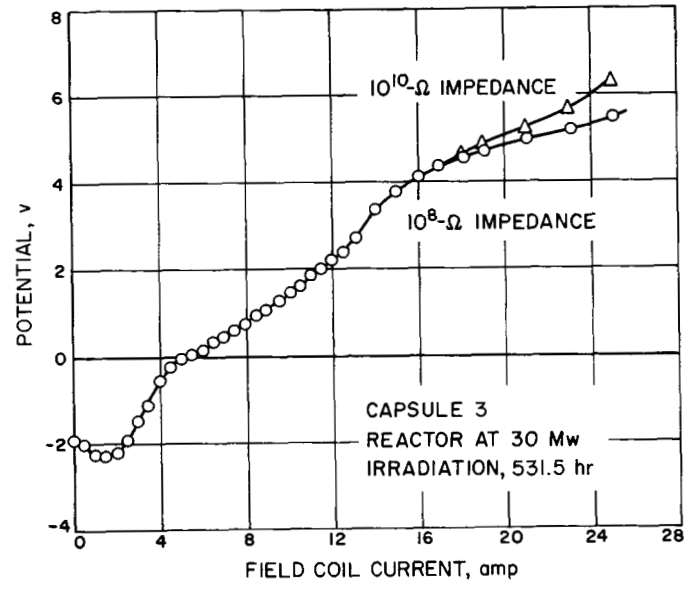

Fig. 33. Magnetron effect: potential buildup (Capsule 3)

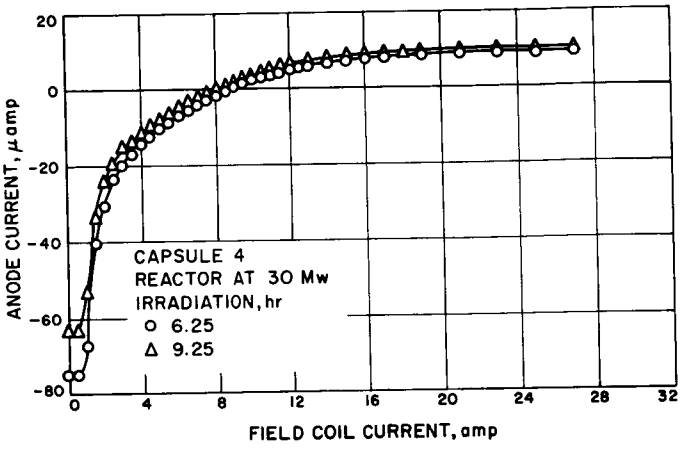

Fig. 34. Magnetron effect: anode current (Capsule 4)

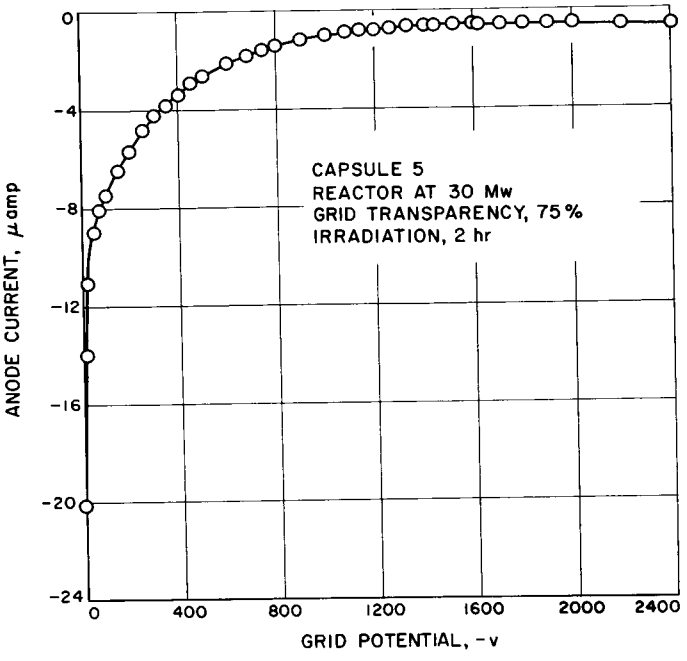

Fig. 36. Electrostatic charge separation: anode current (Capsule 5)

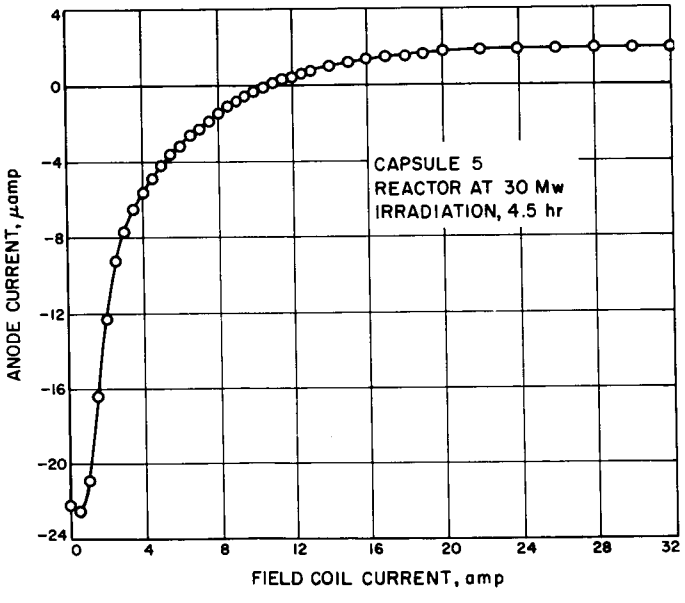

Fig. 35. Magnetron effect: anode current (Capsule 5)

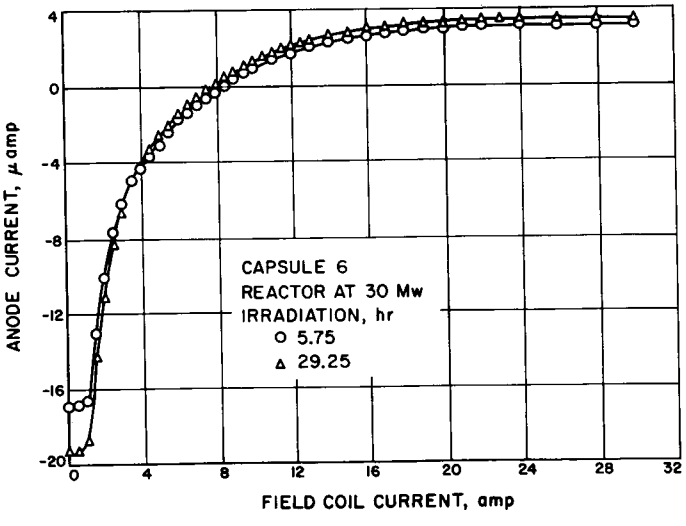

Fig. 37. Magnetron effect: anode current (Capsule 6)

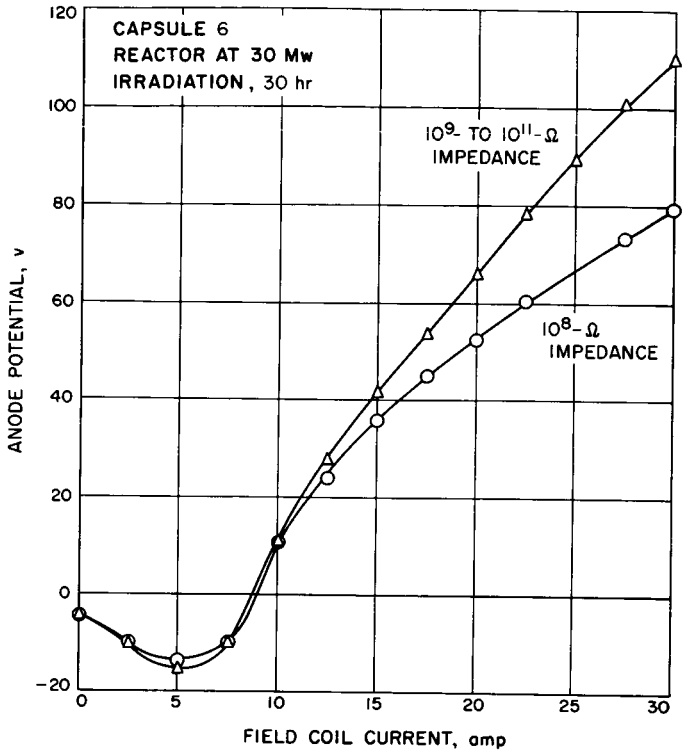

Fig. 38. Magnetron effect: potential buildup (Capsule 6)

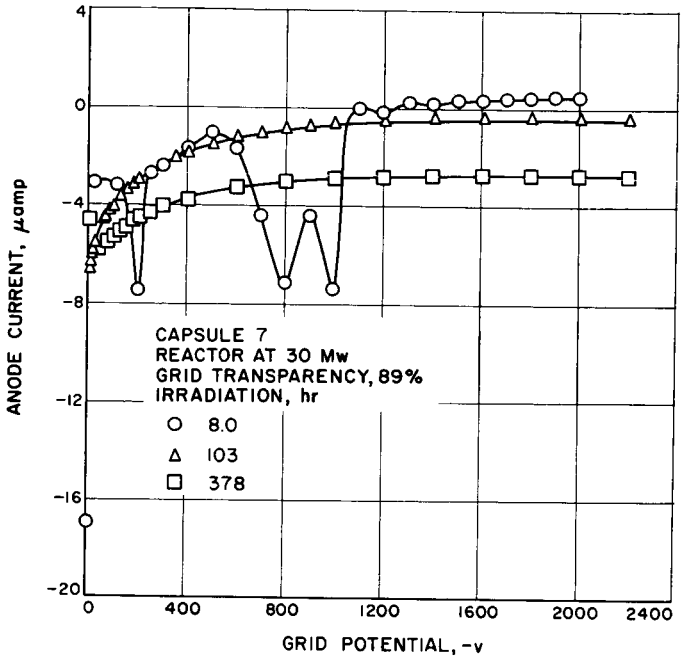

Fig. 40. Electrostatic charge separation: anode current (Capsule 7)

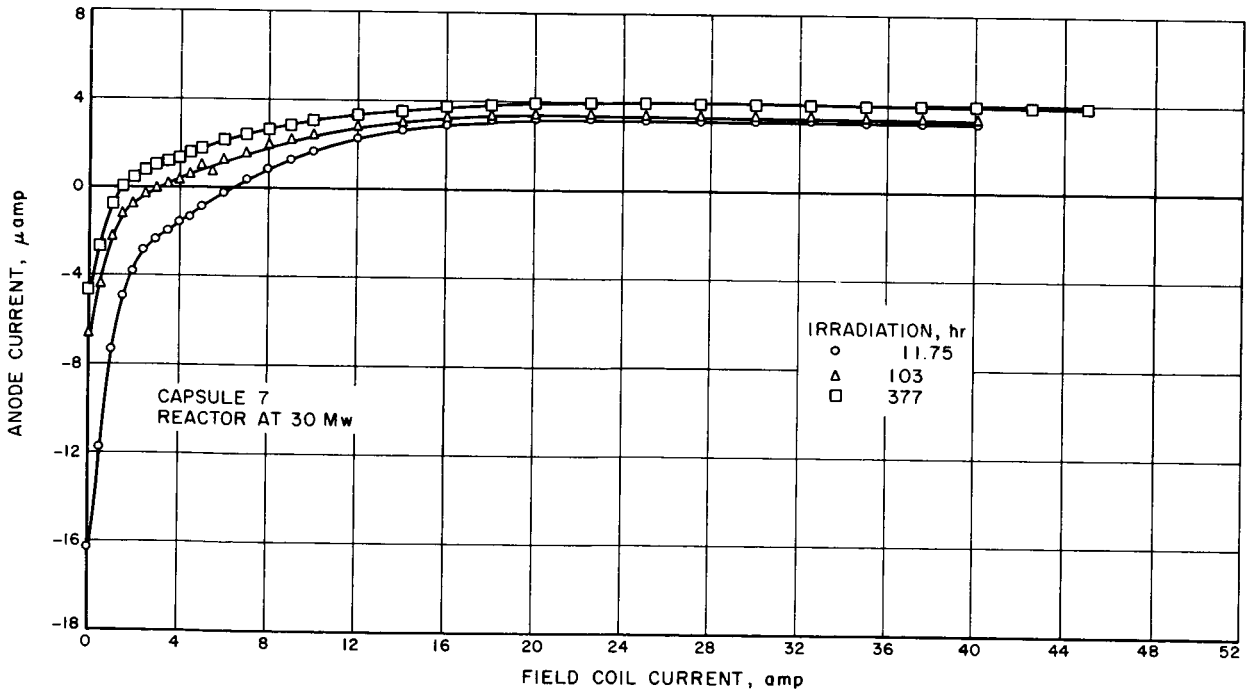

Fig. 39. Magnetron effect: anode current (Capsule 7)

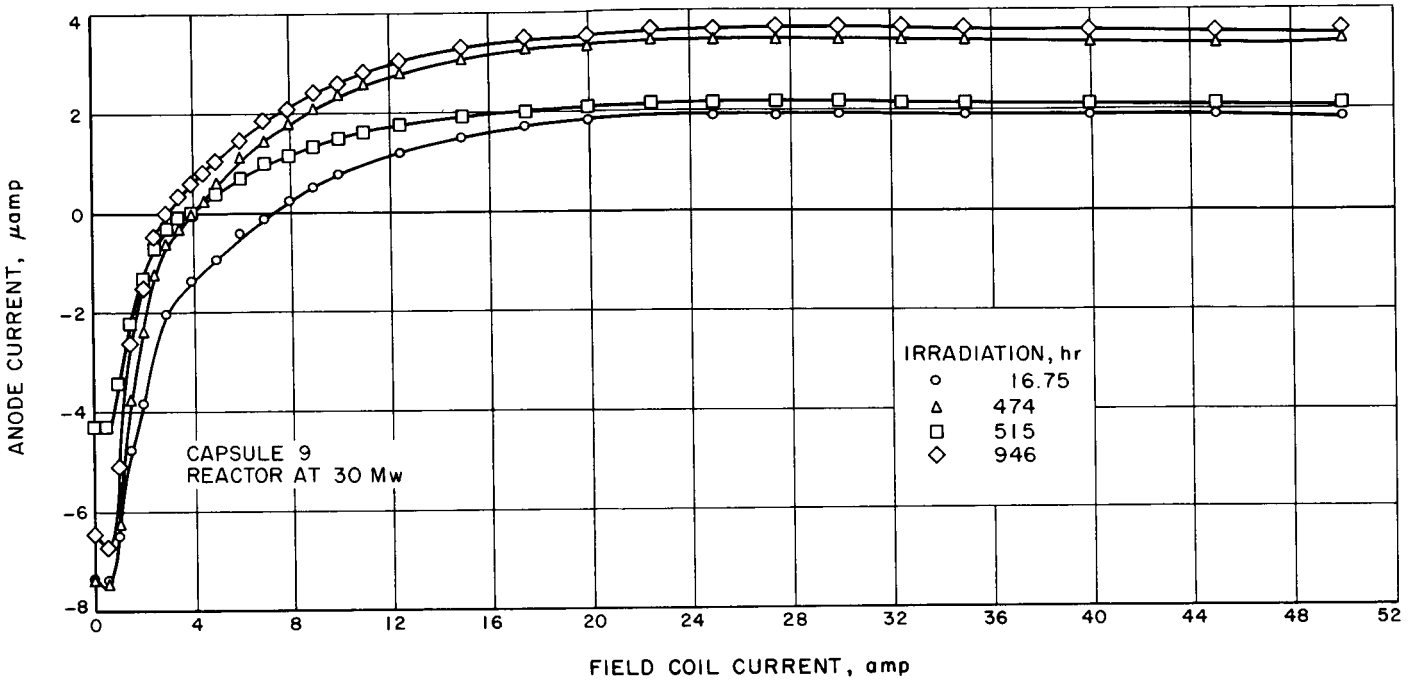

Fig. 41. Magnetron effect: anode current (Capsule 9)

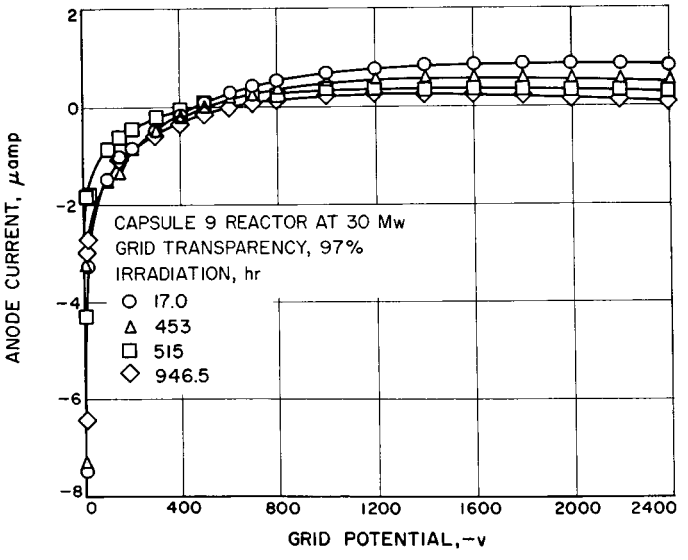

Fig. 42. Electrostatic charge separation: anode current (Capsule 9)

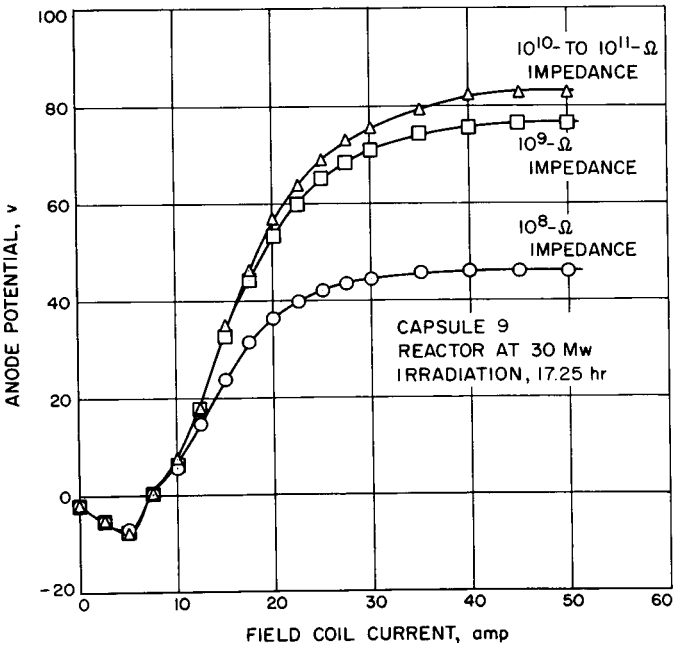

Fig. 43. Magnetron effect: potential buildup (Capsule 9)

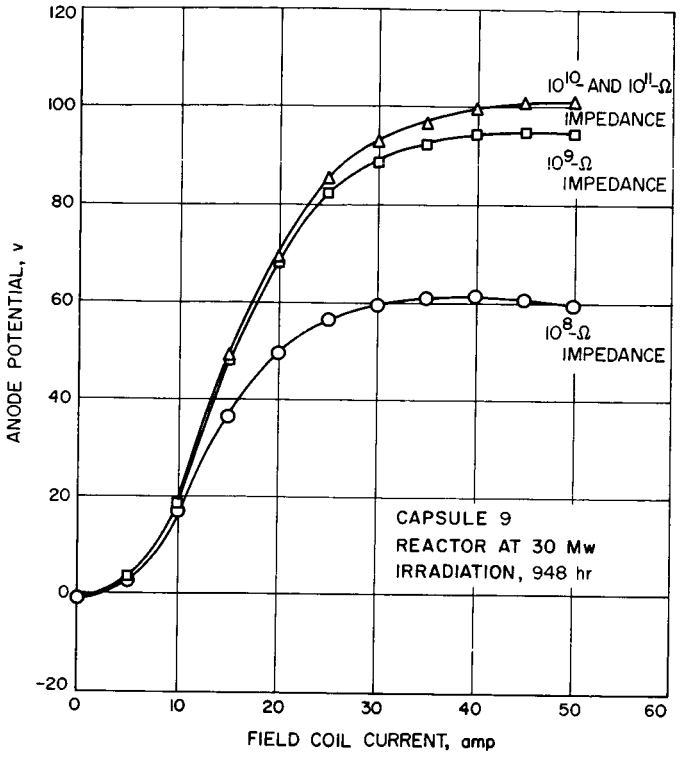

Fig. 44. Magnetron effect: potential buildup with long-term irradiation (Capsule 9)

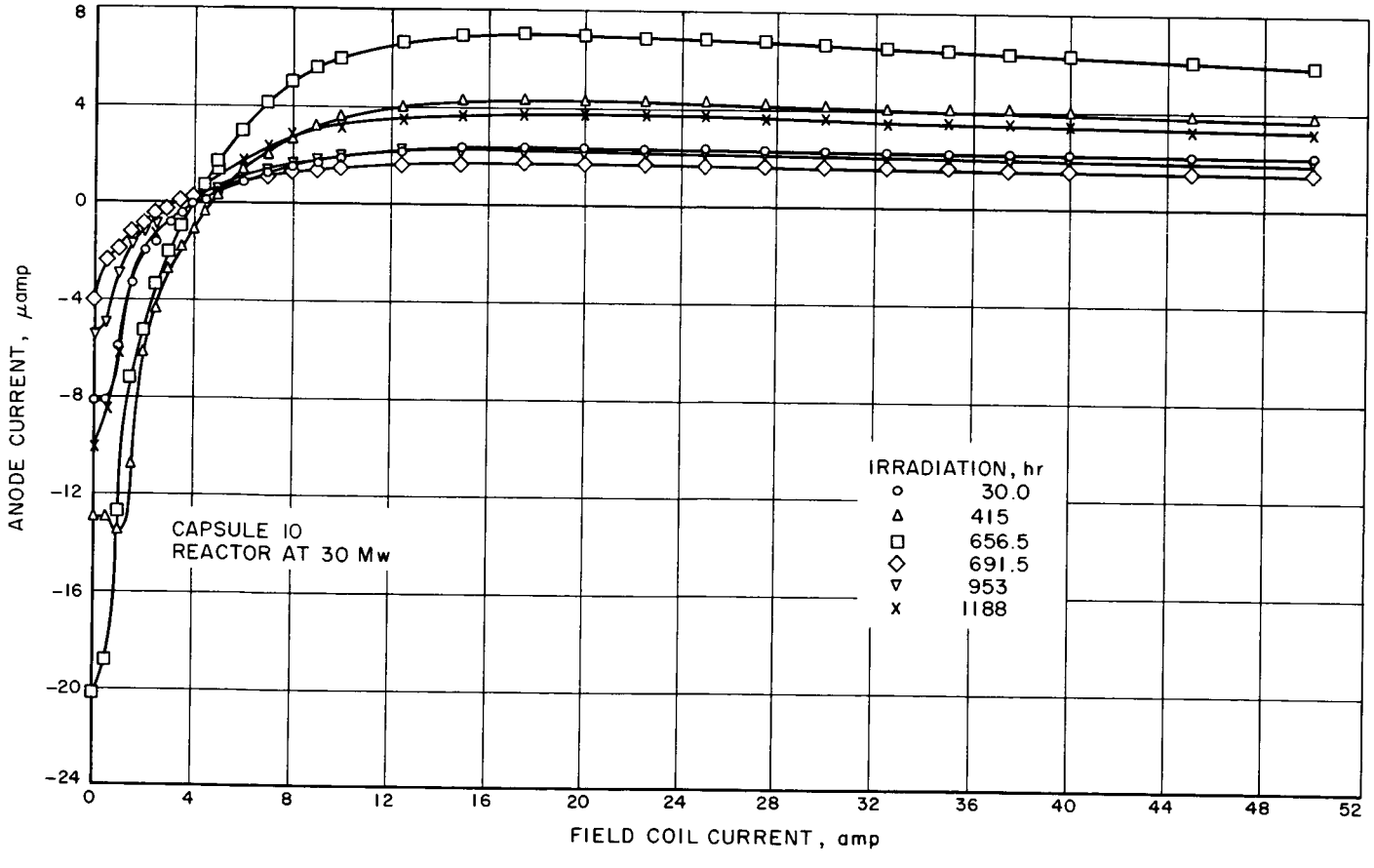

Fig. 45. Magnetron effect: anode current (Capsule 10)

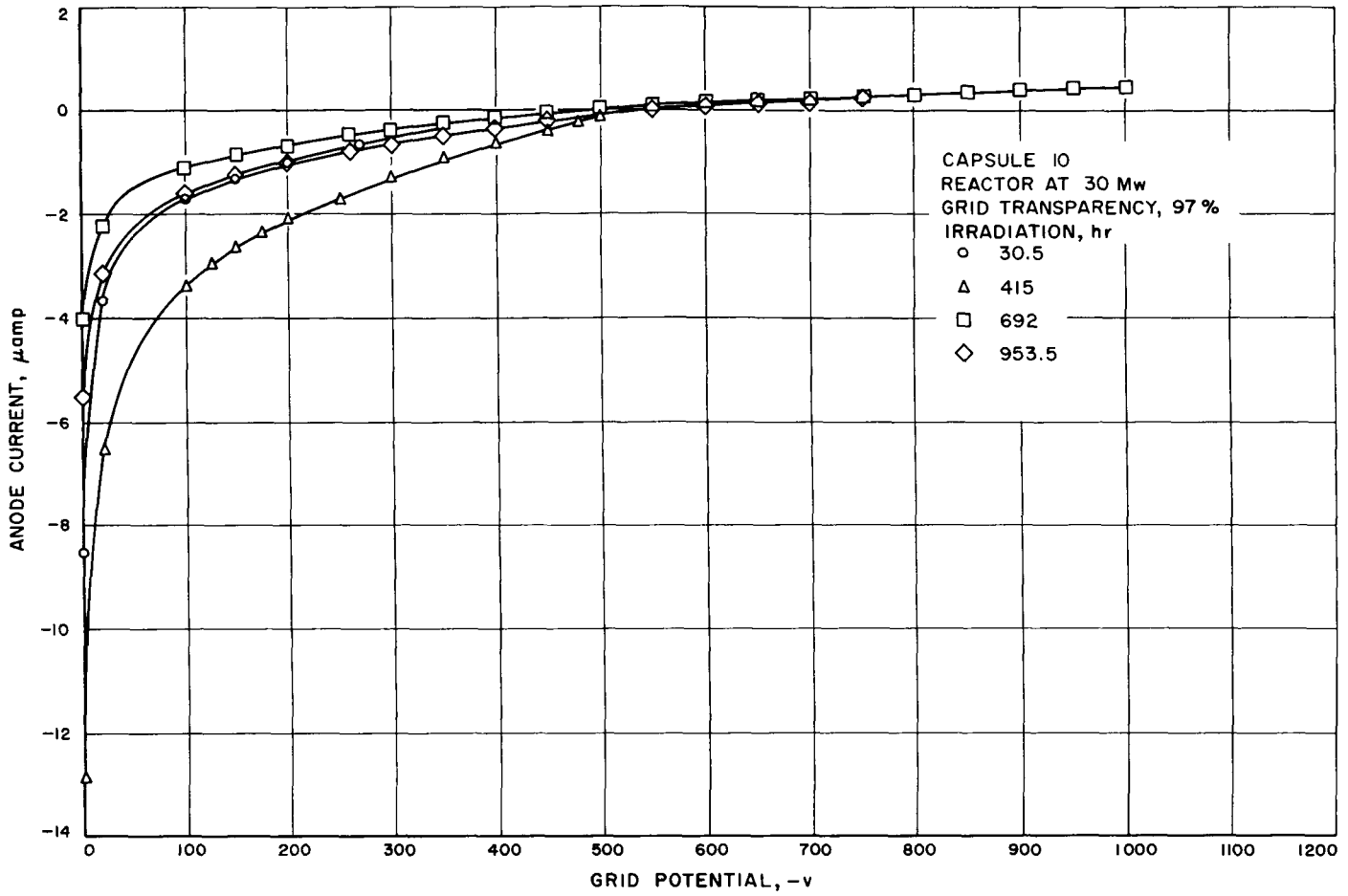

Fig. 46. Electrostatic charge separation: anode current (Capsule 10)

The decrease was consistent with calibration data extrapolated to GETR operating conditions. Differentiation of the curves of capsule current versus magnetic field strength gives a most probable energy of the follow-out electrons of 2.2 ±0.5 ev.

All of the grids used in the various capsules were capable of suppressing the follow-out electrons; however, current reversal was not possible with grids of less than 89% transparency. Capsule 9 was the only one whose grid performed as an adequate electron suppression device throughout the irradiation period. The maximum current with grid suppression was one-half that with magnetic suppression during the initial stages of irradiation, but decreased to a value of one-sixth of it as the irradiation continued. This grid had a transparency of 97%. Fragments intercepted by the grid produce a quantity of electrons in excess of the charge represented by the fragments; these are not suppressed by the grid and are actually accelerated toward the anode. The magnetic field was capable of suppressing the electrons originating from the grid. Deterioration of the grid performance with irradiation was probably the result of accumulation of uranium on its surfaces. This uranium would represent another source of unsuppressed electrons originating from the grid.

A series of leakage-current tests was performed with the various capsules. These tests were performed during the calibration tests and also during irradiation in the reactor. A potential was applied to the anode; the current required to maintain this potential was measured. Several of these tests were performed with different magnetic field strengths. Typical results of the leakage current tests are shown in Figs. 13(a) and (b), 17, 19, and 48 through 53. For Capsule 1, the leakage current is linear with applied potential, for both positive and negative polarity. This would indicate that, over the range tested, there was a single mechanism contributing to the leakage current. For all of the capsules tested in the Spent Fuel Element Facility and in the GETR at full power, there appears to be more than one mechanism

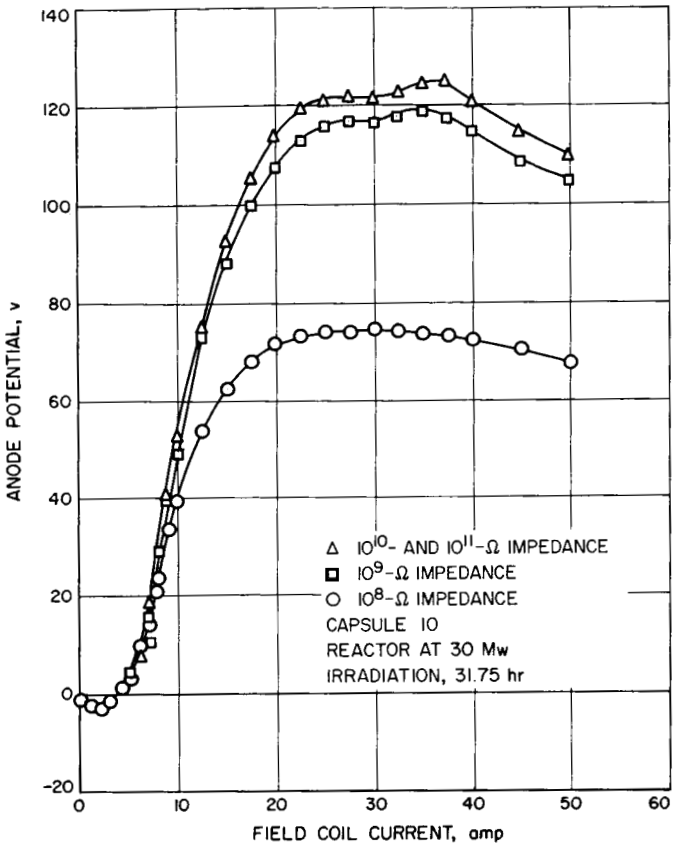

Fig. 47. Magnetron effect: potential buildup (Capsule 10)

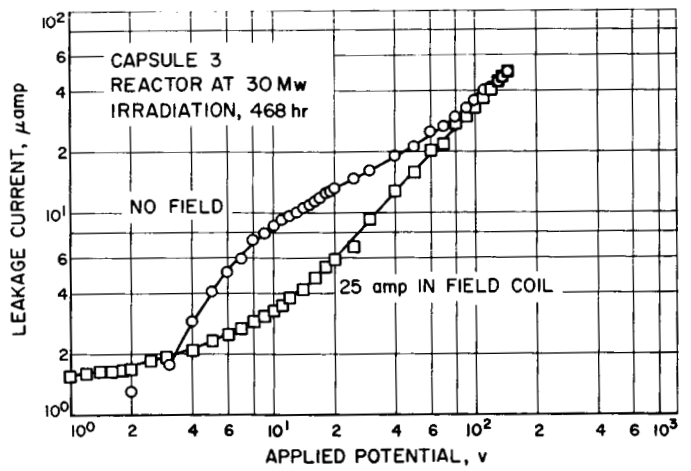

Fig. 48. Leakage current: 136-hr irradiation (Capsule 3)

contributing to the leakage current. At low applied potentials, sweep-out of electrons between the cathode and anode appeared to be the predominant leakage mechanism. This reached saturation at some potential, and

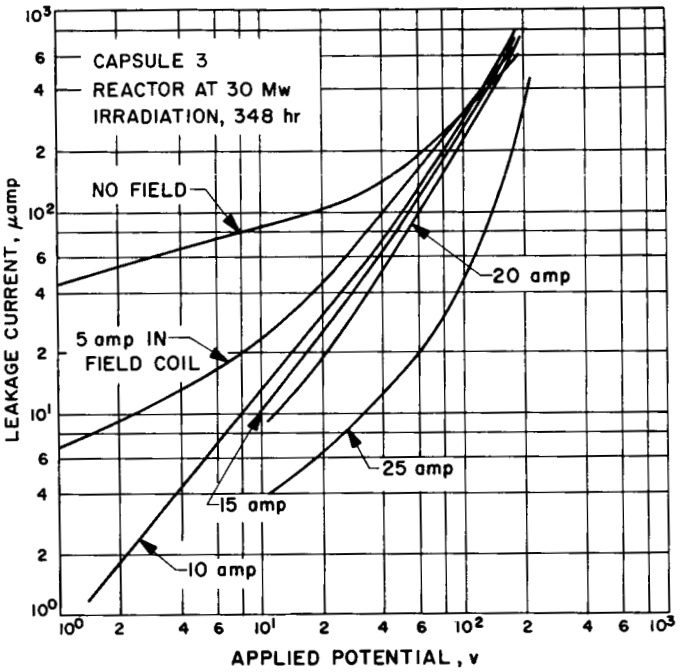

Fig. 49. Leakage current: 348-hr irradiation (Capsule 3)

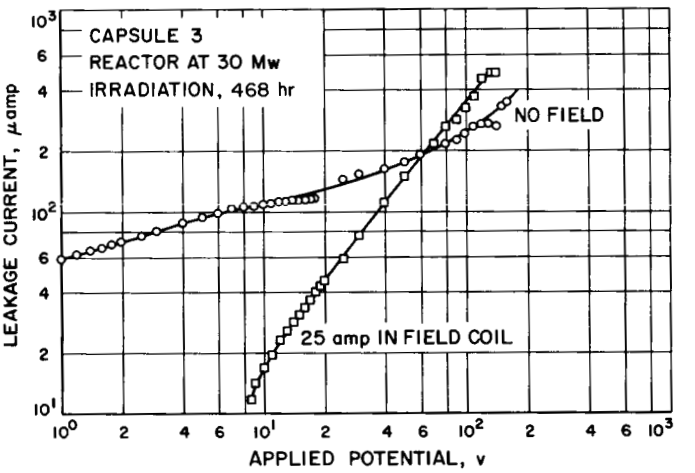

Fig. 50. Leakage current: 468-hr irradiation (Capsule 3)

any further increase in potential would not result in an increase in the leakage current. Capsule 9 is an example of leakage current saturation. The feedthrough insulator of this capsule was removed from the radiation field via vacuum leads. The saturation behavior was evident in both the calibration tests in the Spent Fuel Element Facility and in the reactor with this capsule. A second mechanism of current leakage, which would predominate at the higher potentials, is leakage in the feedthrough

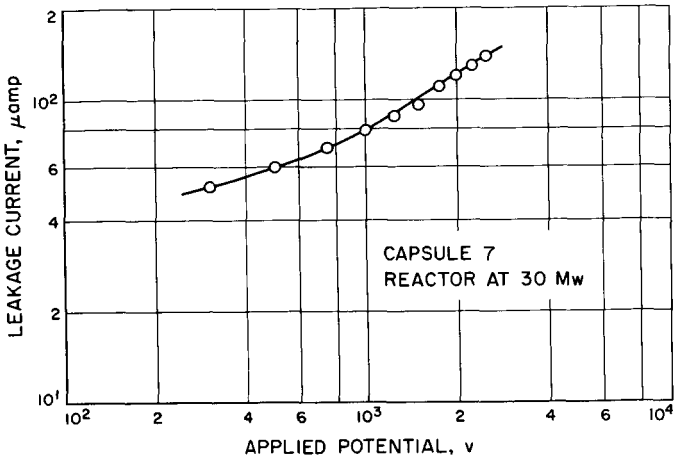

Fig. 51. Leakage current (Capsule 7)

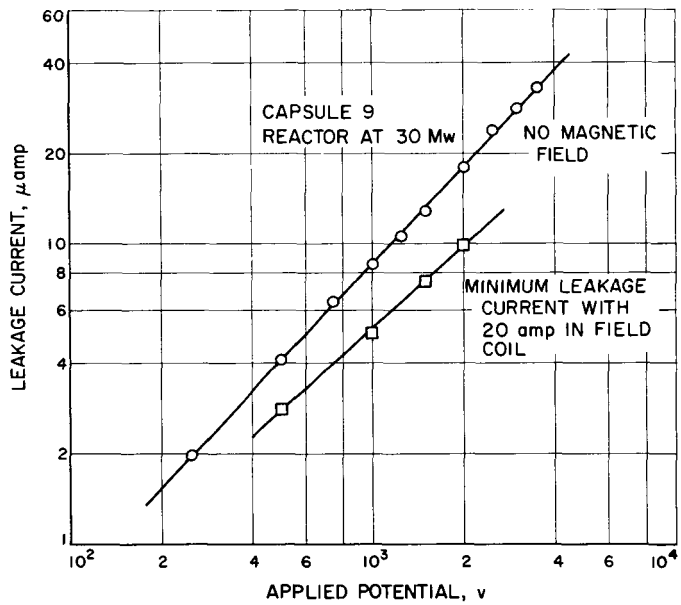

Fig. 52. Leakage current (Capsule 9)

insulator and the leads due to the ionizing radiation. This mechanism is evident in the tests with the capsules whose feedthrough insulators were attached directly to the capsule envelopes.

Leakage current with magnetic field was lower than that without, but approached the zero magnetic field value at large applied potentials. This was true for capsules in which the feedthrough insulators were right at the vacuum envelope. This fact supports the assumption of two different mechanisms for leakage current. It was possible to find magnetic field strengths for which the leakage current was a minimum for the capsules in which

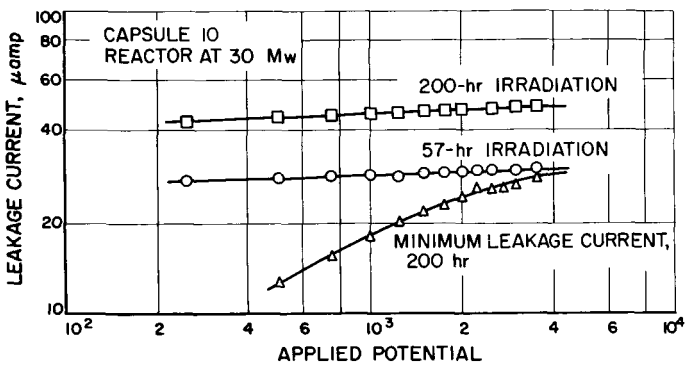

Fig. 53. Leakage current (Capsule 10)

the feedthrough insulators were removed from the high radiation field. For Capsule 9, the minimum leakage current always occurred at the same magnetic field strength independent of the applied potential; for Capsule 10, the magnetic field required for minimum leakage was a linear function of applied potential. These results can be seen in Fig. 54.

There was no problem with glow discharge during the leakage current tests with magnetic field in the NTR and in the Spent Fuel Element Facility; however, the capsules would on occasion break into glow discharge with the crossed magnetic and electrostatic fields present. Once this had happened, several hours of recovery were required before reproducible data could again be taken.

Magnetic fields required for minimum leakage current were always well below the calculated magnetron limitation for the applied potential. The capsules always broke into glow discharge at fields slightly above the field for minimum leakage current. This meant that it would be impossible for the capsules to attain potentials near their calculated magnetron limit. Limits to the po-

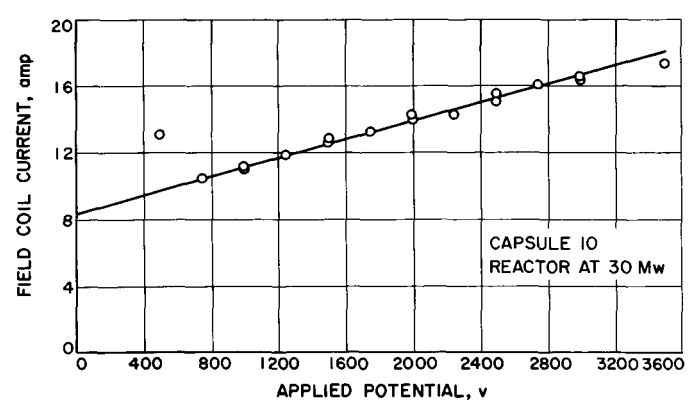

Fig. 54. Field for minimum leakage current

tentials attained by the various capsules were imposed by the maximum probability for an ionizing collision with a neutral atom by the electrons in the inner space between the cathode and the anode, and by the plateau voltage for glow discharge as determined by the cell geometry. The ion pump current gave an indication of noncondensable gas in the electrode inner space; however, because of sputtering of cathode and collector material, the atomic density of material in the inner space is probably much higher. Because of this large atom density, and the large electron density due to follow-out electrons and secondary electrons, capsule potentials would be limited to the few-hundred-volt range, which corresponds to the electron energy for maximum probability of an ionizing collision.

Capsule 8 was irradiated in the NTR to determine the effects of various gases in the capsule terminal chamber on the leakage current in the anode circuit external to the cell region. Evaluation of the effect was made by measuring the maximum voltage developed by the capsule with the chamber pressurized with various gases. The maximum voltage developed by the capsule with helium, or a helium (96%)–butane (4%) mixture, in the chamber was 237 v; 810 v was attained with nitrogen, carbon dioxide, argon, sulfur hexafluoride, air, or a mixture of nitrogen and sulfur hexafluoride in the chamber. These voltages were independent of gas pressures for pressures between 30 and 60 psia. They were also independent of neutron flux levels for reactor power from 200 w to 30 kw.

C. Capsule Disassembly

Disassembly of the capsules was a remote operation performed in a hot cell. Parts were opened and removed by either tool machining or grinding. These operations unfortunately subjected the capsules to severe mechanical shocks in spite of all precautions taken. The field coil was the first part removed; after its removal, the cell subassembly (with the exception of the first two capsules) was gamma scanned. This first scan was to outline the fragment activity to indicate any gross migration of the uranium.

The results of this scan indicated that fragment activity was confined to the cathode and anode region of the cell. There were small peaks on the scans of the aluminum capsules outside the cathode–anode region; however, these corresponded to the welds. Scans of the stainless steel capsules were somewhat more difficult to interpret because of the activity of the structural material. Activity peaks were noted outside of the cathode–anode region; however, they could be accounted for by geometric and material density effects. This is especially true for the base of the working section of the cell. Accumulation of uranium in this bottom section of the cell could not be detected against the high background.

Following the gamma scan of the cell subassembly, the cell was disassembled into its basic components of cathode, anode, and grid (if present). These parts were photographed and placed in suitable containers for gamma scanning. Because of the difficulty of handling the delicate parts remotely, some of the parts were damaged. Any of this damage, however, is clearly distinguishable from that incurred during irradiation.

Figure 55 is a photograph of the Capsule 3 cathode and is an example of the diffusion of base materials

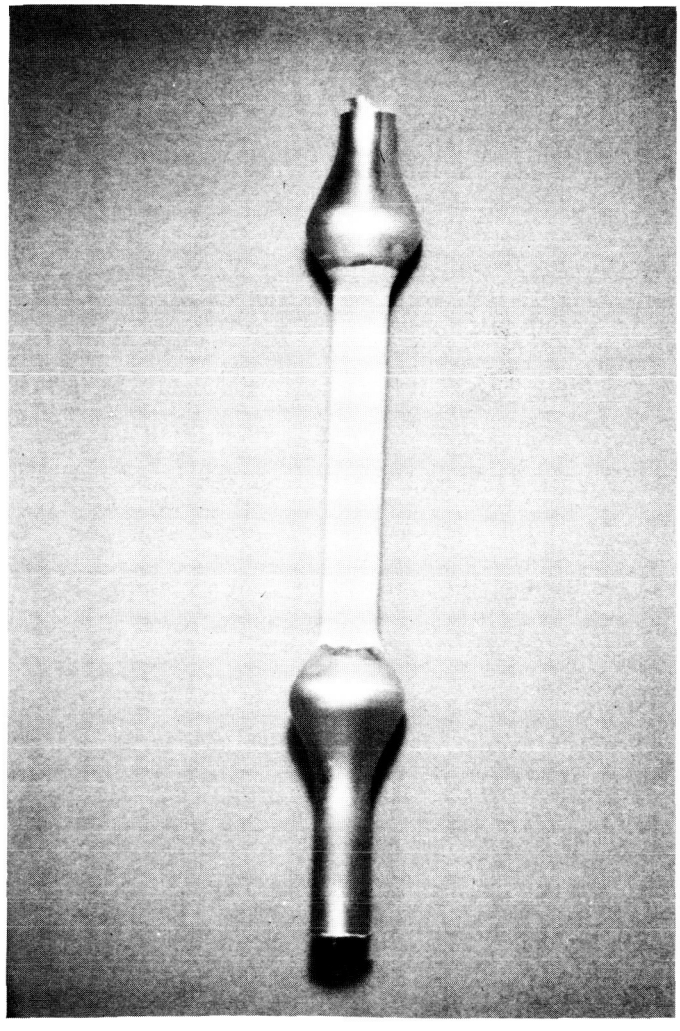

Fig. 55. Cathode after irradiation (Capsule 3)

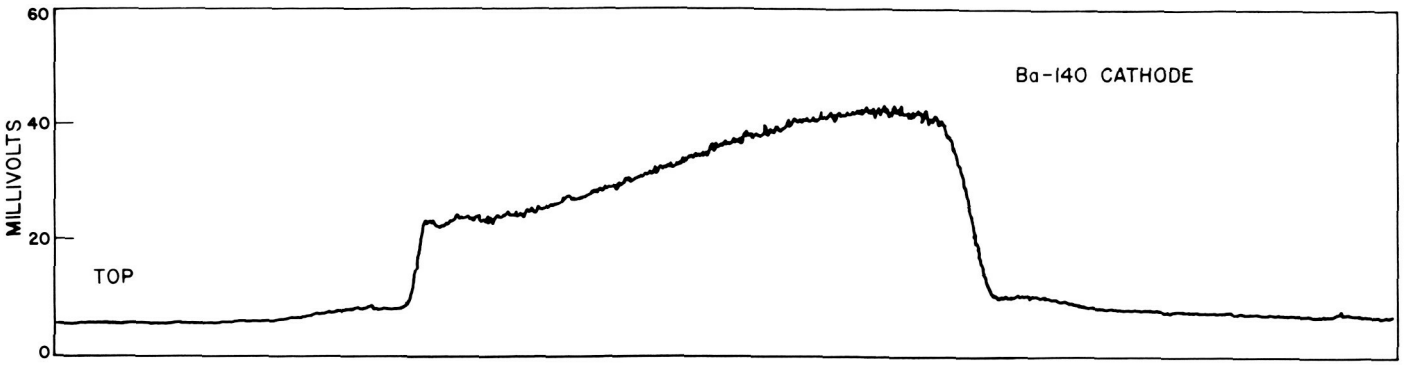

Fig. 56. Scan of cathode for 0.54-Mev gamma activity

through the fissile layer. The sublayer of this capsule was formed by zincating the aluminum surface and then plating with copper followed by zinc. The diffused material appears to be zinc. The gamma scan (Fig. 56) outlines the activity on the cathode. Although the sublayers of Capsule 4 were the same as for Capsule 3, the cathode appearance was quite different. Capsule 4 contained 1.97 times as much uranium as Capsule 3. The fissile layer has a beaded appearance as seen in Fig. 57. The metallic appearing area on the cathode is anode material that sublimed. Fig. 31(a) is a photograph of the anode showing the damaged areas. The distribution of anode

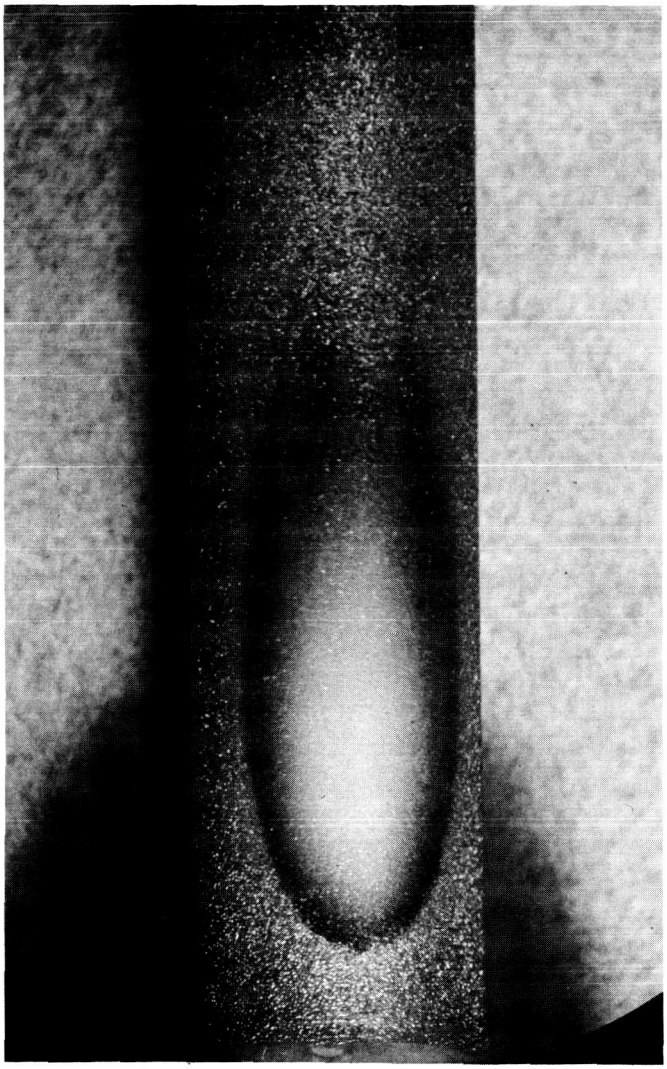

Fig. 57. Cathode after irradiation (Capsule 4)

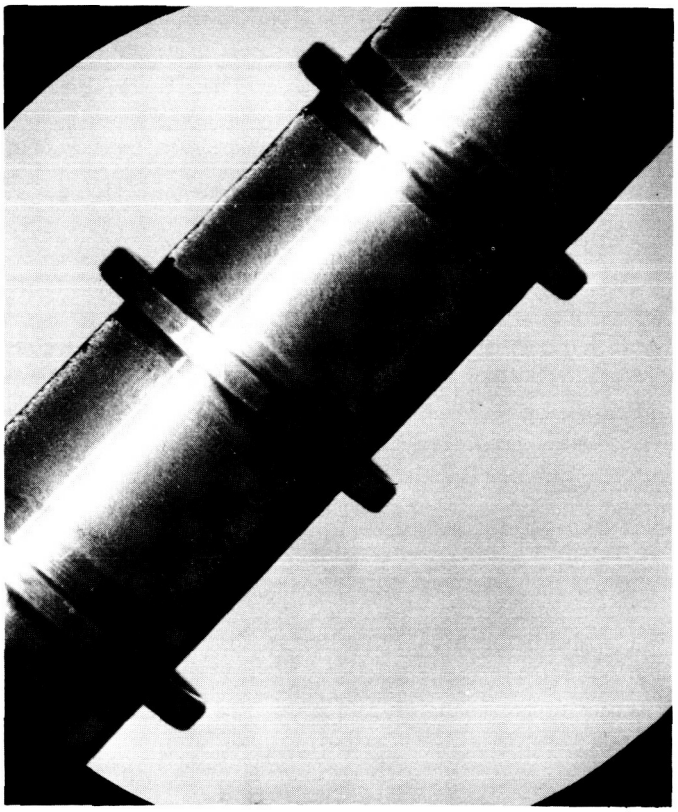

Fig. 58. Cathode after irradiation (Capsule 9)

material on the cathode is proportional to the fragment source distribution that impinged on the damaged areas. Fig. 58 shows the cathode of Capsule 9 in which the fissile layer was in the form of platelets. All of the cathodes can be characterized in appearance by the three shown. A more diffused sublayer was noted in the cathodes with the thinnest fissile layers.

Figure 59 is a photograph of an anode that had a thin layer of platinum on the inner surface. Sublimation of anode material from the outer surface can be discerned from the dull appearance. The inner surface was of the same shiny appearance as before irradiation. Figure 60 is a photograph of the anode of Capsule 9, which had a layer of platinum black on the inner and outer surfaces. The lower section of the anode has a shiny appearance while the upper portion has the characteristic matte finish. The gamma scan of the anode (Fig. 61) indicates a large accumulation of activity in the lower curl of the anode. The glazed appearance is probably due to overheating of the lower portion.

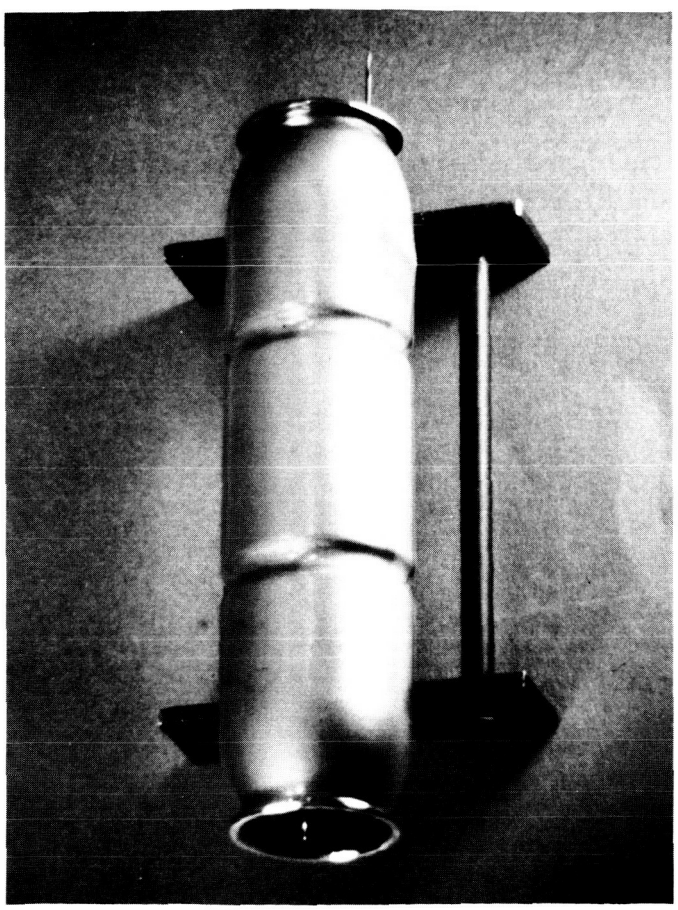

Fig. 59. Platinized anode after irradiation

A typical spiral grid is shown in Fig. 62. The darkened appearance is most likely due to fissile material that sublimed from the cathode to the grid.

Figures 61 and 63 through 74 are typical gamma scans of the components of the various capsules.

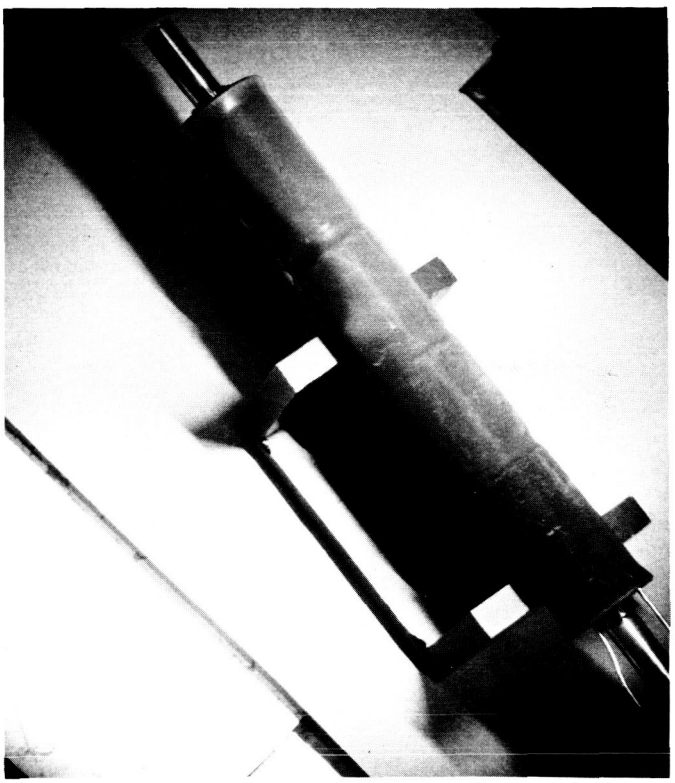

Fig. 60. Platinized anode after irradiation (Capsule 9)

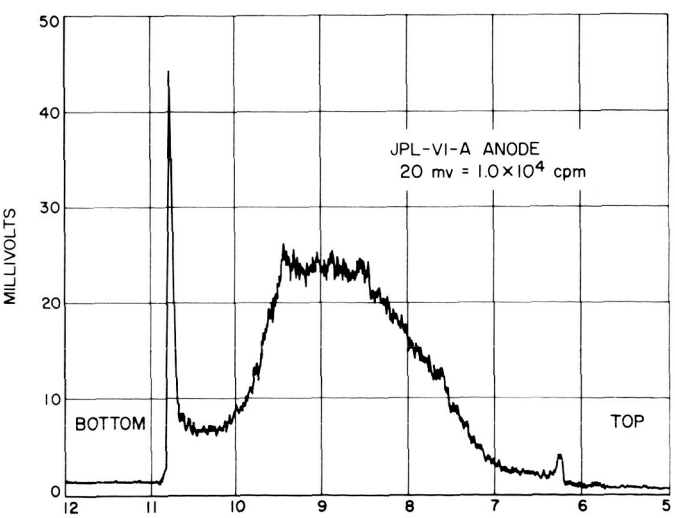

Fig. 61. Gross gamma scan: anode (Capsule 9)

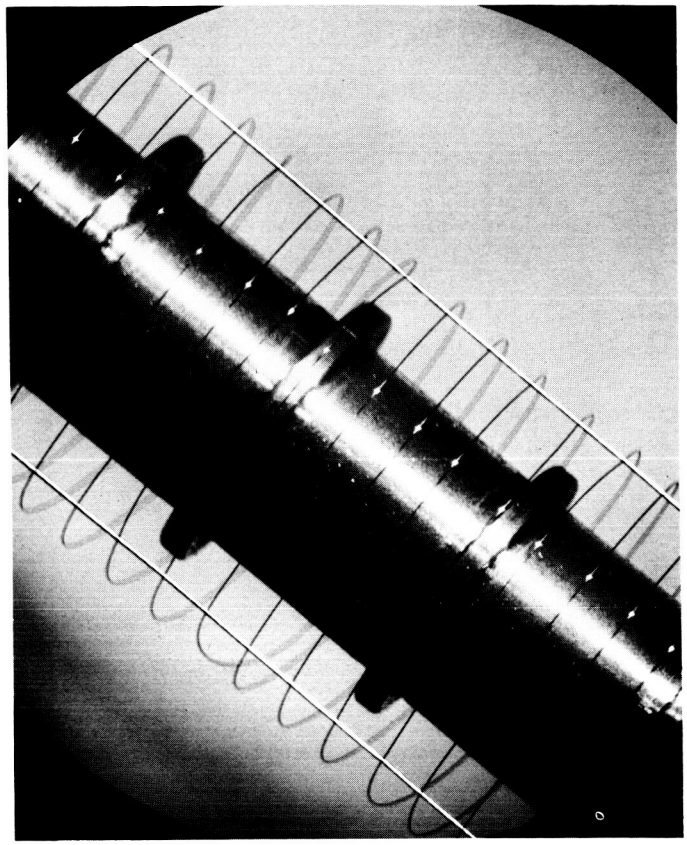

Fig. 62. Spiral grid and cathode

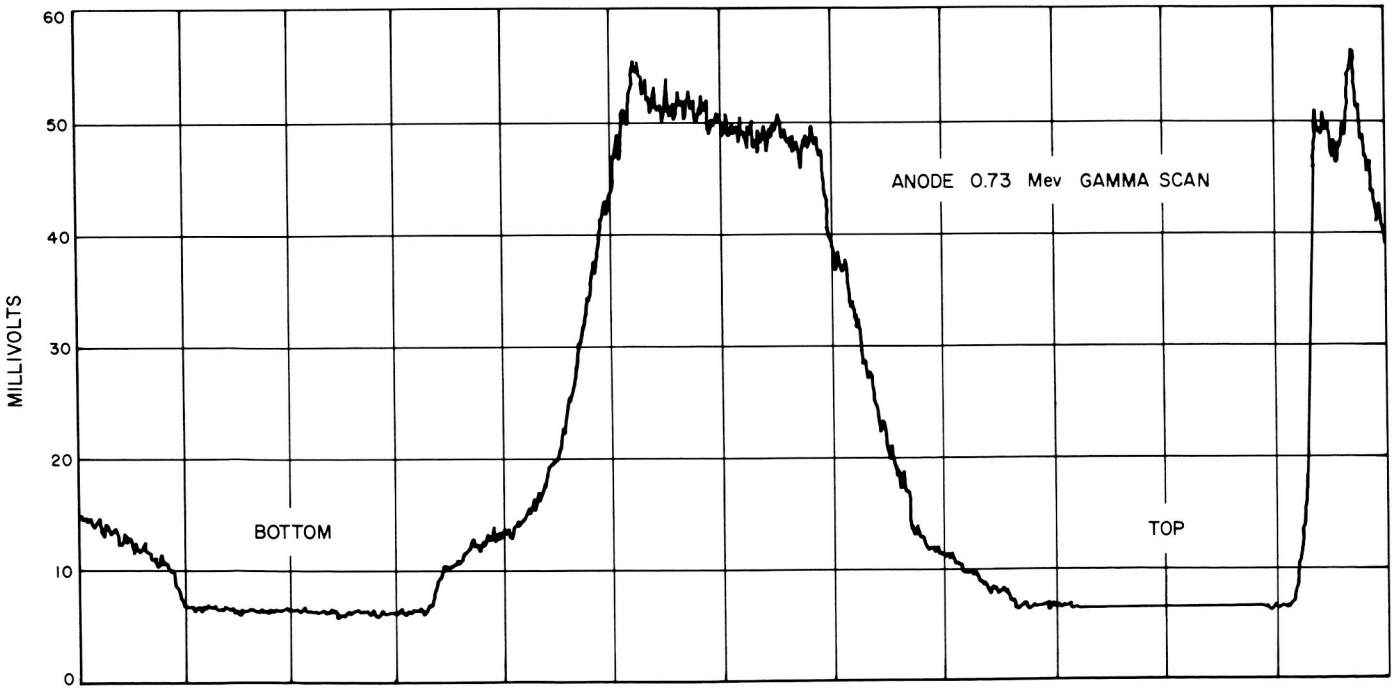

Fig. 63. 0.73-Mev gamma scan: anode (Capsule 4)

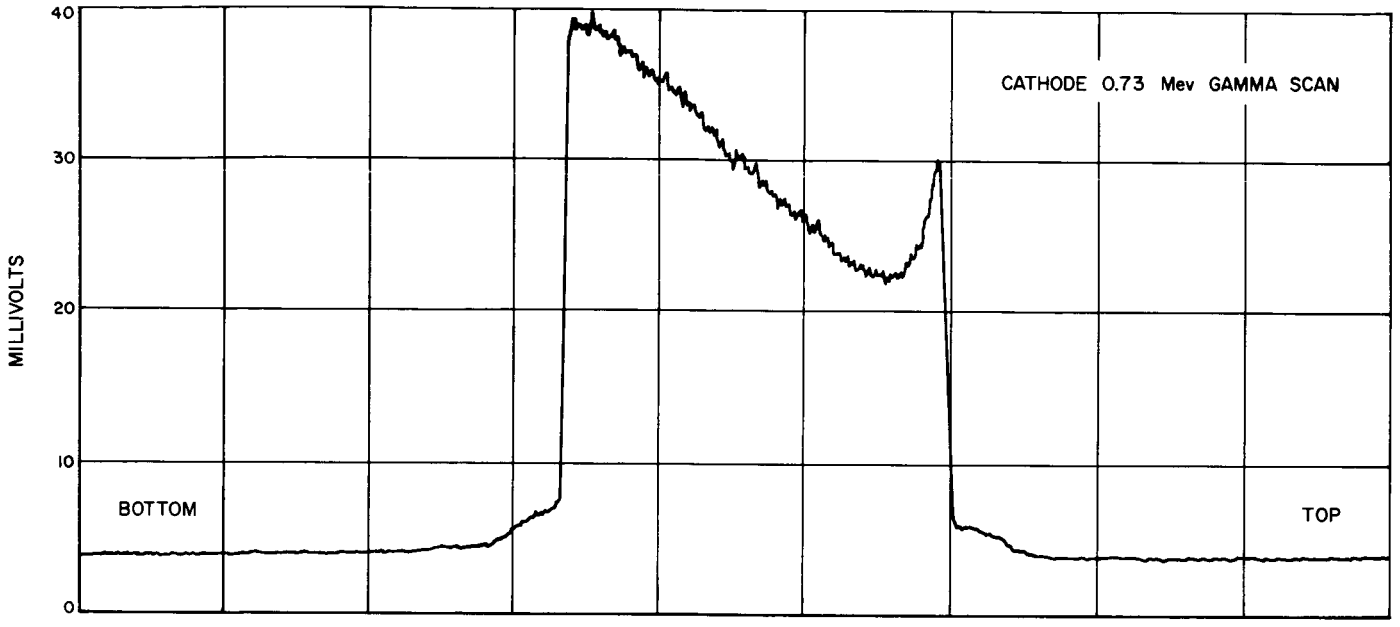

Fig. 64. 0.73-Mev gamma scan: cathode (Capsule 4)

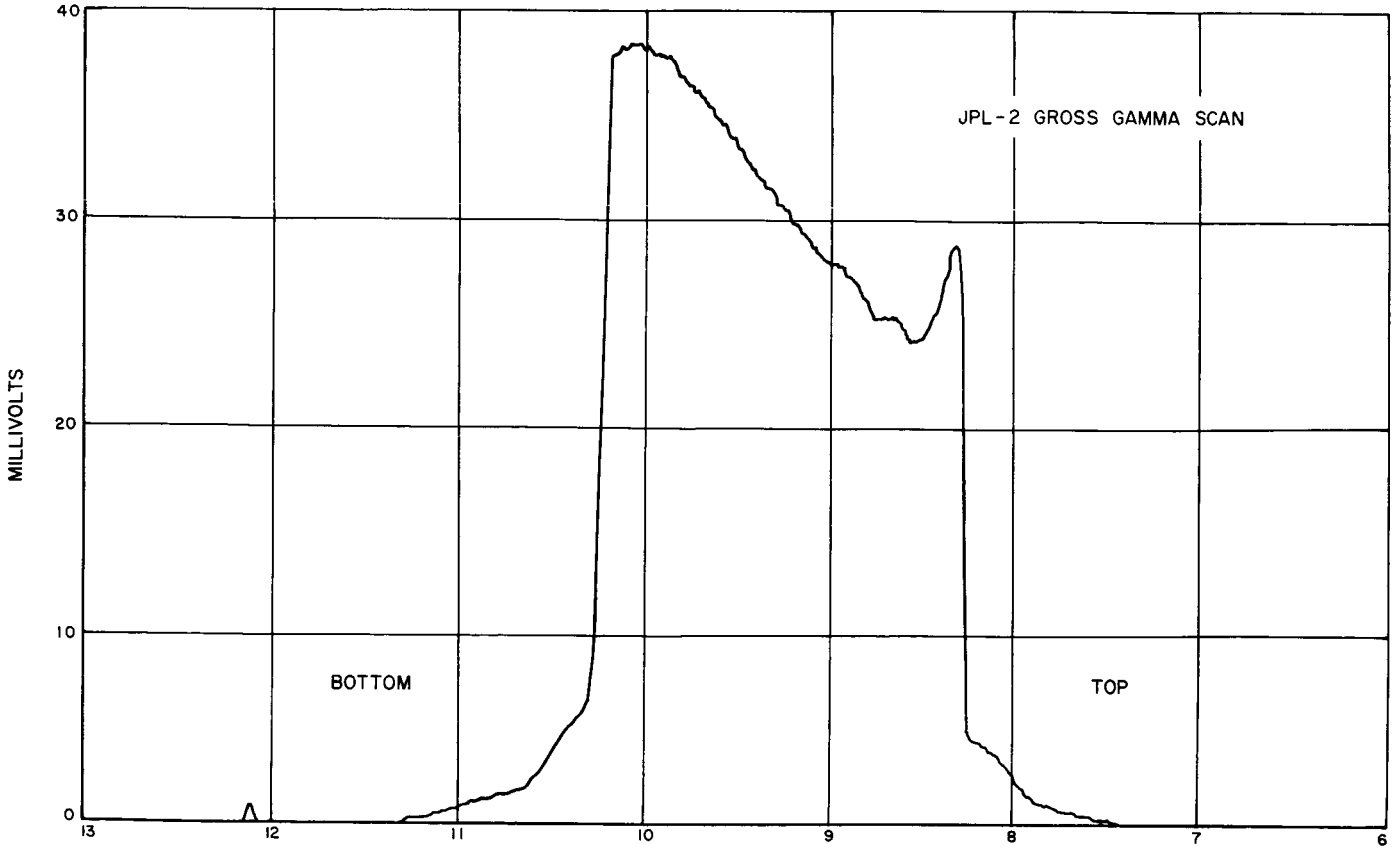

Fig. 65. Gross gamma scan: capsule subassembly (Capsule 4)

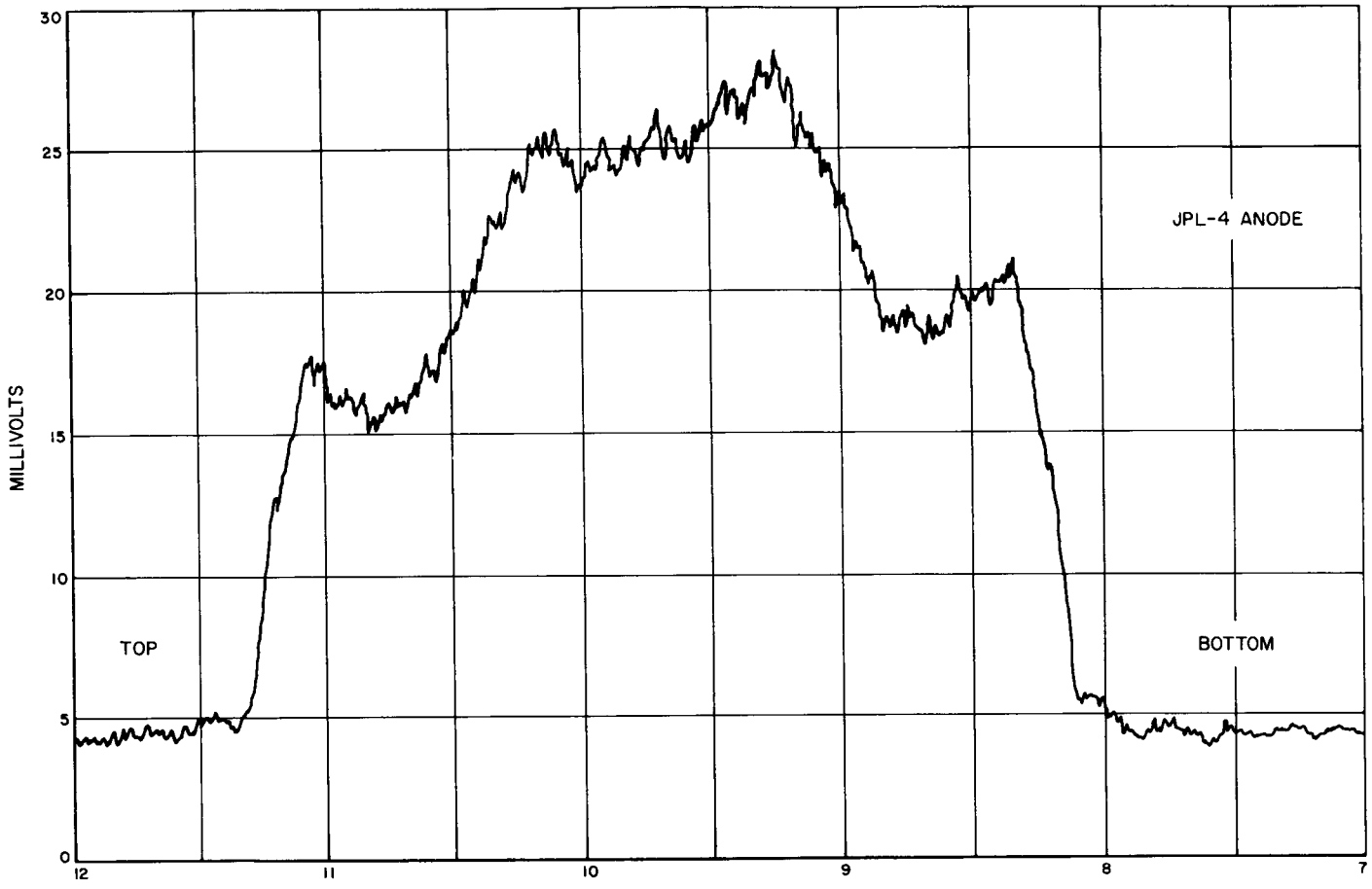

Fig. 66. Gross gamma scan: anode (Capsule 6)

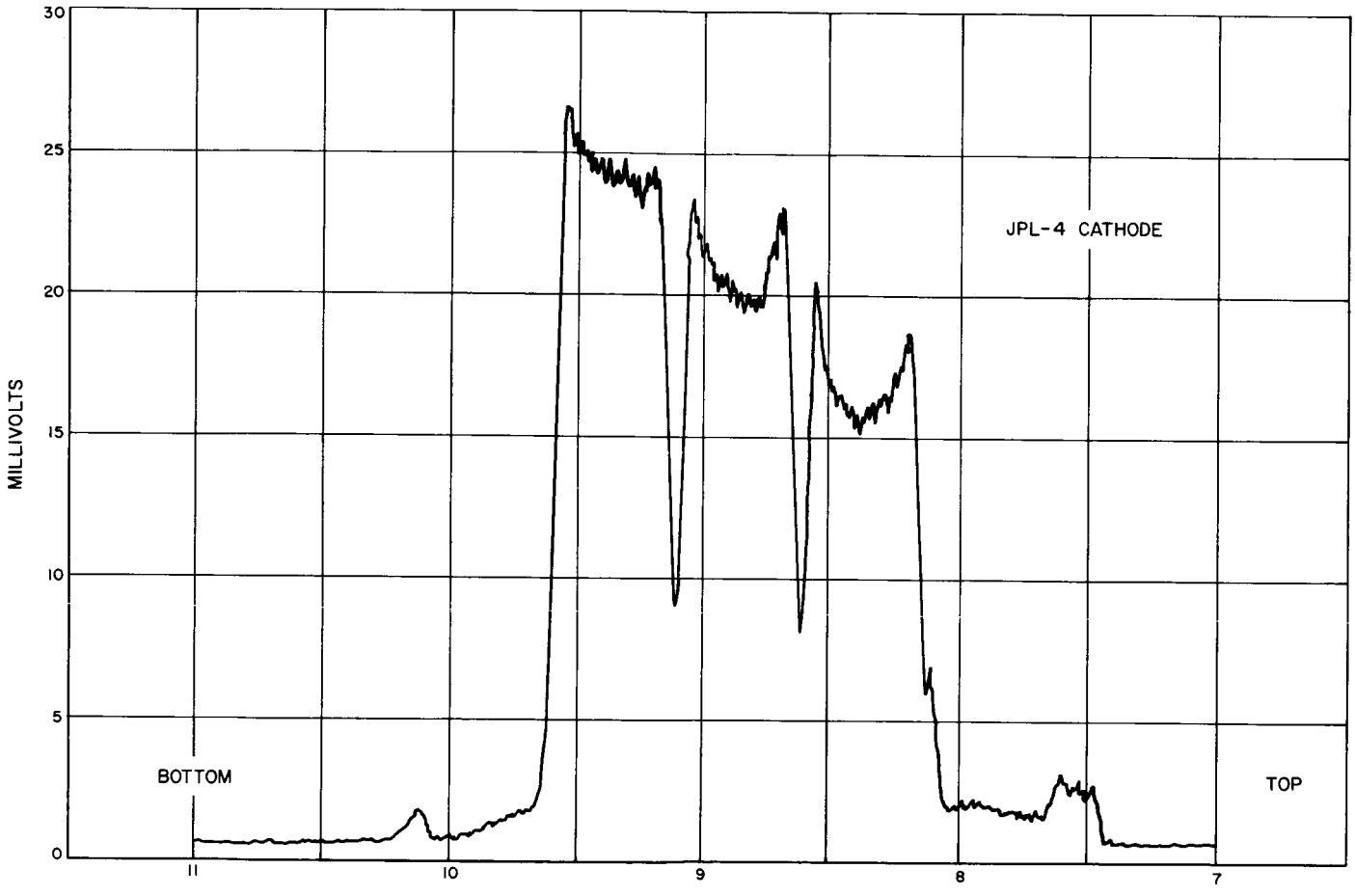

Fig. 67. Gross gamma scan: cathode (Capsule 6)

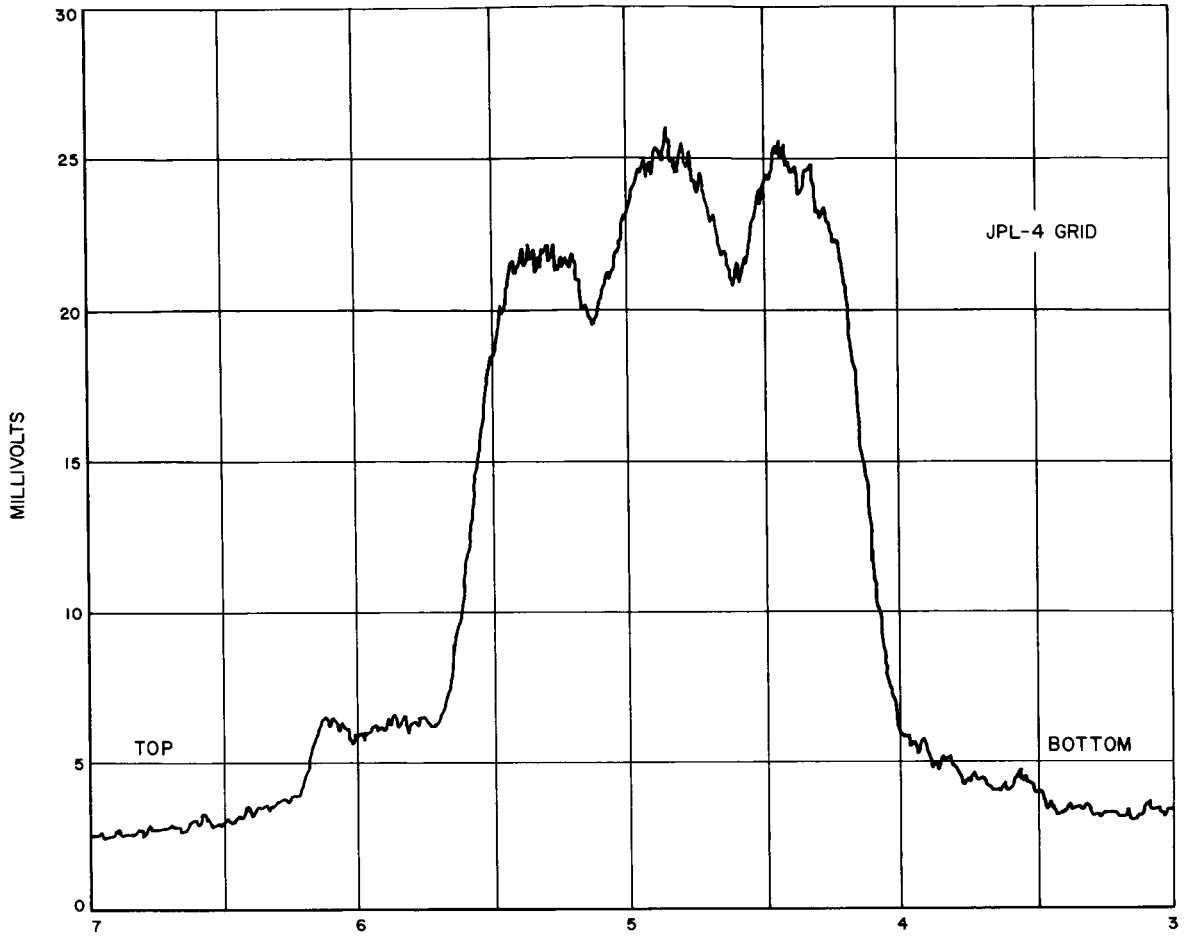

Fig. 68. Gross gamma scan: grid (Capsule 6)

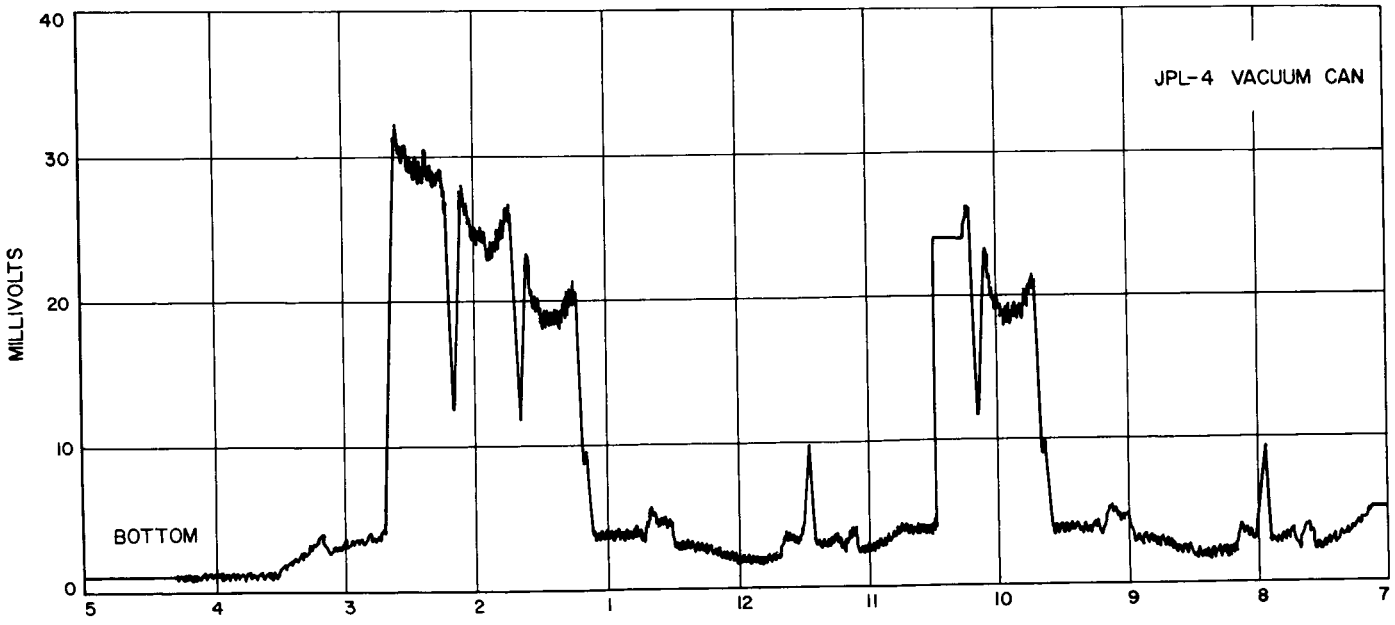

Fig. 69. Gross gamma scan: capsule subassembly (Capsule 6)

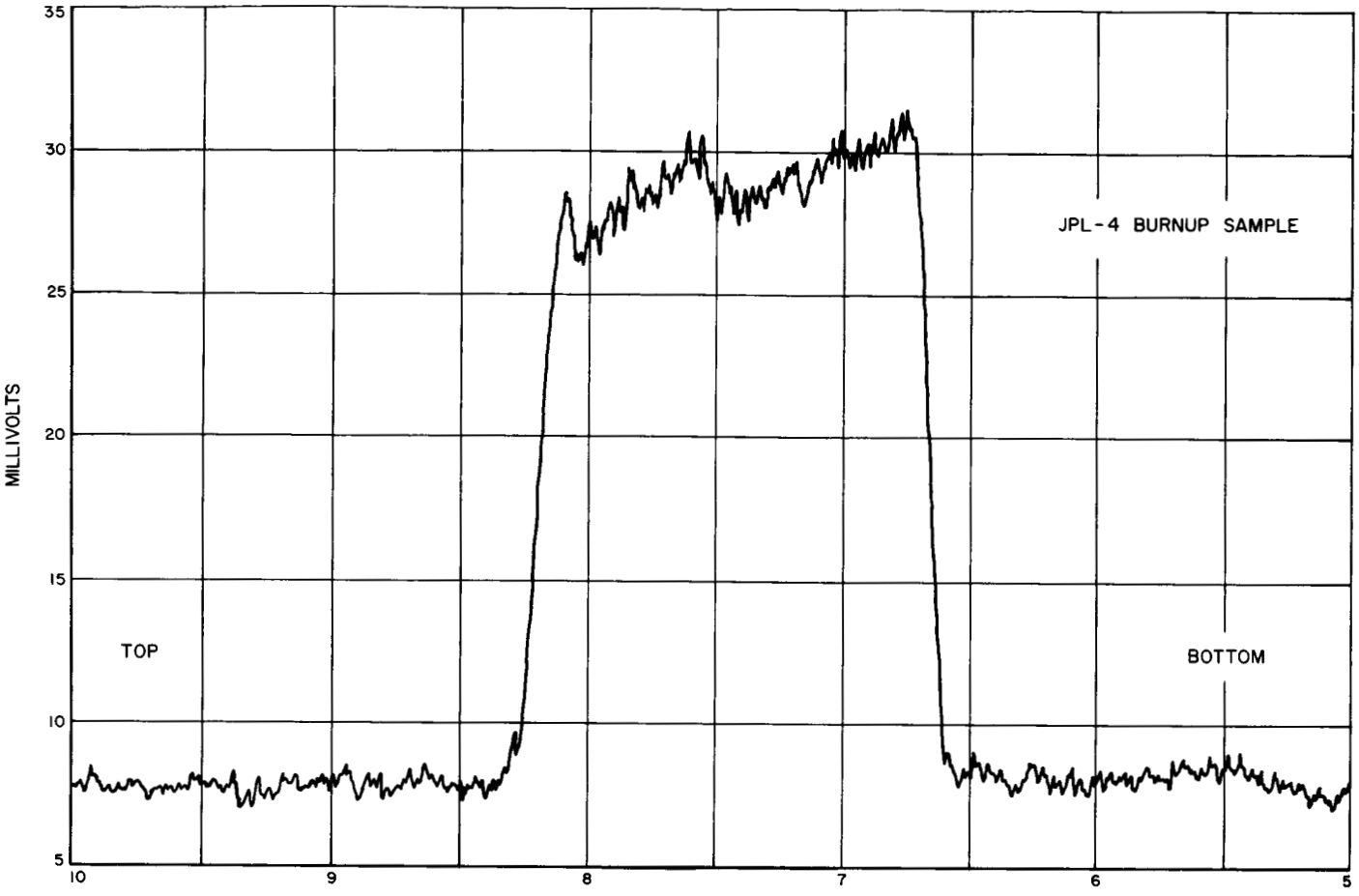

Fig. 70. Gross gamma scan: burnup sample (Capsule 6)

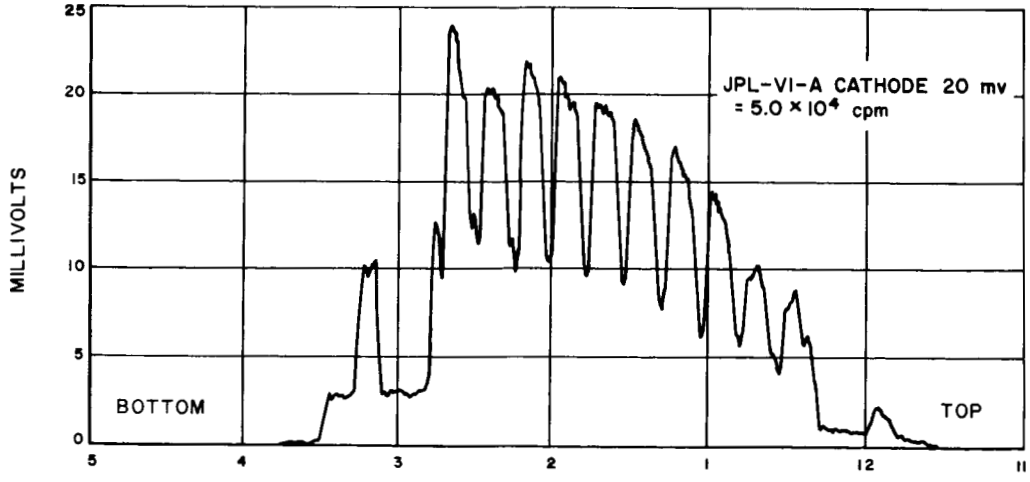

Fig. 71. Gross gamma scan: cathode (Capsule 9)

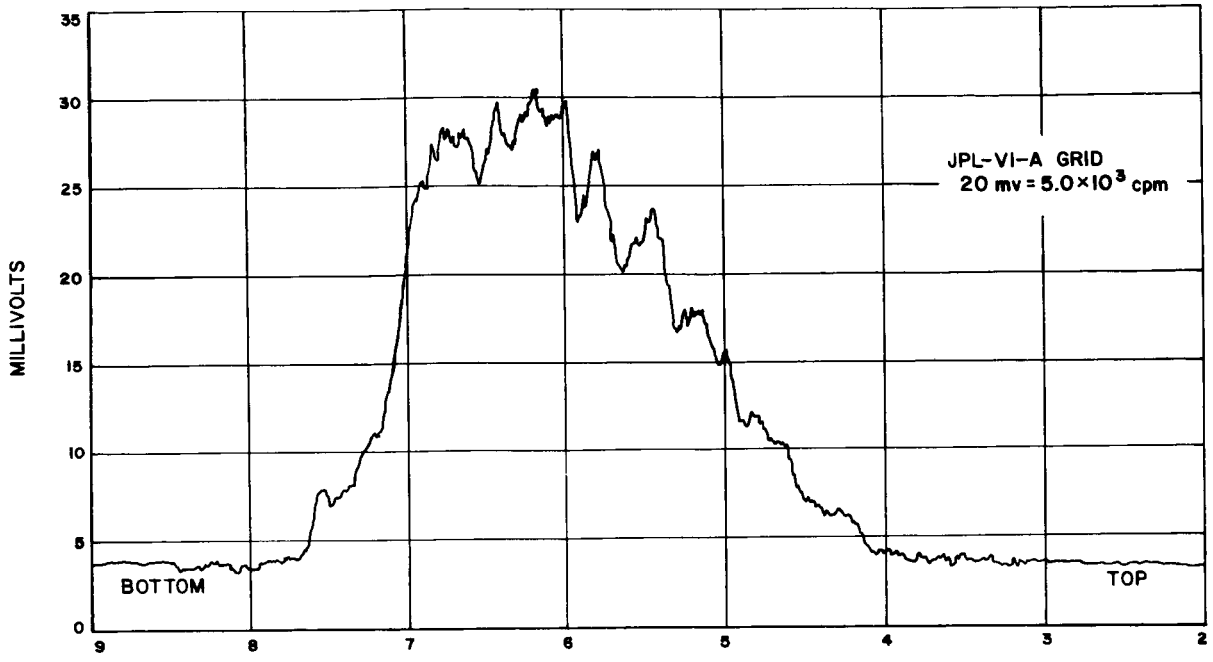

Fig. 72. Gross gamma scan: grid (Capsule 9)

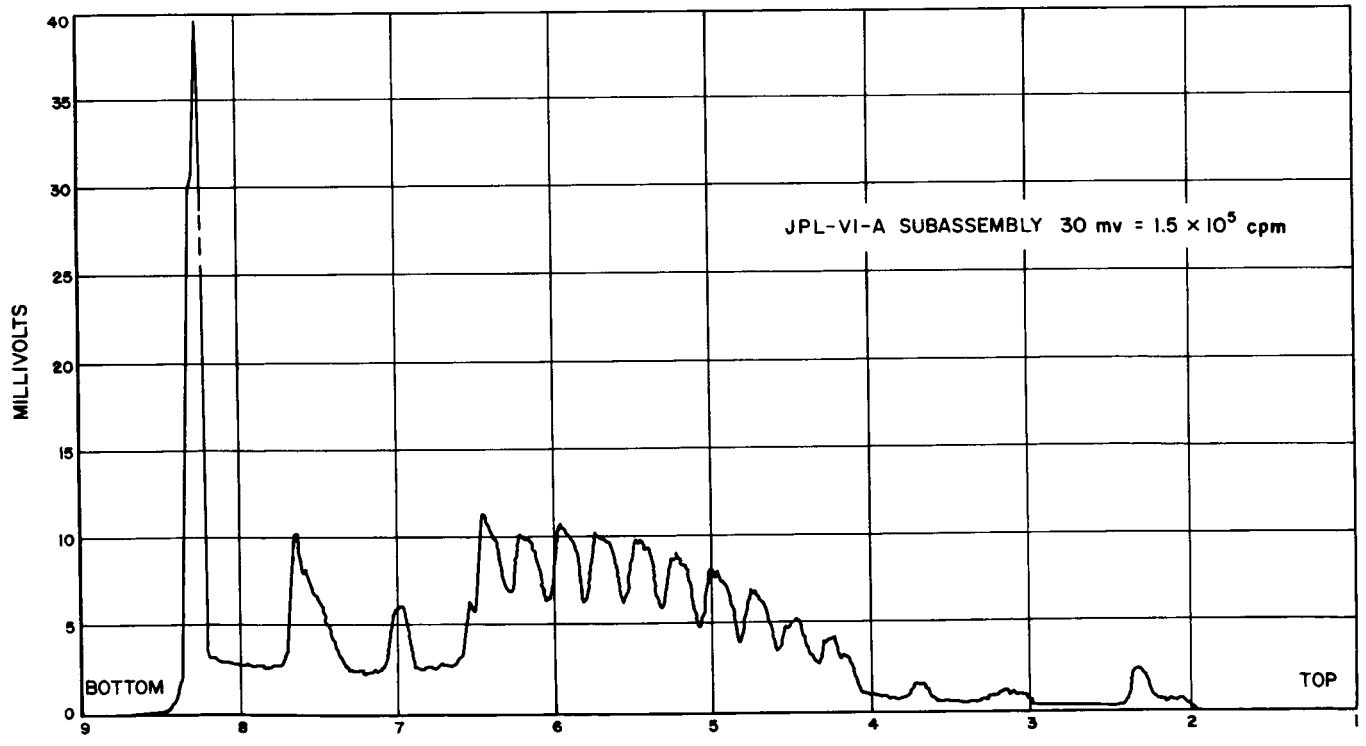

Fig. 73. Gross gamma scan: capsule subassembly (Capsule 9)

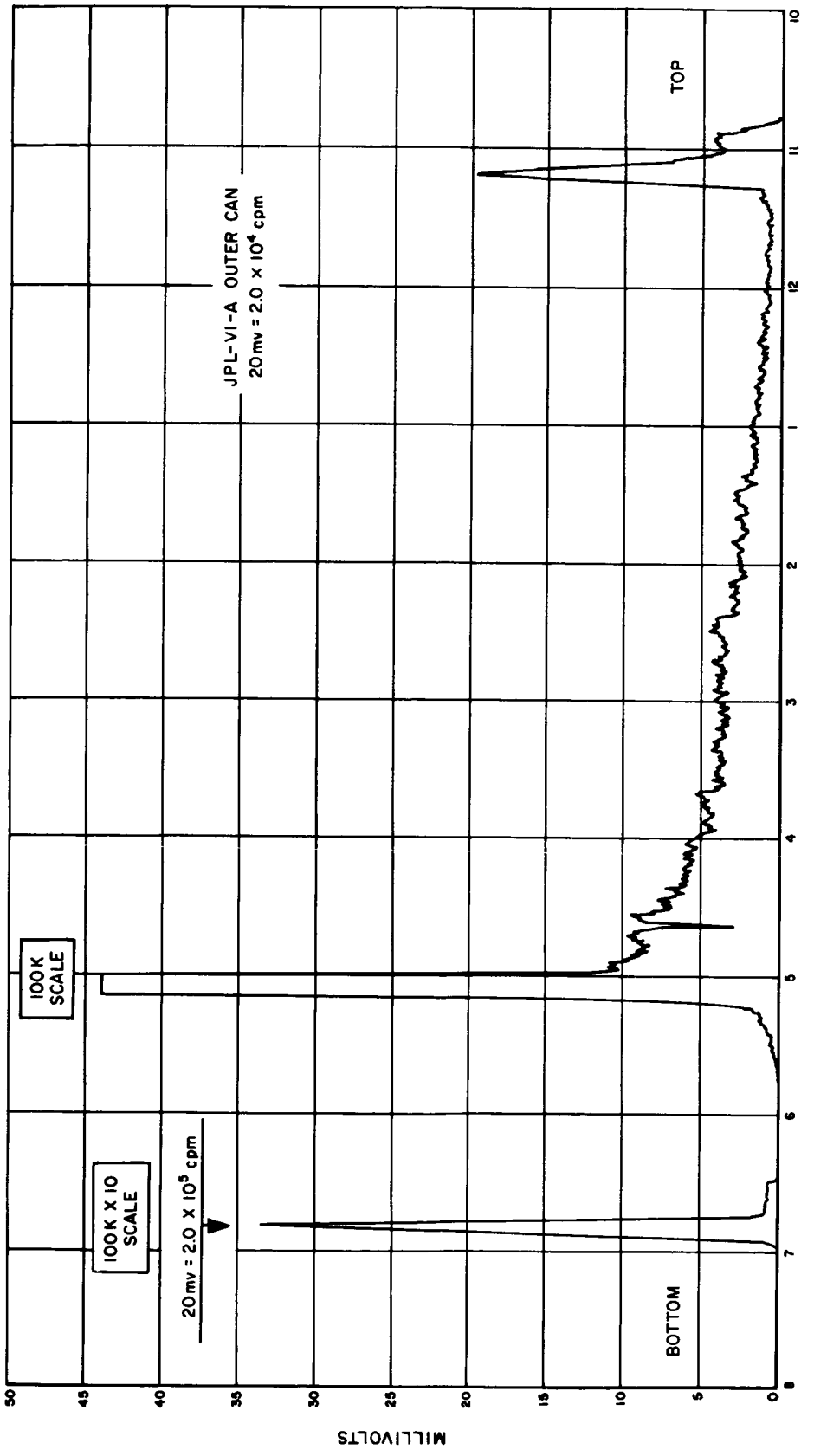

Fig. 74. Gross gamma scan: vacuum envelope (Capsule 9)

D. Radiochemical Analysis

1. Fragment Analysis

The total quantity of a fragment species produced was determined by correcting the quantity found at the time of counting for inpile and out-of-pile decay. Production rate of the fragments (i.e., fission rate) was assumed to be proportional to the averaged position of the reactor control rods. Because the reactor was down at intervals during a cycle, the capsules were subjected to several irradiation periods during a reactor cycle. For long irradiation intervals, the control rod position (and therefore the fragment production rate) increased linearly with time. Averaged value of fission rate was assumed for short irradiation intervals. It was found by this method that the total quantity of a particular fragment produced was only a few percent different than the quantity found by averaging the irradiation intervals.

Because of the small quantity of uranium contained within the capsule (22.2- to 298-mg U-235 total) and the relatively low burnup (1.5 to 3.6%), the total quantity of individual fragment species produced was small. By comparison, there was an extremely large amount of structural material of the various components, especially of the cathode, that had to be dissolved to recover the fragments. Because of this fact, as well as the difficulties of dissolution and the possibility of contamination of the components and solutions within the hot cell, there was considerable scatter in fragment data for individual capsules. However, ratios of the quantity of fragments on the various components of a capsule are fairly consistent, except in cases where solid material remained in the solutions. This was true of the cathode solutions, and a fragment definitely found in the solid residue was Zr-95. A tabulation of the fragment analysis for the capsules is included in Table 2 and discussed in Appendix C.

The fraction of the fragments leaving the cathode and collected on the grid was higher than the optical blockage of the grid. This is as expected because of the angular distribution of the fragments as they emerged from the cathode, and the finite thickness of the grids. Except for Capsule 6, the fraction of the heavy fragments collected on the grids was larger than the light fragments. The ratio of the fraction of the heavy fragments to that of the light fragments collected on the grid increases as the optical transparency of the grid increased. For Capsule 6, in which the reverse was true, the total quantity of both the light and heavy fragments collected on the grid was greater than the quantity collected on the anode. The fraction of the heavy and light fragments collected on the grid is approximately equal for Capsule 5, and this fraction is slightly less than one-third of the total leaving the cathode. The grid had an optical transparency of 75%.

Although Capsules 9 and 10 had grids of the same optical transparencies, a larger fraction of the fragments leaving the cathode was collected on the grid in Capsule 9. This is as expected, since Capsule 10 had a thicker layer of uranium. A thicker uranium layer for layers equal to or less than a fragment range would result in a greater average forward velocity component for the emerging fragments. Also, Capsule 10 had a spiral grid between the electrostatic grid and the cathode, which would cause some collimation of the fragments leaving the cathode.

2. Uranium Analysis

The total quantity of uranium found in each capsule during the chemical analysis was, for all capsules, less than the quantity plated on the cathode. The fraction of the uranium deposited on the cathode which was found in the analysis ranged from 0.127 to 0.727. There is a possibility that, in the course of irradiations, uranium was deposited in regions of the capsules outside of the sections analyzed; however, gross gamma scans of the capsules prior to disassembly did not indicate fragment activity beyond the region of the cathode and anode. Any large migration of uranium during irradiation should have been indicated by fragment activity variations. Some of the uranium may have been jarred loose during the disassembly process. This would be especially true of the cathode, since it had the thickest deposit. Fuel lost in this manner would also be accompanied by the fragments imbedded in the material.

Another possible explanation for the discrepancy in the uranium analysis is incomplete dissolution of the samples. Since the dissolution, storage, and sampling of the various solutions were done in a hot cell facility, a close visual examination of the solutions for residual particulate matter was not possible. Particulate was noted, however, in the cathode solution of Capsule 9. A gamma scan of this particulate material revealed that it contained Zr-95. This was also verified by the fragment analysis. The material in all probability contained uranium. Solutions of the subsequent capsule were refluxed with excess acid for a period of 3 wk. Particulate material that contained Zr-95 still persisted; however, the fraction of the total uranium found to that plated was the highest

Table 2. Radiochemical data: fragment analysis

Capsule	Component	Total atoms produced			
		Y-91	Zr-95	Ba-140	Ce-144
3	Anode		1.570×10^{17}	1.262×10^{17}	
	Cathode[a]		0.597×10^{17}	4.62×10^{15}	
4	Anode		3.50×10^{17}	2.74×10^{17}	1.70×10^{17}
	Cathode		5.71×10^{17}	5.08×10^{17}	3.29×10^{17}
	Total		9.21×10^{17}	7.82×10^{17}	4.99×10^{17}
5	Anode	3.67×10^{16}	2.78×10^{16}	2.03×10^{16}	2.30×10^{16}
	Cathode	6.53×10^{16}	4.66×10^{16}	4.08×10^{16}	4.79×10^{16}
	Grid	1.673×10^{16}	1.320×10^{16}	0.969×10^{16}	1.117×10^{16}
	Total	11.87×10^{16}	8.76×10^{16}	7.08×10^{16}	8.21×10^{16}
	Anode and grid	5.34×10^{16}	4.10×10^{16}	3.00×10^{16}	3.42×10^{16}
6	Anode	2.15×10^{16}	0.364×10^{16}	0.827×10^{16}	0.486×10^{16}
	Cathode	13.77×10^{16}	1.770×10^{16}	7.26×10^{16}	3.48×10^{16}
	Grid	2.49×10^{16}	0.489×10^{16}	0.866×10^{16}	0.511×10^{16}
	Total	18.41×10^{16}	2.623×10^{16}	8.593×10^{16}	4.477×10^{16}
	Anode and grid	4.64×10^{16}	0.853×10^{16}	1.693×10^{16}	0.977×10^{16}
7	Anode	4.30×10^{16}	5.40×10^{16}	1.033×10^{16}	1.86×10^{16}
	Cathode	5.55×10^{16}	6.77×10^{16}	1.478×10^{16}	2.65×10^{16}
	Grid	1.582×10^{16}	1.970×10^{16}	0.400×10^{16}	0.712×10^{16}
	Total	11.43×10^{16}	14.14×10^{16}	2.911×10^{16}	5.22×10^{16}
	Anode and grid	5.88×10^{16}	7.37×10^{16}	1.433×10^{16}	2.57×12^{16}
9	Anode	7.34×10^{16}	5.79×10^{16}	11.12×10^{16}	4.28×10^{16}
	Cathode	19.70×10^{16}	2.64×10^{16}	8.90×10^{16}	7.43×10^{16}
	Grid	0.523×10^{16}	0.423×10^{16}	0.896×10^{16}	0.333×10^{16}
	Total	27.56×10^{16}	8.85×10^{16}	20.92×10^{16}	12.04×10^{16}
	Anode and grid	7.86×10^{16}	6.21×10^{16}	12.02×10^{16}	4.61×10^{16}
10	Anode	1.213×10^{17}	7.35×10^{16}	5.50×10^{16}	6.30×10^{16}
	Cathode	6.17×10^{17}	3.80×10^{16}	33.9×10^{16}	40.5×10^{16}
	Grid	0.486×10^{17}	0.300×10^{16}	0.254×10^{16}	0.268×10^{16}
	Total	7.73×10^{17}	1.145×10^{17}	3.97×10^{17}	4.71×10^{17}
	Anode and grid	1.262×10^{17}	0.765×10^{17}	0.575×10^{17}	0.657×10^{17}

[a]A portion of the cathode solution was lost because of boilover during the dissolution process.

[b]Undissolved material was noted in the cathode solution after the samples for analysis had been taken. A check analysis indicated that Zr-95 was present in the solid material.

for all of the capsules. The results of the uranium analysis are shown in Table 3.

3. Burnup Analysis

Total uranium burnup was determined by obtaining the ratio of the U-235 and U-236 isotopes in the burnup sample before and after irradiation. The sample was sectioned into four parts so that an axial distribution of the burnup could be obtained. The results are shown in Table 3. Capsule 10 did not contain a burnup sample; however, burnup was determined by obtaining the isotope ratios of the material on the cathode, anode, and grid. This gave an averaged value for the capsule. Average fuel burnup for the capsules was in the range of 1.5 to 3.6%.

Table 3. Radiochemical data: uranium analysis

Capsule	Uranium found		Grid, mg	Total	Uranium plated on cathode	Time at full power, hr	Burnup, %
	Anode	Cathode					
3	7.23	45.54[a]		52.77	136.	554	3.27
4	7.74	93.12		100.86	268.	597	3.62
5	0.0513	18.42	0.631	19.10	62.8	454	2.805
6	1.114	24.1	0.886	26.10	94.5	610	3.13
7	0.749	5.55	4.86	11.16	23.8	556	2.81
9	4.67	13.32[b]	1.61	19.60	158.	1089	2.60
10[c]	7.14	221.[b]	0.643	228.7	320.	1290	1.48[d]

[a]A portion of the cathode solution was lost due to boilover during the dissolution process.

[b]Undissolved material was noted in the cathode solution after the samples for analysis had been taken. A check analysis indicated that Zr-95 was present in the solid material.

[c]Components were refluxed in excess acid to attempt complete dissolution.

[d]Burnup was determined by analyzing the uranium on the various components. The cathode value is one used. Burnup, as determined by the anode sample, was 1.26%; the grid sample was 1.64%.

IV. CONCLUSIONS

Pressures of 10^{-4} mm Hg or less in the capsules were required in order to determine the actual output currents under short-circuit conditions. At higher pressures, amplification of the fragment current was experienced and was apparently due to ionization of the residual gas by fragments. Ions produced in this matter would have a net velocity component in the direction of the anode. The resulting electrons would have a more isotropic distribution, which would result in a net flow of positive current from the cathode to the anode due to the ionization process. No voltage buildup was obtained when the vacuum degraded, thus indicating a large internal cell leakage current under these conditions.

There were changes in the appearance of the fuel layer as a result of irradiation. It appeared to change from its original continuous, velvety appearance into a series of droplets or platelets. In some instances, the fuel material was diluted with sublayer and/or anode material. These effects will tend to decrease the efficiency of a cell that is generating electric power.

An equilibrium layer thickness of uranium appeared to build up on the anode. This layer was extremely thin; thus, its effect on cell operation would be small. There may, however, have been a large interchange of material between the electrodes. The effect of this material on cell performance will have to be studied in experiments designed specifically for high-voltage operation.

A large fission electric cell was designed in which a more detailed study of cell performance under irradiation

could be made. Problem areas concerning cell performance have been defined as a result of the capsule experiments; the large cell was designed to isolate them and allow their study under controlled conditions. Experiments with the large cell have been reported in Ref. 9.

APPENDIX A

Uranium Dioxide Plating Procedure

Fuel elements were formed by electro-deposition of uranium dioxide on the selected cathode surface. A cylindrical electrode formed of perforated platinum sheet was used for the anode. The perforations were to enhance circulation of the plating solution into the annular space between the anode and fuel element. An aqueous solution of ammonium oxalate, $(NH_4)_2C_2O_4$, was used as the plating bath. The uranium was introduced as an aqueous solution of uranyl nitrate, $UO_2(NO_3)_2$.

The plating bath temperature was maintained at 80°C during the plating operation. The element to be plated was placed in the bath with a potential applied between it and the anode. Plating current was maintained at 0.10 amp/cm^2 with 8.5 $\pm$0.5 v between the electrodes by increasing or decreasing the ammonium oxalate concentration in the plating bath. Uranyl nitrate was added to the plating bath at the rate of 0.5 to 0.75 mg UO_2/cm^2 of plating surface at 15-min intervals until the desired quantity had been introduced. Areas of the cathode within the plating bath that were not to be plated were masked with latex strippable paint.

Fueled cathodes were removed from the solution with the potential applied. The fuel material would flake off of the cathode if the potential between the electrodes were lost while the element is in the plating solution. Elements were thoroughly rinsed with methyl alcohol after plating, and then heated to approximately 150°C in a vacuum chamber to ensure complete dehydration. Cathode assemblies were weighed before and after plating to determine the quantity of uranium that was deposited. The finished elements were then alpha scanned to check for plating uniformity. Maximum deviation from the average thickness was $\pm$7%.

APPENDIX B

Calibration Experiments

Several different capsules were calibrated in order to determine the magnitude of capsule current due to non-fission events. This current, which results from the presence of structural material, is referred to as background current. The major contributors are electrons produced by Compton scattering of gamma rays by the structural material of the capsules. Although the anodes used in the capsules were thin so that they would be a small source of and essentially transparent to these electrons, and the structural material was thin and of low-density material, this type of electron current will nevertheless make a sizable contribution to the capsule fragment current because of the small quantity of uranium in the capsule. If true fragment output currents from the capsules are to be determined accurately enough to show operational behavior and trends, the non-fission current must be held to a small fraction of the total output currents.

Two capsules of the original basic design were irradiated in the NTR. One contained depleted uranium (0.22% U-235), and the other fully enriched. (See Figs. 12 and 14, which are graphs of their respective output

currents.) The current from Capsule 1, containing the depleted uranium, was positive without magnetic field and increased in value with complete follow-out electron suppression. This is as expected, since there should be a contribution to the capsule current from fissioning of the small amount of U-235 in the depleted uranium. Extrapolation of the results of Capsules 1 and 2 indicated a background current of 1.0 ± 0.2 μamp at GETR operating conditions. This calibration was used for Capsules 3 and 4.

Subsequent capsule calibrations were performed in the Spent Fuel Element Facility of the GETR. In these tests, the capsules were subjected to gamma radiation only. Each individual irradiated fuel element used and the capsules tested were surrounded with a cadmium sheet to eliminate the possibility of photoneutrons irradiating the capsules. Gamma irradiation was sufficient to determine background current, since neutron induced beta activation current with reactor irradiation was only a few percent of the Compton electron current. The first capsule of each series that contained a significant modification was calibrated and was subsequently irradiated in the GETR.

Capsule 5, the first to contain a grid, was calibrated in the Spent Fuel Element Facility. The gamma dose rate was 6×10^6 roentgens/hr for the configuration used. Anode current during this exposure was 11.3 mμamp with no magnetic field and 10.3 mμamp with from 2 to 30 amp in the field coil. The anode current was 5.8 mμamp with from -20 to -1000 v applied to the grid. Extrapolation to GETR conditions indicated a background current of 0.35 μamp with magnetic electron suppression and 0.20 μamp with electrostatic grid suppression. This same calibration data was used for Capsule 6.

Calibration data of Capsule 7 (shown in Figs. 15 and 16) had a gamma dose rate of 10^7 roentgens/hr. In addition to being a gridded capsule, it also had a field coil of copper windings instead of aluminum. The magnetic field affected the background current from this capsule. This was probably due to Compton electrons produced by the lower-energy gammas resulting from the larger mass of material surrounding the capsule. Average Compton electron energies for this configuration would be lower and more affected by the magnetic field.

Leakage current data taken during the calibration tests is shown in Fig. 17. The leakage current appears to become saturated at higher applied potentials. The opposite was true for leakage current data taken with this capsule during irradiation in the GETR (Fig. 51).

Extrapolation of the background current to GETR conditions indicated a background current of 0.9 ± 0.2 μamp with magnetic-field suppression and 0.45 μamp with grid suppression. Decrease of anode current with magnetic suppression at the higher fields during irradiation in the GETR (Fig. 39) is probably entirely due to the decrease in background current with increasing field.

Capsule 8 was irradiated in the NTR and was a voltage buildup experiment under various operating conditions.

Capsule 9 was the first of the two stainless steel capsules irradiated. Calibration data at a gamma dose rate of 10^7 roentgens/hr with electrostatic charge separation is shown in Fig. 18. At these same conditions, the anode current was independent of magnetic-field strength. The value with 50 amp in the field coil was 81.5 mμamp. Extrapolation to GETR conditions indicated a background current of 0.6 ± 0.1 μamp with magnetic-field suppression. Background current averaged over the range of grid operation was 0.3 ± 0.1 μamp. The same calibration data was used for Capsule 10.

Leakage currents with applied potentials were also measured (Fig. 19) during the calibration experiment. Leakage currents decreased with accumulated irradiation time. They appeared to be approaching saturation at the higher potentials with increased irradiation time. These changes were probably due to surface cleanup under irradiation.

APPENDIX C

Post-Irradiation Analysis

All capsules irradiated in the GETR were subjected to a post-irradiation analysis. Visual inspection during capsule disassembly and the gamma scans of the various components yielded information that explained some of the capsule behavior during irradiation. The radiochemical analysis, however, did not produce consistent results.

The total quantity of uranium found on the various components of each capsule by analysis after irradiation was always considerably less than the amount plated on the cathode. In the case of Capsule 3, the cathode solution boiled over, and a portion was lost during dissolution of the cathode. It was obvious that, as shown in Table 2, a large fraction of the fragments on the cathode was lost. Thus, it could be assumed that uranium was also lost. The discrepancy between the quantity of uranium found and the quantity of uranium plated on the cathode was noted for all succeeding capsules, even though steps were taken to ensure no solution loss. Axial gamma scans of all of the capsule assemblies following irradiation gave no indication of fragment activity outside of the cathode–anode region. This would indicate that there was no gross axial movement of the uranium during the irradiation period.

Because the dissolution of the capsule components was done in a hot cell facility, close examination of the solution was not possible. Residual material was noted in the cathode solution of Capsule 9. A gamma analysis indicated that the particulate contained Zr-95. Unfortunately, this was the only fragment checked. An unsatisfactorily small quantity of Zr-95 was found in the radiochemical analysis of the cathode solution, the results of which are shown in Table 2. The solution of the various components of Capsule 10 were refluxed for a period of 3 wk to ensure complete dissolution of the material. Even with this treatment, the Zr-95 analysis on the cathode solution was low, and particulate containing Zr-95 was evident in the solution. However, the total quantity of uranium found by analysis was the largest percent, relative to the amount plated on the cathode, of any of the capsules. It can be concluded from this that uranium was lost, at least from the cathode analyses, by incomplete dissolution of the material.

The uranium on the anode and grid should be in completely dispersed condition. This would increase the probability that the material is completely dissolved. If complete dissolving is assumed, the quantity of uranium on the anode or anode–grid combination appeared to reach an equilibrium value, and this value was independent of the thickness of the material on the cathode.

The analytical results for total quantity of fission fragments found in each capsule are inconsistent among the various species and the uranium by both the amount plated and the amount found. There is no correlation between the amount of a particular fragment found and the half-life of its noble gas precursor. Table C-1 shows the total quantity of fragments of the various species found in each capsule along with the quantities that should be present based on the burnup, the fission yield (Ref. 8), and the quantity of uranium plated on the cathode and also by the quantity found by analysis.

For Capsules 4, 5, 7, and 10, the ratio of the fragments found on the anode or anode–grid combination to the total found in the capsule establish a consistent trend. These ratios are shown in Table C-2. The light fragment groups had higher values for these ratios than did the heavy fragments. This indicates, as expected, that the light fragments have a longer range than the heavy ones. For Capsules 4, 5, and 7, the ratios for the fragments are larger than expected from range data; and for 10, they are smaller. In calculating the ratios, no correction was made for the fragments that would be generated and collected on the anode and grid because of the presence of uranium on these components.

A time averaged fragment current for the various capsules was calculated from the quantity of the fragments found on the anode, their fission yield, and the total time of irradiation; it is shown in Table C-3 along with an average measured fragment current. The calculated average fragment current is less than the measured value for all of the capsules. An average charge of $20e^+$ was used for the light fragments and $22e^+$ for the heavy. The lower calculated values would indicate that a portion of the fragments intercepted by the anode was missing. The fraction of the individual fragments not accounted for is random and does not correlate with precursor half-life or with vapor pressure of the fragment material. Best correlation between measured and calculated current is

Table C-1. Radiochemical data: comparison of analysis samples

Capsule		Y-91	Zr-95	Ba-140	Ce-144
3	(a)		7.11×10^{17}	7.28×10^{17}	
	(b)		2.85×10^{17}	2.92×10^{17}	
	(c)		2.17×10^{17}	1.31×10^{17}	
4	(a)		1.542×10^{18}	1.581×10^{18}	1.493×10^{18}
	(b)		6.02×10^{17}	6.17×10^{17}	5.83×10^{17}
	(c)		9.21×10^{17}	7.82×10^{17}	4.99×10^{17}
5	(a)	2.44×10^{17}	2.80×10^{17}	2.87×10^{17}	2.71×10^{17}
	(b)	7.64×10^{16}	8.76×10^{16}	8.98×10^{16}	8.48×10^{16}
	(c)	1.187×10^{17}	8.76×10^{16}	7.08×10^{16}	8.21×10^{16}
6	(a)	4.08×10^{17}	4.69×10^{17}	4.80×10^{17}	4.54×10^{17}
	(b)	1.164×10^{17}	1.338×10^{17}	1.370×10^{17}	1.293×10^{17}
	(c)	1.841×10^{17}	0.262×10^{17}	0.895×10^{17}	0.448×10^{17}
7	(a)	0.925×10^{17}	1.061×10^{17}	1.089×10^{17}	1.028×10^{17}
	(b)	4.46×10^{16}	5.12×10^{16}	5.25×10^{16}	4.95×10^{16}
	(c)	1.14×10^{17}	1.414×10^{17}	2.91×10^{16}	5.22×10^{16}
9	(a)	5.70×10^{17}	6.54×10^{17}	6.70×10^{17}	6.33×10^{17}
	(b)	7.26×10^{16}	8.33×10^{16}	8.54×10^{16}	8.06×10^{16}
	(c)	2.76×10^{17}	8.85×10^{16}	2.09×10^{17}	1.204×10^{17}
10	(a)	6.56×10^{17}	7.54×10^{17}	7.22×10^{17}	7.30×10^{17}
	(b)	4.77×10^{17}	5.47×10^{17}	5.24×10^{17}	5.30×10^{17}
	(c)	7.73×10^{17}	1.145×10^{17}	3.97×10^{17}	4.71×10^{17}

Note:
(a) Calculated from burnup data and the amount of uranium plated on the cathode.
(b) Calculated from burnup data and the amount of uranium found.
(c) Total quantity of fragments found corrected for in- and out-of pile decay.

for Capsule 4. For this capsule, the fraction of a particular fragment that is missing is proportional to its vapor pressure. If sublimation were the means by which the fragments were lost, these missing fragments should have appeared in the cathode analysis. The ratio of the quantity of fragments found between the anode and the cathode, and the total found indicate that this could not have been the case. It is possible that they were lost in the analysis.

The burnup data analysis results were in agreement with the NVT data determined from cobalt wire calibrations made in the vicinity of the capsule position.

Changes in surface characteristics were the most noteworthy observations made during the post-irradiation analysis. These changes are characterized by the migration of material between the electrodes and diffusion of material on the electrodes.

The post-irradiation view of the cathode of Capsule 3 in Fig. 55 shows a lack of the characteristic black coloring of uranium dioxide in the fueled region of the cathode. This is due to the migration of the zinc underlayer through the UO_2 layer. This type of behavior would cause fuel dilution which would result in a smaller fraction of the fragments reaching the anode than for a pure fuel layer.

An examination of the photographs of the anode of Capsule 4 in Fig. 31(a) shows that some portions sublimed and some may have been melted. Figs. 31(b) and 57 show regions of nickel deposited on the cathode from the anode. No evidence of anode damage was noted for Capsule 3; however, approximately one-half the quantity of uranium was plated on Capsule 3 as on Capsule 4. The uranium on the cathode of Capsule 4 shown in Fig. 57 appears to have formed into droplets or beads, which is in contrast to the original matte finish. Although the sublayer for Capsule 4 was the same as for Capsule 3, there is no evidence that zinc was mixed with the uranium.

The interior surface of the anode of Capsule 5 was platinum plated; there was no evidence from the visual observation of sublimation of anode material from this surface. However, there was indication of sublimation

Table C-2. Radiochemical data: fragment distribution

Capsule	Fragment species	Fraction fragment leaving cathode (c)			Fraction of leaving fragments on the grid	Grid transparency, %
		Experimental	Calculated			
			(a)	(b)		
3	Zr-95	—	0.221	0.551	—	—
	Ba-140	—	0.173	0.433	—	—
4	Zr-95	0.380	0.223	0.581	—	—
	Ba-140	0.350	0.173	0.445	—	—
	Ce-144	0.341	0.114	0.292	—	
5	Y-91	0.491	0.219	0.700	0.314	75
	Zr-95	0.468	0.146	0.468	0.322	
	Ba-140	0.424	0.105	0.334	0.323	
	Ce-144	0.416	0.126	0.417	0.326	
6	Y-91	0.252	0.114	0.398	0.537	70
	Zr-95	0.325	0.182	0.064	0.573	
	Ba-140	0.189	0.035	0.124	0.511	
	Ce-144	0.223	0.022	0.077	0.513	
7	Y-91	0.514	0.636	1.318	0.269	89
	Zr-95	0.521	0.694	1.440	0.267	
	Ba-140	0.494	0.132	0.274	0.279	
	Ce-144	0.493	0.250	0.520	0.277	
9	Y-91	0.285	0.138	1.082	0.0665	97
	Z-95	0.702	0.095	0.745	0.0680	
	Ba-140	0.575	0.180	1.410	0.0745	
	Ce-144	0.382	0.073	0.572	0.0722	
10	Y-91	0.170	0.192	0.265	0.0385	97
	Zr-95	0.667	0.101	0.140	0.0392	
	Ba-140	0.145	0.080	0.110	0.0442	
	Ce-144	0.139	0.090	0.124	0.0409	

Note:
(a) Calculated from total uranium on the cathode and burnup data. Experimental data used for quantity of this fragment on anode and grid.
(b) Calculated from total uranium found in capsule from the chemical analysis and burnup data. Experimental data used for the quantity of fragments on anode and grid.
(c) No correction for fragment that originated on anode and found on anode.

Table C-3. Time averaged fragment current

Capsule	Calculated fragment current, μamp					Measured fragment current, μamp		
	Y-91	Zr-95	Ba-140	Ce-144	Average	Anode current	Background current	Fragment current
3		4.07	3.20		3.63	9.7	1.0	8.7
4		8.41	6.44	4.23	6.36	9.5	1.0	8.5
5	1.33	0.88	0.63	0.75	0.90	1.9	0.35	1.55
6	0.58	0.09	0.19	0.12	0.24	3.2	0.35	2.85
7	1.27	1.39	0.26	0.50	0.86	3.6	0.90	2.7
9	1.11	0.76	1.43	0.58	0.97	2.75	0.60	2.15
10	1.55	0.82	0.60	0.72	0.92	3.75	0.60	3.15

from the exterior anode surface because of its matte appearance as seen in Fig. 59. The fuel layer of this capsule was covered with a layer of extraneous material as is evidenced in Fig. C-1. The origin of the material could have been molybdenum from the grid or nickel from the uranium sublayer.

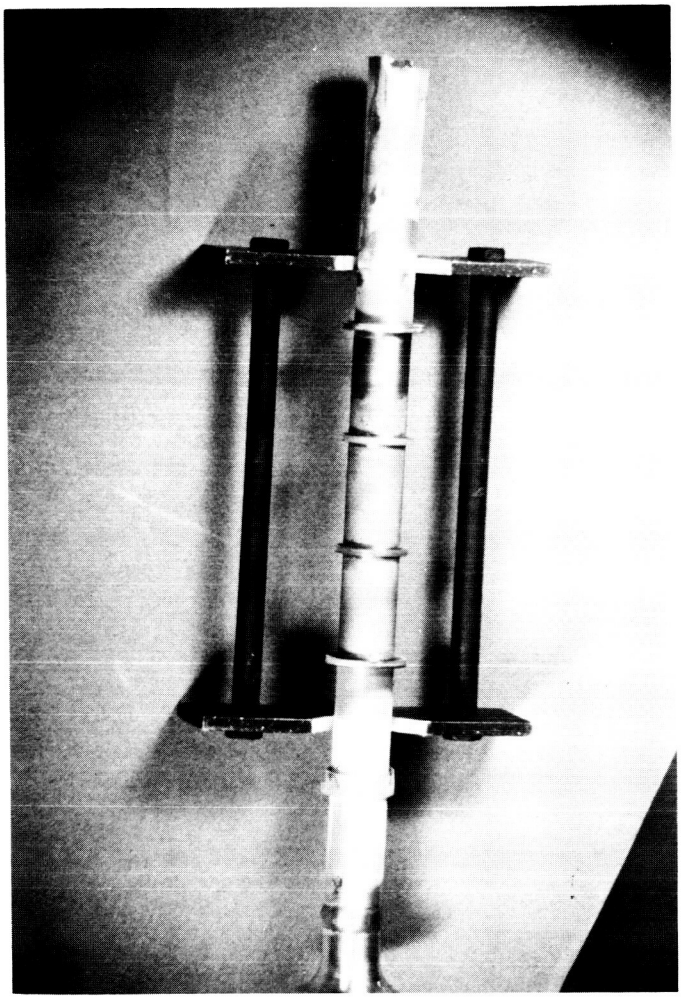

Fig. C-1. Cathode after irradiation (Capsule 5)

Both the interior and exterior surfaces of the anode of Capsule 6 were platinum plated; there was no evidence of gross movement of anode material. Small scratch marks visible in Fig. C-2 that were on the anode prior to irradiation were still visible after. Blistering of the nickel sublayer in the fuel region as a result of the irradiation can be seen in Fig. C-3.

Following irradiation, the fuel on the cathode of Capsule 7 had a metallic appearance as shown in Fig. C-4 rather than the characteristic black of UO_2. This appearance could have been due to a coating of extraneous anode or grid material or the platinum sublayer material of the cathode.

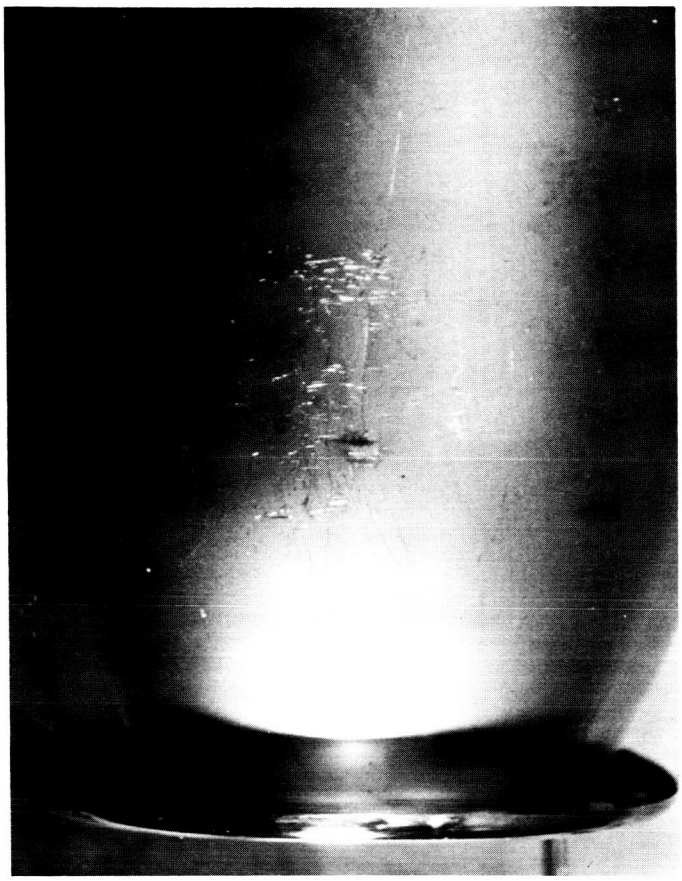

Fig. C-2. Anode closeup after irradiation (Capsule 6)

The glazed appearance of the platinum black finish in Fig. 60 on the lower portion of the anode of Capsule 9 indicates that it was subjected to extreme heating. The gamma scan of the anode shown in Fig. 61 indicated that the maximum activity on the anode was located at the bottom. This was probably due to accumulation of uranium in the termination curl at the base of the anode. The end curls of the anodes for the stainless steel capsules turned in while those for the aluminum turn out. The uranium layer on the cathode following irradiation has a metallic rather than a black color, and the materials appear to be in the form of platelets as shown in Fig. C-5 rather than the original matte-finish.

The cathode of Capsule 10 was plated with approximately twice the uranium of Capsule 9. Following irradiation, the uranium on Capsule 10 had a beaded appearance as shown in Fig. C-6.

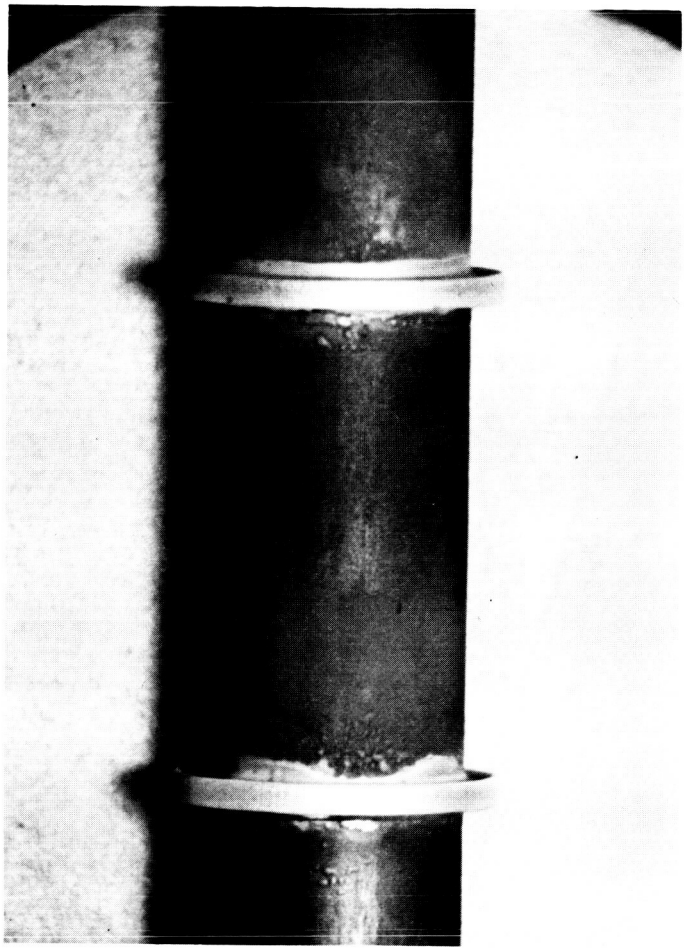

Fig. C-3. Cathode closeup after irradiation (Capsule 6)

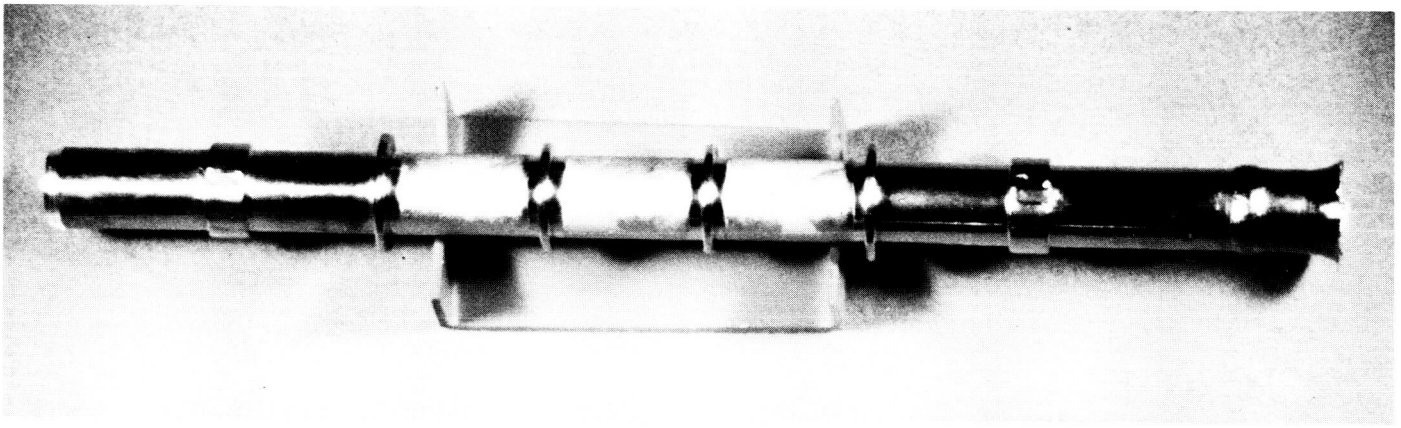

Fig. C-4. Cathode after irradiation (Capsule 7)

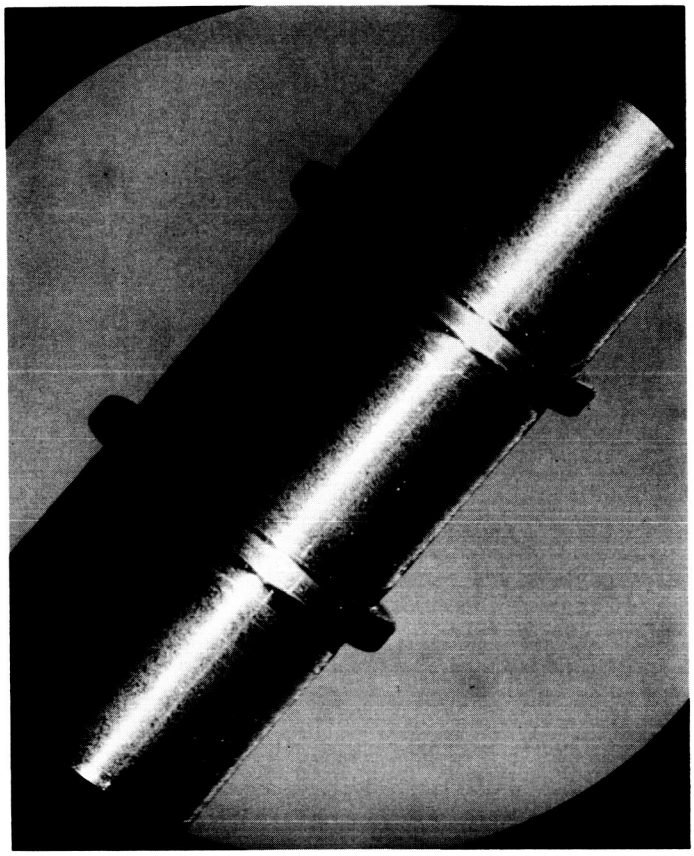

Fig. C-5. Cathode closeup after irradiation (Capsule 9)

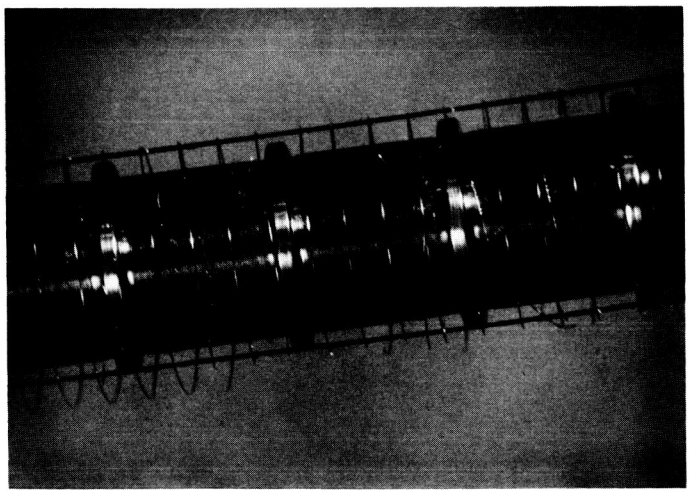

Fig. C-6. Cathode after irradiation (Capsule 10)

REFERENCES

1. Safonov, G., *Direct Conversion of Fission to Electric Energy in Low Temperature Reactors*, RM-1870, Rand Corporation, Santa Monica, California, 1957.
2. Safonov G., *The Fission-Electric Cell Project (A Report on 1963 Operations)*, Final Report, Contract AT (04-3)-482, March 1964.
3. Shock, A., *A Direct Nuclear Electrogenerator-Analysis of Cylindrical Electrode Configuration*, AFOSR TN 59, 590, 1959.
4. Heindl, C. J., *Comparison of Fission-Electric Cell Geometries*, Technical Report No. 32-101, Jet Propulsion Laboratory, Pasadena, California, September 1, 1961.
5. Heindl, C. J., Krieve, W. F., and Meghreblian, R. V., "Fission-Fragment Conversion Reactor for Space," *Nucleonics*, Vol. 21, No. 4, p. 80, April 1963.
6. Smythe, W. R., *Static and Dynamic Electricity*, p. 491, First Edition, McGraw-Hill Book Co., Inc., New York, 1939.
7. Dow, W. G., *Fundamentals of Electrical Engineering*, pp. 104 and 109, Second Edition, John Wiley & Sons, Inc., New York, 1952.
8. Katcoff, S., "Fission-Produce Yields From Neutron-Induced Fission," *Nucleonics*, Vol. 18, No. 11, pp. 201–208, November 1960.
9. Krieve, W. F., *JPL Fission-Electric Cell Experiment*, Technical Report No. 32-981, Jet Propulsion Laboratory, Pasadena, California, November 15, 1966.